The Islamic University–Gaza
Research and Postgraduate Affairs
Faculty of Science
Master of Physics

الجامعة الإسلامية– غزة
شئون البحث العلمي والدراسات العليا
كلية العلوم
ماجستير الفيزياء

Simulation of Human Head Model Exposed to RF Radiation from Dipole Antenna Using Finite Difference Time Domain Method

محاكاة رأس الإنسان المعرض للإشعاع الكهرومغناطيسي الناتج عن ثنائي القطبية باستخدام طريقة الفروق المنتهية في مدى الزمن

Heba-Allah Abdul-Mahdi Abo Amra

Supervised by

Prof. Dr. Mohammad M. Shabat
Prof. of Theoretical Physics and Applied Mathematics

Dr. Khitam Y. Elwasife
Associate Prof. of Physics

A thesis submitted in partial fulfillment of the requirements for the degree of Master of Science in Physics

February, 2017

إقـــــرار

أنا الموقع أدناه مقدم الرسالة التي تحمل العنوان:

Simulation of Human Head Model Exposed to RF Radiation from Dipole Antenna Using Finite Difference Time Domain Method

محاكاة رأس الإنسان المعرض للإشعاع الكهرومغناطيسي الناتج عن ثنائي القطبية باستخدام طريقة الفروق المنتهية في مدى الزمن

أقر بأن ما اشتملت عليه هذه الرسالة إنما هو نتاج جهدي الخاص، باستثناء ما تمت الإشارة إليه حيثما ورد، وأن هذه الرسالة ككل أو أي جزء منها لم يقدم من قبل الآخرين لنيل درجة أو لقب علمي أو بحثي لدى أي مؤسسة تعليمية أو بحثية أخرى.

Declaration

I understand the nature of plagiarism, and I am aware of the University's policy on this.

The work provided in this thesis, unless otherwise referenced, is the researcher's own work, and has not been submitted by others elsewhere for any other degree or qualification.

Student's name: هبة الله عبد المهدي أبو عمرة :اسم الطالب

Signature: :التوقيع

Date: :التاريخ

بسم الله الرحمن الرحيم

الجامعة الإسلامية غزة
The Islamic University of Gaza

مكتب نائب الرئيس للبحث العلمي والدراسات العليا هاتف داخلي 1150

الرقم: ج س غ/35/ Ref:

التاريخ: 18/04/2017 Date:

نتيجة الحكم على أطروحة ماجستير

بناءً على موافقة شئون البحث العلمي والدراسات العليا بالجامعة الإسلامية بغزة على تشكيل لجنة الحكم على أطروحة الباحثة/ **هبة الله عبد المهدي علي أبو عمرة** لنيل درجة الماجستير في **كلية العلوم** قسم **الفيزياء** وموضوعها:

محاكاة رأس الإنسان المعرض للإشعاع الكهرومغناطيسي الناتج عن ثنائي القطبية باستخدام طريقة الفروق المنتهية في مدى الزمن

Simulation of Human head model exposed to RF radiation from dipole antenna using Finite Difference Time Domain Method

وبعد المناقشة العلنية التي تمت اليوم الثلاثاء 21 رجب 1438هـ، الموافق 2017/04/18م الساعة الواحدة ظهراً بمبني اللحيدان، اجتمعت لجنة الحكم على الأطروحة والمكونة من:

أ.د. محمد موسى شبات	مشرفاً و رئيساً	.....
د. ختام يوسف الوصيفي	مشرفاً	.....
د. ماهر عمر الغصين	مناقشاً داخلياً	.....
أ.د. هناء محمد موسى	مناقشاً خارجياً	.....

وبعد المداولة أوصت اللجنة بمنح الباحثة درجة الماجستير في كلية العلوم/ قسم الفيزياء.

واللجنة إذ تمنحها هذه الدرجة فإنها توصيها بتقوى الله ولزوم طاعته وأن تسخر علمها في خدمة دينها ووطنها.

والله ولي التوفيق،،،

نائب الرئيس لشئون البحث العلمي والدراسات العليا

أ.د. عبدالرؤوف علي المناعمة

Abstract

The rapid evolution of the wireless communication technology and the widespread use of mobile phone lead to the increase of public concerns of the influence of the electromagnetic (EM) radiation on the human body. Cell phones emit radio frequency energy, a form of non-ionizing electromagnetic radiation, which can be absorbed by tissues closest to the place the phone is held. The amount of radio frequency power that a cell phone user is exposed to depends on technology of the phone, the distance between the phone's antenna and the user, and the extent and type of use.

In the past, the mobile phone had external antenna on the top of the phone which badly affects human head. Nowadays, the internal antenna is used more than the external antenna because the internal antenna has a good relation with Specific Absorption Rate (SAR).

This thesis aims to study the effect of radio frequency (RF) radiation emitted from dipole antenna on the human head and to explore the impact of following parameters: first, the distance between human head and the phone at (5cm, 10cm, 15cm, 20cm, 25cm, and 30cm), the effect of frequency at (900MHz, and 1800MHz) on SAR, power density, second, the distribution of electromagnetic fields by a planar multi-layered model to human head; its (Skin, Dura, Cerebrospinal Fluid, Brain, and Cerebellum) by Matlab program, and Finite Difference Time Domain (FDTD) method, third, High Frequency Structural Simulator (HFSS) software for the simulation and design calculations of the dipole antennas.

The study found that the electric and magnetic fields attenuate speed because when it hits human head, it penetrates the skin until it reaches zero in the cerebellum layer. It was found that decreasing the distance between mobile phone radiation and the human head makes electromagnetic wave radiations penetrate deeper up to the cerebellum layer, in addition, we note that the power density and SAR have maximum value at the skin and dura layers. Also, Figures show that the effect of frequency 900MHz by mobile phone global system mobile (GSM) is higher than the frequency 1800 MHz on human head.

الملخص

التطور السريع لتكنولوجيا الاتصالات اللاسلكية والاستخدام الواسع النطاق للهواتف المحمولة أدى إلى تزايد المخاوف بين العامة حول تأثير الإشعاع الكهرومغناطيسي علي جسم الإنسان. تنبعث من الهواتف المحمولة طاقة الترددات الراديوية وشكل من أشكال الإشعاع الكهرومغناطيسي غير المؤين، والتي يتم امتصاصها من قبل الأنسجة الأقرب إلي الهاتف الحمول.

تعتمد كمية الطاقة للترددات الراديوية عندما يتعرض لها مستخدم الهاتف المحمول علي تكنولوجيا الهاتف، والمسافة بين هوائي الهاتف والمستخدم، و مدى و نوع الاستخدام.

تهدف هذه الأطروحة إلي دراسة تأثير الموجات الراديوية المنبعثة من هوائي ثنائي القطب علي رأس الإنسان، واستكشاف أثر المتغيرات التالية: المسافة بين الرأس والهاتف عند (٥سم، ١٠سم، ١٥سم، ٢٠سم، ٢٥سم، ٣٠سم)، وتأثير التردد عند (٩٠٠ميجاهيرتز، ١٨٠٠ ميجاهرتز) على كل من معدل الامتصاص النوعي وكثافة الطاقة وتوزيع الحقول الكهرومغناطيسية من خلال نموذج متعدد الطبقات من رأس الإنسان ممثلاً بخمس طبقات وهي (الجلد، الجمجمة، السائل النخاعي، المخ، المخيخ) باستخدام برنامج الماثلاب وطريقة الفروق المنتهية في مدى الزمن وكذلك رسم الهوائي الخاص بالهاتف المحمول باستخدام برنامج HFSS.

وجدت الدراسة أن المجالات الكهربائية والمغناطيسية عندما تضرب رأس الإنسان تخترق الجلد ثم تخفف سرعتها حتي تصل إلى الصفر في طبقة المخيخ. ووجدت أيضا أنه كلما قلت المسافة بين إشعاعات الهاتف المحمول ورأس الإنسان فإن إشعاعات الموجة الكهرومغناطيسية تخترق بعمق أكبر حتى طبقة المخيخ، بالإضافة إلى أن كثافة الطاقة ومعدل الامتصاص النوعي لديها أقصى قيمة في طبقة الجلد والجمجمة عن غيرها من باقي الطبقات الخمسة.

ولوحظ أن تأثير تردد ٩٠٠ ميجاهيرتز من الهاتف المحمول هو أكثر من تردد ١٨٠٠ ميجاهيرتز على رأس الإنسان.

Dedication

To those whom the Almighty Allah recommends to obey and relates his content to their content my dear parents: mother and father, who did their best to get me to the highest degree of success, I dedicate this work.

This thesis is dedicated to my husband, Suleiman, who has been a constant source of support and encouragement during the challenges of graduation and life as a whole. I am truly thankful for having him in my life.

To my sisters Hana, Nada, and Abeer, I also dedicate this work.

To my daughter, Mira I also dedicate this thesis.

I never forget to dedicate this work to everyone who helped me to finish this work.

Acknowledgment

Praise is to Allah for blessing me to accomplish this thesis, and I beg Him to accept this among my good deeds.

I would like to thank Prof. Dr. Mohammed M. Shabat, at the Faculty of Science, Department of Physics, at The Islamic University of Gaza, for his valuable guidance and directions to me throughout this work.

In addition, I'd like to thank Dr. Khitam Y. Elwasife, at the Faculty of Science, Department of Physics at The Islamic University of Gaza, for her many valuable suggestions, fruitful discussions, and constructive pieces of advice throughout this work.

Special thanks and much respect go for my lovely husband, Suleiman Abo Amra, for his patience and encouragement till I finish my work.

I'd like to thank my family, my parents, my sisters Hana, Nada, and Abeer for their unflagging love and unconditional support throughout my life and my study.

Also I'd like to thank Mr. Ismail Abo Amra for his great help.

Table of Contents

List of Tables

List of Figures

List of Annexes

Chapter One

Introduction

Chapter One
Introduction

Since cellular phones were produced, the scientific community has gained substantial knowledge about the interaction between a wireless transmitter and the electromagnetic (EM) energy absorption in the user's head in the immediate vicinity of the transmitter. The fundamental absorption mechanism of high frequency fields in biological bodies is essentially based on the induction of eddy currents on the skin and in the tissue due to the electromagnetic fields caused by the radio frequency (RF) currents on the antenna and device (Christ, Samaras, Klingen, and Kuster, 2006).

This chapter offers a review to electromagnetic radiation. Moreover, it aims to study the types of electromagnetic radiation based on the severity of the radiation. Also, it summarizes reviews of human head tissues as a model of multilayered structure subject to the radiation of dipole antenna, so the proposed structure contains five layers as biological body tissue as skin, dura, CSF, brain and cerebellum.

1.1 Electromagnetic Radiation

Electricity and magnetism were once thought to be separate forces. However, in 1873, Scottish physicist James Clerk Maxwell developed a unified theory of electromagnetism. The study of electromagnetism deals with the way electrically charged particles interact with each other and with magnetic fields (Jensen, 2007). There are four main electromagnetic interactions: the force of attraction or repulsion between electric charges is inversely proportional to the square of the distance between them, magnetic poles come in pairs that attract and repel each other, much as electric charges do, an electric current in a wire produces a magnetic field whose direction depends on the direction of the current, and a moving electric field produces a magnetic field, and vice versa (Cheng, 1998).

Electromagnetic (EM) radiation is created when an atomic particle, such as an electron, is accelerated by an electric field, causing it to move. The movement produces oscillating electric and magnetic fields, which travel at right angles to each other in a bundle of light energy called a photon. Electromagnetic radiation has

properties in common with other forms of waves such as reflection, refraction, diffraction, and interference. Moreover, it may be characterized by the frequency with which it varies over time or by its wavelength. Electromagnetic radiation, however, has particle-like properties in addition to those associated with wave motion (Cheng, 1998).

In electromagnetic radiation (Mohsenin, 1984; Butcher, n.d): the electric field is perpendicular to the magnetic field, and both are perpendicular to the direction of propagation as shown in Figure (1.1) (Tempfli, Kerle, Huurneman, and Janssen, 2009).

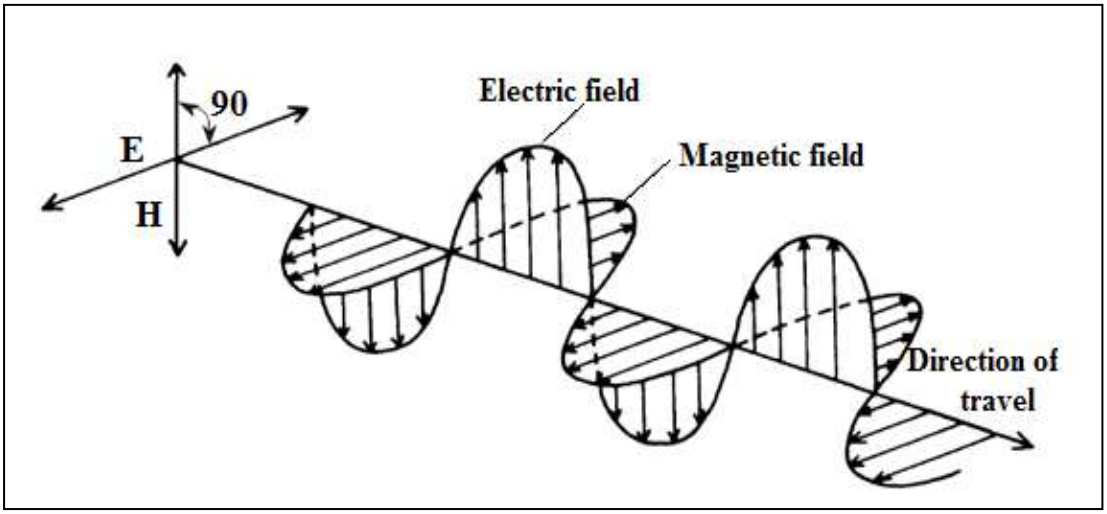

Figure (1.1): The two oscillating components of EM radiation: an electric and a magnetic field (Tempfli, Kerle, Huurneman, and Janssen, 2009).

Electromagnetic radiation spreads in the vacuum at a constant speed, the speed of light, these rays move from the source to the receiver with energy, its energy equation is: $E = h f$, where the constant h is Planck's constant $h = 6.6 \times 10^{-34}$ J.s, the unit uses electron volts to express electromagnetic radiation energy $1e.v = 1.6 \times 10^{-19}$J.

1.2 The Spectrum of Electromagnetic Radiation

EM radiation spans an enormous range of wavelengths and frequencies. This range is known as the electromagnetic spectrum. The EM spectrum is generally divided into seven regions, in order of decreasing wavelength and increasing energy and frequency.

The common designations include radio waves, microwaves, infrared (IR), visible light, ultraviolet (UV), X-rays, and gamma rays. Typically, lower-energy radiations include radio waves, microwaves, infrared, visible, and UV light; and the higher-energy radiation, such X-rays, and gamma rays as shown in Figure (1.2) (Andrews, 2009; Kraus, 1997). The speed of electromagnetic radiation is given by the equation $c = \lambda f$ (Andrews, 2009).

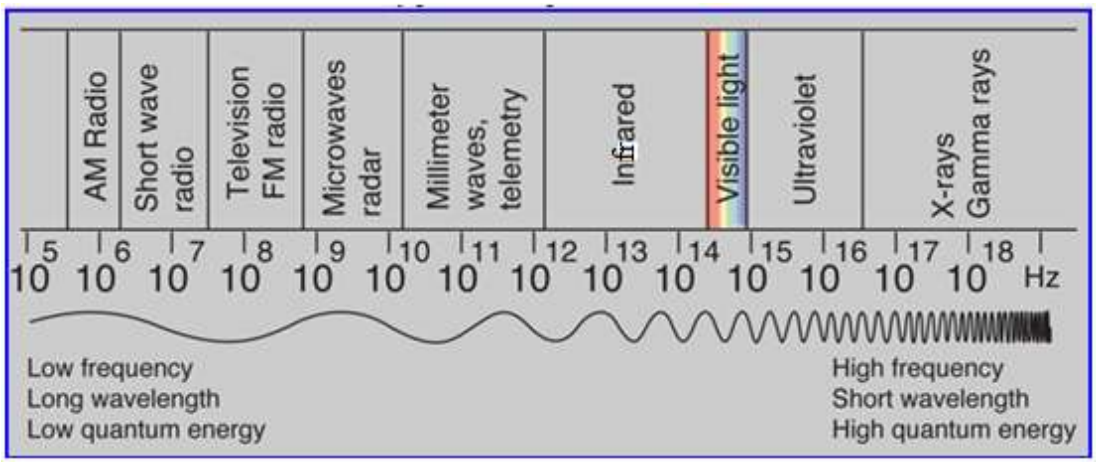

Figure (1.2): Electromagnetic spectrum with light highlighted (Andrews, 2009).

Radio waves:

The experiments of scientists such as Hertz, Maxwell and Faraday, and the invention of Telegraph by scientist Marconi credited with the discovery of radio waves, and they are understood and used in many applications (Carr, 2001).

Radio waves are at the lowest range of the EM spectrum, with frequencies of up to about 30 billion hertz, or 30 gigahertz (GHz), and wavelengths greater than 10 millimeters (0.4 inches), have the lowest energy levels (Lucas, 2015).

Radio is used primarily for communications including radio broadcasts, TV broadcasts, and even cell phones. In addition, Radio waves are used in remote sensing. They are also used in radar systems, where they release radio energy and collect the bounced energy back. Especially useful in weather, radar systems are used to illustrate maps of the surface of the Earth and predict weather patterns since radio energy easily breaks through the atmosphere (Hernandez, Patel, and VO, 2015).

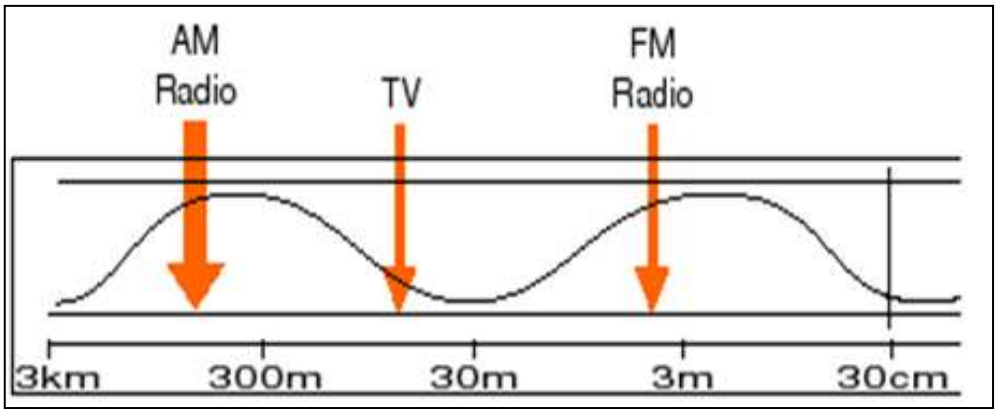

Figure (1.3): Radio Wave Region of the Electromagnetic spectrum (Hernandez, Patel, and Vo, 2015).

1.3 Types of Electromagnetic Radiation

Electromagnetic Radiation is also categorized in two groups: ionizing and non-ionizing, based on the severity of the radiation (Wikipedia, 2014; Mousa, 2011; Retriev, 2011):

1) Ionizing Radiation

This type of radiation has enough energy to remove bound electrons from the orbit of an atom. It becomes an ionized atom, this type of radiation contains enough electromagnetic energy to strip atoms and molecules from the tissue and alter chemical, deoxyribonucleic acid (DNA) cells of the body, and some of these changes may lead to an imbalance in the atomic liquid of human. The symptoms of radiation ionizing may occur over a long period. There are three main types of ionizing radiation that may be found in man-made radiation as well as in the radiation of the natural alpha particles, beta particles, and gamma rays in addition to cosmic rays, and X-rays.

2) Non-ionizing Radiation

Non-ionizing radiation does not have the sufficient energy to ionize (change) the atoms, and it is typically safe. It causes some heating effect, but it is usually not enough to cause any type of long-term damage to tissue, which is characterized by

low frequency long wave length; the eye is the most vulnerable. Laser and electromagnetic radiations include radio, radar, and television waves, infrared, UV, microwave, visible light, Mobile phones that generate a modulated radio frequency electromagnetic field (RF- EMF).

1.4 Human Body Structure

The human body is a single structure but it is made up of billions of smaller structures of four major kinds (Assefa, and Tsige, 2003):

a- Cell: The cell is a chemical system that is able to maintain its structure and reproduce itself; it is the fundamental unit of life. Cell is the structural and functional unit of the human body.

b- Tissues: Tissues are materials made up of groups of similar cells. Cells are of various types, and tissues vary according to the types of cells in their structure; they are specialized to carry out particular functions. There are four major or primary types of tissue in the human body: epithelium, muscle, connective tissue, and nervous tissue.

c- Organs: Organs are more complex units than tissues. An organ is an organization of several different kinds of tissues so arranged together that they can perform a special function. For example, the stomach is an organization of muscle, connective, epithelial, and nervous tissues. Muscle and connective tissues form its wall, epithelial and connective tissues form its lining, and nervous tissues extend throughout both its wall and its lining (Hoehn, and Nicpon, 2007).

d- Systems: Systems are the most complex component unit of the human body. A system is an organization of varying numbers and kinds of organs so arranged together that they can perform complex functions for the body (Hoehn, and Nicpon, 2007; Rettner, 2016).

1.4.1 The Brain

The brain is the main part of the central nervous system, which also includes the spinal cord. It controls all of the body’s processes. Most of the signals from the brain

reach the body via the spinal cord (Morris, and Fillenz, 2003; "The human brain," 2016). What makes the human brain unique is its size. Our brains have a larger cerebral cortex, or cerebrum, relative to the rest of the brain more than any other animal. This enables us to have abilities such as complex language, problem-solving, and self-control ("Know Your Brain," 2012). The brain is protected by layers as shown in Figure (1.4):

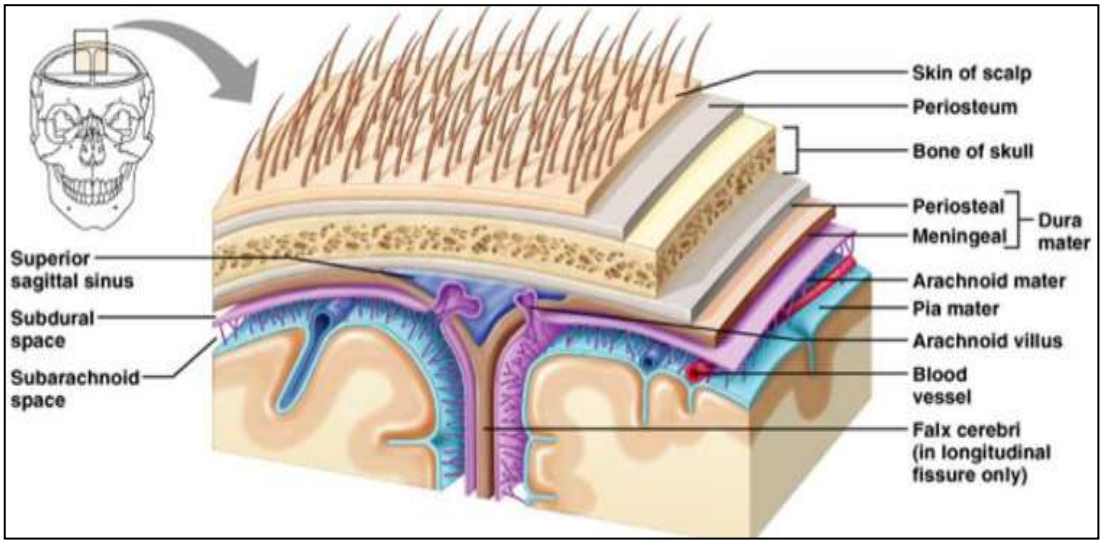

Figure (1.4): Section of brain, showing layers that protect the brain ("Know Your Brain," 2012).

1- Skin Tissue

Skin is the outermost tissue of the body and the largest organ in terms of both weight and surface area. Skin has a very complex structure that consists of many components. Cells, fibers and other components make up several different layers that give skin a multi-layered structure. Skin performs a wide variety of functions resulting from chemical and physical reactions inside these components. The major function of skin is to act as a barrier to the exterior environment. It protects the body from friction and impact wounds by its flexibility and toughness (Derrickson, and Gerard, 2005; Igarashi, Nishino, and Nayar, 2005).

2- The Skull

The skull or Cranial is a bony structure that forms the head of the skeleton in most vertebrates. It supports the structures of the face and provides a protective

cavity for the brain. The skull is composed of two parts: the cranium and the mandible (Morris, and Fillenz, 2003).

3- The Meninges

The meninges are membranous coverings of the brain that lie immediately internal to the cranium. The meninges perform a variety of functions which include (Student bmj, 2011): covering and protecting the brain, protecting blood vessels, enclosing venous sinuses, containing cerebrospinal fluid (CSF), and forming partitions within the skull.

The meninges are composed of three membranous connective tissue layers, such as dura Mater. Dura is a tough thick membrane composed of dense collagen fibers, closest to the skull. The dura creates little folds or compartments. There are two special dural folds, the falx and the tentorium. The other layer is Pia Mater**,** which is in a direct contact with the brain. The pia mater has many blood vessels that reach deep into the brain ("The human brain," 2016; Morris, and Fillenz, 2003).

4- Cerebrospinal Fluid

Cerebrospinal fluid is a transparent, colourless ultrafiltrate of plasma. It is separated from the rest of the body's blood stream by the 'blood-brain barrier,' which also serves to protect the brain from infection and fluctuations in hormones and other substances in the blood. This helps to keep the environment of the brain constant and consistent with the spinal cord at the foramen magnum at the base of the skull (Encyclopædia Britannica, 2016). Cerebrospinal Fluid (CSF performs a variety of functions which are:

- Forming a liquid cushion that gives buoyancy to the CNS organs.
- Preventing the brain from crushing under its own weight.
- Protecting the CNS from blows and other trauma.
- Nourishing the brain and carrying chemical signals throughout it.

The brain consists of four major components as shown in Figure (1.5) (Bender, Harding, Jackson, Kennedy, Lee, and Stokes, 2005):

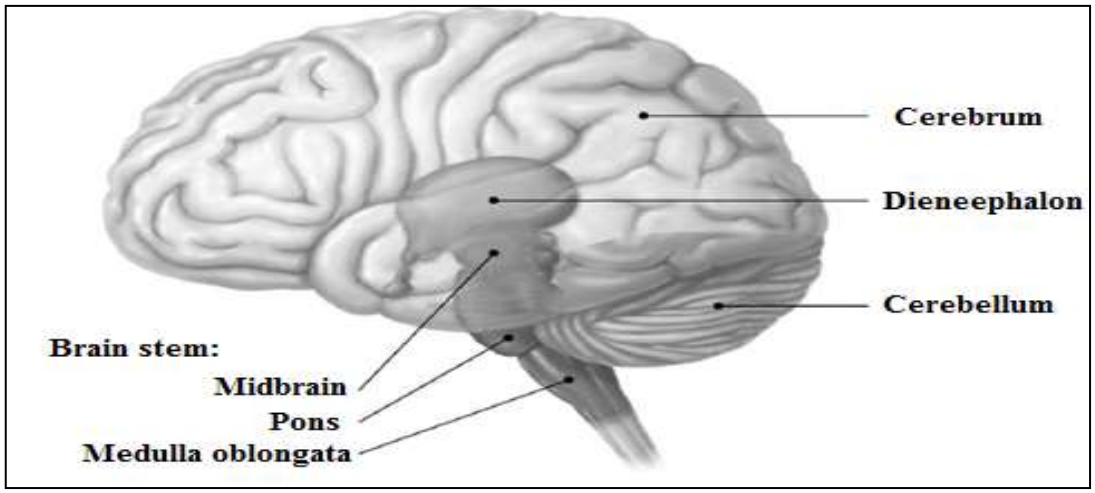

Figure (1.5): General anatomy of the human brain (Bender, Harding, Jackson, Kennedy, Lee, and Stokes, 2005).

1- **Cerebrum,** the largest part of the brain has a right and a left hemisphere; both are separated by a deep groove the longitudinal fissure. The cerebrum performs higher functions like interpreting touch, vision and hearing, speech, reasoning, emotions, learning, and fine control.

2- **The brainstem,** which is normally continuous with the spinal cord, it includes the midbrain, pons, and medulla oblongata. It acts as a relay center connecting the cerebrum and cerebellum to the spinal cord. It performs many automatic functions such as breathing, heart rate, body temperature, sleep cycles, digestion, and swallowing, etc.

3- **Diencephalon,** called the "between brain" area of the forebrain between the midbrain and cerebral hemispheres. It includes the thalamus and the hypothalamus.

4- **The cerebellum,** also known as the hindbrain, is located behind the top part of the brain stem (where the spinal cord meets the brain) and is made of two hemispheres (halves). The cerebellum receives information from the sensory systems, the spinal cord, and other parts of the brain and then regulates motor movements. The cerebellum coordinates voluntary movements such as posture, balance, coordination, and speech, resulting in smooth and balanced muscular activity. It is also important for learning motor behaviors. It is a relatively small portion of the brain about ten percent of the total weight, but it contains roughly

half of the brain's neurons, specialized cells that transmit information via electrical signals.

1.5 Objective

The aim of this work is to evaluate effect of electromagnetic fields produced from dipole antenna on layered biological tissues (human head model) by Finite Difference Time Domain (FDTD) method. It is a numerical analysis technique used for modeling computational electrodynamics. This method can cover a wide range of frequencies to study energy absorption (power density), electric field, magnetic field, and specific absorption rate (SAR) by a planar multi-layered model to human head; its (Skin, Dura, Cerebrospinal Fluid, Brain, and Cerebellum) at the frequencies 900 MHz and 1800 MHz at distances from the body at 5 cm, 10 cm, 15 cm, 20 cm, 25 cm, and 30 cm by Matlab program.

We used High Frequency Structural Simulator (HFSS) software for the simulation and design calculations of the dipole antennas. Ansoft HFSS is an interactive software package for calculating the electromagnetic behaviour of a structure. The software also includes post-processing commands for analyzing the electromagnetic behaviour of a structure in more detail. Ansoft HFSS is a full-wave finite element electromagnetic (EM) simulator that enables engineers to design three-dimensional (3D) high-frequency structures such as connectors, IC packages and antennas found in cellular telephones, broadband communications systems, microwave circuits, and waveguide. Mathematical Method used in HFSS is a numerical technique called the finite element method.

1.6 Importance of the Study

The importance of the study is to explain the relation of the distance between mobile phone radiation, the human head, and the extent of penetration electromagnetic wave radiation in a planar multi-layered model to human head. The study also explores the relation of frequency at (900 MHz, and 1800 MHz) on SAR, power density, second, and the distribution of electromagnetic fields by a planar multi-layered model to human head.

This study can increase the awareness of the people about the potential health hazards due to the absorption of electromagnetic (EM) energy emitted by mobile phone. The study used specific absorption rate (SAR) and power density in dosimetric at the exposure for mobile phone radiation.

Chapter Two

Antennas and FDTD Solution to Maxwell's Equation

Chapter Two

Antennas and FDTD Solution to Maxwell's Equation

Introduction

With the recent rapid increase in the use of portable telephones and wireless local area networks (WLANs), public concern regarding potential health hazards due to the absorption of electromagnetic (EM) energy emitted by these applications has been growing. Safety guidelines for protecting the human body from Radio Frequency (RF) exposure have been issued in various countries.

Specific absorption rate (SAR) parameter has been widely used to determine the possibility of health hazards in the human head due to RF radiation. It is defined as the transferred power divided by the mass of the object. However, very little is known about possible biological effects of localized SAR, since the SAR is a physical quantity, which causes tissue heating due to RF exposure.

This chapter aims to study antenna and its parameters. Moreover, it will talk about mobile phones antenna. In the current chapter, the researcher will focus on the dipole antenna commonly used in radio and telecommunications. This chapter presents the effect of mobile phone radiation on human health and the dosimetric parameters in a human head exposed to an electromagnetic field emitted from a handheld cellular phone operating in global system mobile (GSM). Considering GSM system one of the most popular cellular system all over the world and being the one which is adopted and operating in Palestine, then the operating frequency is at 900MHz, and 1800MHz (Mousa, 2011). Also, the researcher presented simple explanations for FDTD method and the FDTD Yee Algorithm for Maxwell's equations.

2.1 Antenna

Antennas are a very important component of communication systems. By definition, an antenna is a device used to transform a RF signal into an electromagnetic wave often referred to as radio waves in free space (Skolnik, 1962, 1990).

For antennas, several parameters determine the type of antenna and quality of sending and receiving signals, such as (Balanis, 2005; Bath, Thakur, Sharma, Prasad, 2014; Chatterjee, 2001; Chatterjee, and Neelakanta, 2003; Grove, n.d.; Hawkins, 1936; Kraus, 1997; Schelkunoff, and Friis, 1952; Zhang, 2011):

1) Radiation Pattern

Radiation pattern is a shape outside the beam of the antenna, where it has a certain shape and a certain direction through which we can locate the signal reception. It's defined as a mathematical function or a graphical representation of the radiation properties of the antenna as a function of space coordinates.

There are two common types of antenna pattern: the first one is a power pattern, and the second is field pattern. The first type is described as the power radiation through the antenna, which depends on its direction and the position of the spherical coordinate. The second type depends on the kind of field with the position of spherical coordinate. The radiation pattern in the region close to the antenna is not exactly the same as the pattern at large distances. The term near-field refers to the field pattern that exists close to the antenna; the term far-field refers to the field pattern at large distances. The far-field is also called the radiation field, while the near-field is called the induction field.

2) Return Loss

It is the loss of signal power resulting from the reflection caused at the discontinuity in a transmission line or an optical fiber. This discontinuity may mismatch with the terminating load or with a device inserted in the line. It is usually expressed as a ratio in decibels (dB).

3) Directivity

Directivity is one of the antenna parameters that guide us to measure the direction of the radiation pattern. The directivity helps us to determine the efficiency of the antenna and the directivity of isotropic antenna equal to 1 (0 dB). Mobile phone antenna should have a low directivity, because it is not useful to use an antenna with

high directivity, which is the received signal from different directions. On the other hand, the base station needs a high directivity.

4) Polarization

One of the antenna parameters for any types of antennas is the direction of the electrical field vector of the electromagnetic wave. The polarizations of electromagnetic wave depend on the electrical field, which is perpendicular with the magnetic field at the earth's surface. It depends on antenna shape and place with regard to the land surface. It identifies the direction of an antenna in send-and-receive process, such as vertical and horizontal polarization.

5) Input Resistance or Impedance

It is a measure of the value of the impedance on the income of the antenna where it is supposed to be suitable for the value of the output impedance of the cable which is used to transfer the signal of the antenna in order to move the largest possible amount of signal energy, the cables presented in the market often have impedances 50Ω, 75Ω, 300Ω.

6) Gain

One of the antenna parameters to measure the capacity of an antenna is to focus energy emerging from it in a particular area, which increases signal quality in that region.

7) VSWR

Voltage Standing Wave Ration or S_{11} that describes the reflection power coefficient or the return losses of the antenna.

2.2 Mobile Phones Antenna

A mobile phone is a portable telephone which receives or makes calls through a cell site (base station) or a transmitting tower. Radio waves are used to transfer signals to and from the cell phone. Mobile phones are connected to the base stations via radio frequency electromagnetic waves (RF-EMF). These mobile phones should be in the coverage area of a certain cell; the base station of this cell must assign this mobile phone the necessary RF channel to maintain the connection. To achieve this link, the mobile should use certain transmission power to connect with the base station (uplink), and the base station should use the required power to connect with the mobile phone (down link) (Mousa, 2011).

Older mobile phone was so heavy, big and had external antenna on the top of the chassis through the end of 1990s. The external antennas had a drawback of having high SAR (Zhang, 2011). In addition, through the end of 1990s, mobile phones having internal antennas started to be released to the market. The main reason of this is that the internal antenna has a good relation with SAR, on the other, hand the size of the phone became smaller (Fung, 2011). Since mobile phones have evolved immensely both in design and function; the bulky devices that were once used exclusively for making and receiving voice calls are currently light, compact, used to send and receive emails, take pictures, play music, game, FM radio and TV. Moreover, easy access to internet for the internet obsessed societies opens a world of opportunities to every user, and yet, this is just the beginning (Orfanidis, 1999; Stallings, 2005).

Mobile phone consists of several antennas for several purposes such as Wi-Fi antenna, GPS antenna, low and high frequencies antennas. Each type of antennas is designed according to certain considerations. Dipole antenna is a useful type of antennas; easy to be constructed, and integrated in cell phones (Balanis, 2005; Connor, 1989). For this, the evolution of a dipole antenna into a cellular phone antenna became a consistent need. This process is illustrated in Figure (2.1) ("smartphone cellular mobile phone antenna design", 2015).

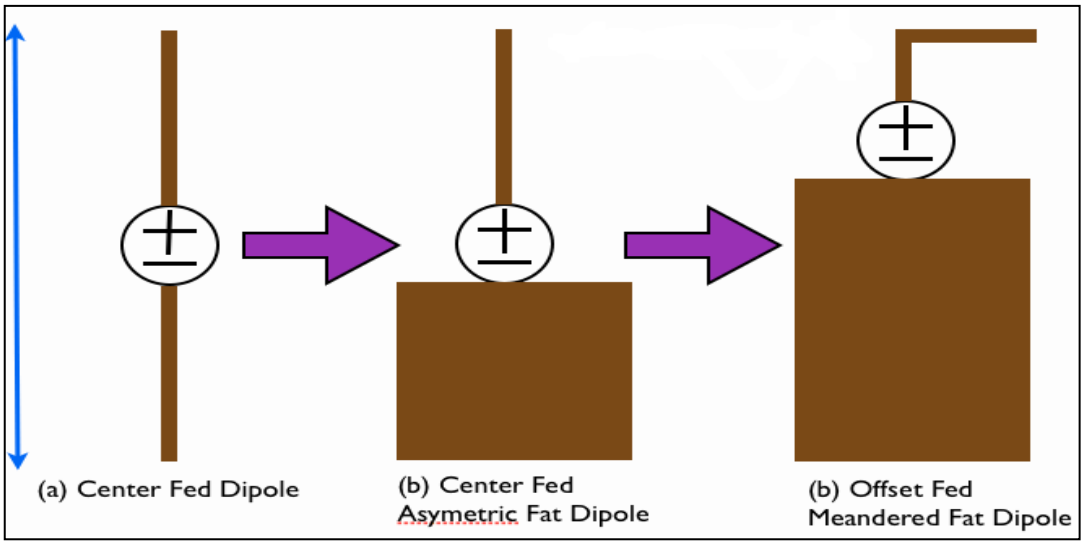

Figure (2.1): Evolution of Dipole Antenna to a Mobile Phone Cell Antenna ("smartphone cellular mobile phone antenna design", 2015).

Dipole Antennas

The dipole antenna is one of the most important and commonly used types of RF antenna. Also, it is incorporated into many other RF antenna designs where it forms the driven element for the antenna (Fung, 2011).

The dipole antenna is omni-directional, propagating radio frequency (RF) energy 360 degrees in the horizontal plane (Ackson, and David, 1999). These devices are constructed to be resonant at a half or quarter wavelength of the frequency being applied. It is made up of two similar conductive elements such as metal wires or rods that are generally bilaterally symmetrical (Tawde, 2015; Parameswari, and Kumar, 2015). The most common type of dipole is two straight rods or wires which are connected end to end on the same axis, with the feed line connected to the two adjacent ends. So, the length of the dipole elements is calculated by the wavelength of the radio waves (Grove, n.d.; James, 1991; Kraus, 1997; Fung, 2011).

2.2.1 The Effect of Mobile Phone Radiation on Human Health

Today, the effect of mobile phone radiation on human health becomes the subject of recent interest and study, because of the enormous increase in the use of wireless mobile telephony throughout the world. In 2016, there were 7.4 billion

subscriptions worldwide (but some have more than two). So, 4.230 million users in 2014 give better picture, then there were about 97 phones per 100 citizens (Wikipedia, 2015; Fujimoto, 1999).

There has been a growing concern about the possible adverse health effects resulting from exposure to radio frequency radiations (RFR), such as those from mobile communication devices. Mobile communication is that signal which is transferred via electromagnetic wave through radio frequency and microwave signals. This signal produces electromagnetic radiation in the form of thermal radiation that consists of harmful ionizing radiation and harmless non-ionizing radiation. When using mobile phone, electromagnetic wave is transferred to the body, causing health problems especially at the place near ear skull region where they are known to affect the neurons. The radiations interfere with the electrical impulses with which two neurons connect each other. These concerns have induced a large body of research in animals and in humans (Bhargavi, KE, and Nageswar, 2013; Kenneth and Repacholi, 2004).

Some of the symptoms and health problems that may occur as a result of frequent use of mobile devices and presence of mobile device transmitters include (Hyland, 2000; Sharma, (n.d.); Attwood, 1995; Adey, 1997; Nicolas, and Lautru, 2001; Gandhi, and Lazzi, 1996) feeling of heat and numbness around ear, headaches, tinnitus acoustic nerve tumours, impaired concentration and memory, chronic fatigue, sleeping difficulties, depression, restlessness and heart palpitations, and increased susceptibility to infection. In light of the above, numerous research findings recommended that children under 12 years of age should not use mobile phones at all.

2.2.2 Dosimetric Parameters at the Exposure for Mobile Phone Radiation

Electromagnetic dosimetry is the science of predicting the dose of the electromagnetic field present at any point inside or outside the body. It is used to determine the amount of power, fields, and current occurring in various parts of the body from different field exposures. Determining if they are safe or not requires an

understanding of the biological effects of these fields. For instance, it is used to predict the strength of fields in the head from cell phones to determine if a particular design meets regulatory guidelines. Dosimetry consists of two main parts: first, the incident E and H fields must be defined; second, the E and H fields inside the tissues must be determined. The relationship between the incident EM fields and the internal EM fields is a function of the frequency of the incident fields and the electromagnetic properties of the body. However, the relationship between the incident fields and the internal fields is very complicated (Gandhi, and Lazzi, 1996).

These effects have been used to define allowable guidelines or regulations for electromagnetic field exposure. In addition, the allowable exposure strengths and the allowed frequencies are generally specified in the guidelines. Limits on whole body absorbed power (as defined by SAR) were established by the Institute of Electrical and Electronics Engineers (IEEE C95.1) in 1991 and adopted by the American National Standards Institute (ANSI) in 1992 (Nicolas, and Lautru, 2001). The most important parameters are:

1) Specific Absorption Rate (SAR)

The specific absorption rate is defined as the dissipated power divided by the mass of the object. It is the unit of measurement of the amount of RF energy absorbed by the body when using a mobile phone. Its unit is watts per kilogram (W/kg) (Z. El Dein, and Amr, 2010).

SAR is the basic parameter that institutions take into consideration for the evaluation of the exposure hazards in the RF and microwave range. The word “Specific” refers to the normalization to mass, and the term “absorption rate” refers to the rate of energy absorbed by the object.

SAR is determined at the highest certified power level in laboratory conditions. However, the actual SAR level of the phone while operating can be below this value. This is because the phone is designed to use the minimum power required to reach the network (Paker, 1998).

The Specific Absorption Rate (SAR) maximum levels for modern handset is set to 1.6 W/kg averaged over 1 g of body tissue, or 2 W/kg averaged over 10 g of body tissue, in USA and Europe, respectively. If the SAR level is above the limit, it may cause both thermal and non-thermal effects on the body, especially on the ear and head since these body parts are at the "near Field" of the radiation (Tan, 2012).

SAR is measured using the following formula (Rahman, 2013):

$$\mathrm{SAR} = \frac{\sigma|\mathrm{E}|^2}{2\rho}\,[\mathrm{W/Kg}] \qquad (2.1)$$

Where:

σ: conductivity of the tissue [S/m], E: is the root mean square (r.m.s) value of the electric field strength [v/m], and ρ: density of the tissue [Kg/m^3]. SAR is calculated as a function of position from the estimates of local fields and tissues properties. An integral of SAR over a volume of tissue containing a given mass gives the absorbed power. This is typically expressed in units of mW/cm^3 (for a given tissue density) averaged over 1g.

Since it is very difficult to quantify the SAR directly in the living human body, the 20osimetry is compelled to rely mainly on a computer simulation with high-resolution numerical human models. Many techniques have been developed to simulate all these situations.

2) Power Density

Power density is defined as the amount of power per unit area in a radiated microwave field or other type of electromagnetic field (Stewart, 2007). Power density is measured using the following formula (Sabbah, 2010).

$$\mathrm{P} = \frac{\sigma|\mathrm{E}|^2}{2} = \rho\ \mathrm{SAR}\ [\mathrm{W/m^3}] \qquad (2.2)$$

2.3 Finite-Difference Time-Domain (FDTD)

The Finite-Difference Time-Domain method (FDTD) is numerical analysis technique used for modeling computational electrodynamics. FDTD solutions can cover a wide frequency range with a single simulation run (Chen, 2010). It is today's one of the most popular techniques for the solution of electromagnetic problems. It has been successfully applied to an extremely wide variety of problems, such as scattering from metal objects and dielectrics, radar signature technology, antennas, wireless communications devices, digital interconnects, biomedical imaging/ treatment, microstrip circuits, and electromagnetic absorption in the human body exposed to radiation. The main reason of the success of the FDTD method resides in the fact that the method itself is extremely simple (Umashankar, and Taflove, 1982; Taflove, 2016).

The FDTD method belongs to the general class of grid-based differential numerical modeling methods (finite difference methods). The time-dependent Maxwell's equations (in partial differential form) are discretized using central-difference approximations to the space and time partial derivatives. The resulting finite-difference equations are solved in either software program: the electric field vector components in a volume of space are solved at a given instant in time. Then, the magnetic field vector components in the same spatial volume are solved at the next instant in time; and the process is done repeatedly until the desired transient or steady-state electromagnetic field behavior is fully evolved (Wikipedia, 2016, c; "Computational electromagnetic," 2016; Taflove, 1980).

When Maxwell's differential equations are examined, the change in the E-field in time (the time derivative) is dependent on the change in the H-field across space (the curl). This results in the basic FDTD time-stepping relation. In which, at any point in space, the updated value of the E-field in time is dependent on the stored value of the E-field and the numerical curl of the local distribution of the H-field in space (Taflove, and Brodwin, 1975). The H-field is time-stepped in a similar manner. At any point in space, the updated value of the H-field in time is dependent on the stored value of the H-field and the numerical curl of the local distribution of the E-field in

space. Iterating the E-field and H-field updates results in a marching-in-time process wherein sampled-data analogs of the continuous electromagnetic waves under consideration propagate in a numerical grid stored in the computer memory (Smitha, and Narayanan, 2016; Umran, and Robert, 2011).

So, to implement an FDTD solution of Maxwell's equations, first a computational domain must be established. The computational domain is simply the physical region over which the simulation will be performed. The E and H fields are determined at every point in space within that computational domain. The material of each cell within the computational domain must be specified. Typically, the material is either free-space (air), metal, or dielectric. Any material can be used as long as the permeability, permittivity, and conductivity are specified (Kunz, and Luebbers, 1993; Elsherbeni, and Demir, 2009). Second, a source is specified; the source can be a current on a wire, applied electric field or impinging plane wave (Wikipedia, 2016, c; Kunz, and Luebbers, 1993; Elsherbeni, and Demir, 2009).

2.4 The FDTD Yee Algorithm for Maxwell's Equations

The Yee Algorithm simultaneously deals with both electric and magnetic fields in time and space using the coupled form of Maxwell's curl equations, rather than solving the wave equation for either the electric field or the magnetic field alone (Schneider, 2016).

2.4.1 Maxwell's Equations

Maxwell's equations represent one of the most elegant and concise ways to state the fundamentals of electricity and magnetism. Where James Clark Maxwell published the famous Maxwell's equations, which mathematically describe the interdependence of the electric field and the magnetic field. Maxwell suggested the existence of electromagnetic waves, which were discovered later by other scientists. Differential form of time-dependent Maxwell's equations (Sullivan, 2000; Taflove, and Hagness, 2000):

$$\nabla \times \mathbf{E} = -\frac{\partial \mathbf{B}}{\partial \mathrm{t}} \qquad \text{Faraday's Law} \qquad (2.3)$$

$$\nabla \times \mathbf{H} = \frac{\partial \mathbf{D}}{\partial t} + \mathbf{J} \qquad \text{Ampere's law} \qquad (2.4)$$

$$\nabla \cdot \mathbf{D} = \rho \qquad \text{Gauss's law} \qquad (2.5)$$

$$\nabla \cdot \mathbf{B} = 0 \qquad \text{No magnetic monopoles} \qquad (2.6)$$

where, **E** is electric field intensity (V/m), **H** is magnetic field intensity (A/m), **D** is electric flux density (C/m^2), **B** is magnetic flux density (Wb/m^2), $\mathbf{J} = \sigma\mathbf{E}$ is electric current density (A/m^2), σ is electrical conductivity in (S/m), which represents conducting properties of material, and ρ is total electric charge density (C/m^3).

The above Maxwell's equations (2.3 – 2.6) form the basis of Yee's FDTD scheme. There are a number of finite-difference schemes for Maxwell's equations, but the Yee scheme persists as it is very robust and versatile (Kunz, and Luebbers, 1993; Elsherbeni, and Demir, 2009).

The flux densities and the field intensities are related through the constitutive relations. For linear, isotropic media, these are:

$$\mathbf{D} = \varepsilon\mathbf{E} = \varepsilon_\circ\varepsilon_r\mathbf{E} \qquad (2.7)$$

$$\mathbf{B} = \mu\mathbf{H} = \mu_\circ\mu_r\mathbf{H} \qquad (2.8)$$

Where ε_o is the free-space permittivity (8.854×10^{-12} f/m), ε_r is the relative permittivity, and ε is the permittivity (f/m) of the media. Similarly, μ_o is the free-space permeability ($4\pi \times 10^{-7}$ H/m), μ_r is the relative permeability, and μ is the permeability (H/m) of the media. In general, μ_r and ε_r are frequency dependent.

Maxwell's Curl Equations in the one Dimensional Cartesian Coordinates

Substituting Eq. (2.7) and Eq. (2.8) into Eq. (2.3) and Eq. (2.4), we obtain the Maxwell's curl equations involving E and H for any linear, isotropic, media with material constants ε, μ and σ, are given as:

$$\nabla \times \mathbf{E} = -\mu\frac{\partial \mathbf{H}}{\partial t} \qquad (2.9)$$

$$\nabla \times \mathbf{H} = \varepsilon_{\circ}\varepsilon_{r}\frac{\partial \mathbf{E}}{\partial t} + \sigma \mathbf{E} \tag{2.10}$$

E and **H** are vectors in three dimensions. Expansion of the vector components of the curl operators of Eq. (2.9) and Eq. (2.10) yields, so Eq. (2.3) and Eq. (2.4) each one gives them three coupled scalar equations under a Cartesian coordinate, as follows:

For Eq. (2.9)

$$\begin{vmatrix} \hat{x} & \hat{y} & \hat{z} \\ \dfrac{\partial}{\partial x} & \dfrac{\partial}{\partial y} & \dfrac{\partial}{\partial z} \\ E_x & E_y & E_z \end{vmatrix} = -\mu\frac{\partial \mathbf{H}}{\partial t}$$

$$\left[\left(\frac{\partial E_z}{\partial y} - \frac{\partial E_y}{\partial z}\right)\hat{x} + \left(\frac{\partial E_x}{\partial z} - \frac{\partial E_z}{\partial x}\right)\hat{y} + \left(\frac{\partial E_y}{\partial x} - \frac{\partial E_x}{\partial y}\right)\hat{z}\right] = -\mu\left(\frac{\partial H_x}{\partial t}\hat{x} + \frac{\partial H_y}{\partial t}\hat{y} + \frac{\partial H_z}{\partial t}\hat{z}\right)$$

Equating the vector components, we obtain:

$$\frac{\partial H_x}{\partial t} = \frac{1}{\mu}\left(\frac{\partial E_y}{\partial z} - \frac{\partial E_z}{\partial y}\right) \tag{2.11}$$

$$\frac{\partial H_y}{\partial t} = \frac{1}{\mu}\left(\frac{\partial E_z}{\partial x} - \frac{\partial E_x}{\partial z}\right) \tag{2.12}$$

$$\frac{\partial H_z}{\partial t} = \frac{1}{\mu}\left(\frac{\partial E_x}{\partial y} - \frac{\partial E_y}{\partial x}\right) \tag{2.13}$$

Also, for Eq. (2.10)

$$\begin{vmatrix} \hat{x} & \hat{y} & \hat{z} \\ \dfrac{\partial}{\partial x} & \dfrac{\partial}{\partial y} & \dfrac{\partial}{\partial z} \\ H_x & H_y & H_z \end{vmatrix} = \varepsilon_{\circ}\varepsilon_{r}\frac{\partial \mathbf{E}}{\partial t} + \sigma \mathbf{E}$$

$$\left[\left(\frac{\partial H_z}{\partial y}-\frac{\partial H_y}{\partial z}\right)\hat{x}+\left(\frac{\partial H_x}{\partial z}-\frac{\partial H_z}{\partial x}\right)\hat{y}+\left(\frac{\partial H_y}{\partial x}-\frac{\partial H_x}{\partial y}\right)\hat{z}\right]$$
$$=\varepsilon_\circ\varepsilon_r\left(\frac{\partial E_x}{\partial t}\hat{x}+\frac{\partial E_y}{\partial t}\hat{y}+\frac{\partial E_z}{\partial t}\hat{z}\right)+\sigma\left(E_x\hat{x}+E_y\hat{y}+E_z\hat{z}\right)$$

We obtain three more equations,

$$\frac{\partial E_x}{\partial t}=\frac{1}{\varepsilon_\circ\varepsilon_r}\left(\frac{\partial H_z}{\partial y}-\frac{\partial H_y}{\partial z}-\sigma E_x\right) \tag{2.14}$$

$$\frac{\partial E_y}{\partial t}=\frac{1}{\varepsilon_\circ\varepsilon_r}\left(\frac{\partial H_x}{\partial z}-\frac{\partial H_z}{\partial x}-\sigma E_y\right) \tag{2.15}$$

$$\frac{\partial E_z}{\partial t}=\frac{1}{\varepsilon_\circ\varepsilon_r}\left(\frac{\partial H_y}{\partial x}-\frac{\partial H_x}{\partial y}-\sigma E_z\right) \tag{2.16}$$

We assume that ε and μ are not time-dependent. The system of six coupled partial differential equations (2.11)–(2.16) forms the basis of the FDTD numerical algorithm for modeling electromagnetic wave interactions with arbitrary three-dimensional objects.

Yee's FDTD scheme discretizes Maxwell's curl equations by approximating the time and space first-order partial derivatives with central differences, and then solving the resulting equations by using a leapfrog scheme.

2.4.2 The Yee Algorithm

In 1966, Kane S. Yee derived an elegant, yet simple, time-dependent solution of Maxwell's equations based on their differential form using central difference approximations of both the space and the time-derivatives (Balanis, 2011; Yee, 1966). The formulation is based on discretizing the volume domain with a regular, structured, staggered, rectangular grid. Similar to the one-dimensional transmission-line equations, Yee discovered that in order to maintain second-order accuracy of the central difference operators, the electric and magnetic fields must be staggered in both space and time (Rao, 2004).

The Yee's algorithm positions its **E** and **H** components at the centers of the grid lines and surfaces such that each **E** component is surrounded by four **H** components, and vice versa. This provides an elegant yet simple picture of three-dimensional space being filled by interlinked arrays of Faraday's law and Ampere's law contours. Thus, it is possible to identify the **E** components associated with the displacement current flux linking with the **H** loops and, correspondingly, the **H** components associated with the magnetic flux are linked with the **E** loops, as shown in Figure (2.2) (Rhattoy, Lahmer, and Zatni, 2010; Kawano, and Kitoh, 2001).

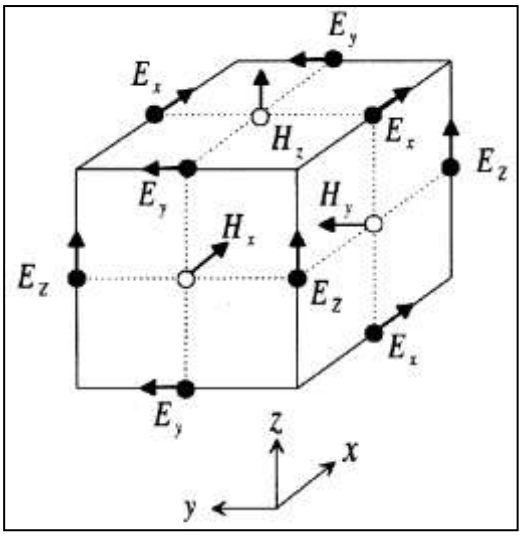

Figure (2.2): Positions of the field components in a unit cell of the Yee's lattice (Kawano, and Kitoh, 2001).

Considering a uniformly spaced rectangular grid in three-dimensions, each grid cell has dimensions Δx , Δy, and Δz along each Cartesian axis. The coordinate of a node of the grid can be expressed in discrete form as:

$$(x, y, z)_{i,j,k} = (i\Delta x\,, j\Delta y, k\,\Delta z\,) \tag{2.17}$$

Similarly, time is uniformly discretized as $t = n\Delta t$, where Δx, Δy, Δz are respectively the lattice space increments in the x, y, and z-axes, Δt is the time increment, and j, k, n, and I are integers. We denote any function F of space and time evaluated at a discrete point in time as (Chu, and Chaudhuri, 1995):

$$F\,(x, y, z, t) = F(i\Delta x\,, j\Delta y, k\,\Delta z, n\Delta t\,) = F^{\,n}{}_{i,j,k} \tag{2.18}$$

2.4.3 Finite Difference Approximations

Finite difference approximations are used to solve the above-mentioned partial differential equations. For higher accuracy, represent the derivatives in Maxwell's curl equations by finite differences. Using central finite difference approximation (central-difference) expressions for the space and time derivatives that are both simply programmed and second-order accurate in the space and time increments, it becomes (Jurgens, Taftove, Umashanker, and Moore, 1992; Millgan, 2011):

$$\frac{\partial F^n(i,j,k)}{\partial x} = \frac{F^n(i+1/2,j,k) - F^n(i-1/2,j,k)}{\Delta x} + O[(\Delta x)^2] \qquad (2.19)$$

Partial derivative of F is expressed for the first time, being evaluated at the fixed space point (i, j, k), as by analogy follows:

$$\frac{\partial F^n(i,j,k)}{\partial t} = \frac{F^{n+1/2}(i,j,k) - F^{n-1/2}(i,j,k)}{\Delta t} + O[(\Delta t)^2] \qquad (2.20)$$

Now, $\pm 1/2$ the increment is in the n superscript (time coordinate) of F, denoting a time finite-difference over $\pm 1/2\,\Delta t$. Yee chose this notation because he wished to interleave his **E** and **H** components in time at intervals of $\pm 1/2\,\Delta t$ for purposes of implementing a leapfrog algorithm. FDTD is implemented by discretizing the space into a number of cells. Discretization means that both **E** and **H** should be determined only at discrete spatial locations (x_i, y_i, z_i) where i is the i^{th} cell in the spatial lattice.

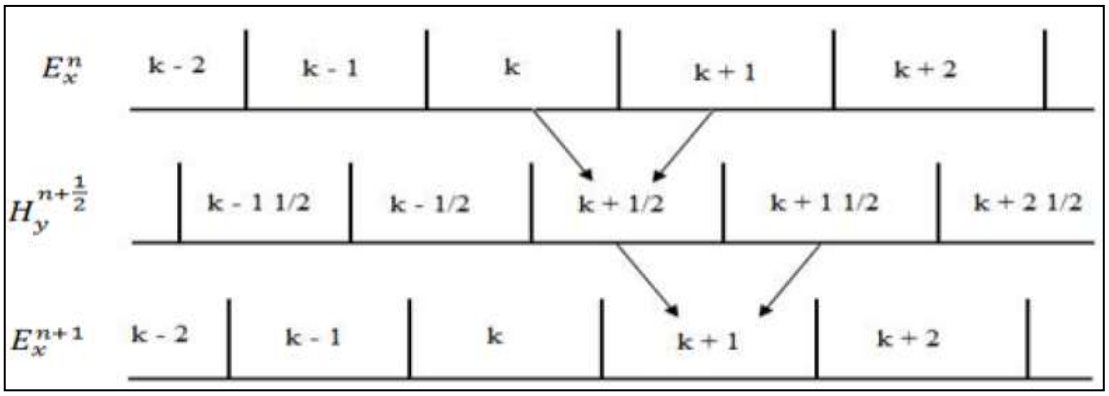

Figure (2.3): Interleaving of the E and H fields in space and time in FDTD formulation (Sullivan, 2000).

As shown in Figure 2.3, both E and H are interleaved such that their components positions satisfy the differential form of Maxwell's equations. Also, both the E and H field components are off by half a time step leading to a leap-frog scheme. Therefore, the electric field components are calculated at integer time steps, and magnetic field components are calculated at half-integer time steps, and they are offset from each other by $\frac{\Delta t}{2}$ as shown in Figure (2.3) (Sullivan, 2000).

Chapter Three

Simulation of Dipole Antenna with 900MHz and 1800MHz by HFSS

Chapter Three
Simulation of Dipole Antenna with 900MHz and 1800MHz by HFSS

Introduction

Half-wave dipole is the most common antenna. It is a two-wire antenna with copper or aluminum being straight, where they feed each of the parties by a double cable so that the length of the wire is equal to 1/4 wavelength. The length of the two-wire is equal to 1/2 wavelength which leads to the best reception and sending largest energy of signal, where wavelength λ is equal to the speed of light over the center frequency. The antenna is a means to operate at the range of frequency in which half-wave dipole operates at around 3 KHz to 300GHz. This antenna is used in all transmitters that are broadcast in all directions parallel to the surface of the ground or in the receptors that pick up signals from all directions (Bath, Thakur, Sharma, and Prasad, 2014; Tawde, 2015; Parameswari, and Kumar, 2015). The applications of half-wave dipole antenna include the devices to send and receive radio and television broadcasting, cellular phones, and products for enterprises, homes, and office modems (Hallas, (n.d.); Huang, and Boyle, 2008; James, 1991).

The planar dipole antenna is very useful in antenna applications because of its ease of fabrication and better compactness. In recent years, planar dipole antennas have been widely used for various communication systems due to good omni-directional coverage and stable radiation performance. In order to meet more real applications, there are several design challenges for dipole antennas، such as compact size, multiband operation and easy fabrication (Orugu, Srinivas, Raju, Krishna, and Babu, 2013). In the current study, the researcher designed a new half wave dipole antenna and planar dipole antenna using the HFSS (high-frequency structural simulator). A software is used for the simulation and calculations of the dipole antennas. The return loss, VSWR, directivity, gain, and radiation pattern are evaluated.

3.1 Design and Model of Dipole Antenna

The half wavelength dipole antenna (wire antenna) operating at 0.9 GHz and 1.8GHz can be modeled in HFSS as two cylinders separated by a small gap as shown in Fig. (3.1).

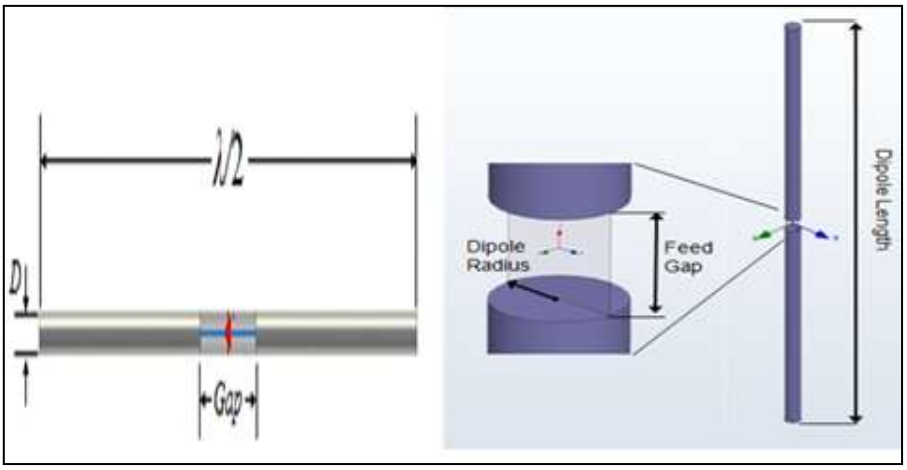

Figure (3.1): The half wave dipole antenna (wire antenna).

Dimensions of the antenna changes are based on the resonant frequency, as a resonant frequency 0.9GHz and 1.8GHz has been chosen. The parameters used in the final model are shown in Table (3.1), and Table (3.2).

Table (3.1): Design parameters of the half wave dipole antenna operating in 0.9GHz.

Parameter	Value	Unit
Resonant frequency(f)	0.9	GHz
Length of dipole (L)	149.99	mm
Port Impedance(Z_0)	50	Ω
Feed Gap (G)	2.5	mm
Radius of dipole(R)	2.5	mm

Table (3.2): Design parameters of the half wave dipole antenna operating in 1.8GHz.

Parameter	Value	Unit
Resonant frequency(f)	1.8	GHz
Length of dipole (L)	74.99	mm
Port Impedance(Z_0)	50	Ω
Feed Gap (G)	1.25	mm
Radius of dipole(R)	1.25	mm

The planar dipole antenna operating at 0.9 GHz and 1.8GHz can be modeled in HFSS as shown in Fig. (3.2).

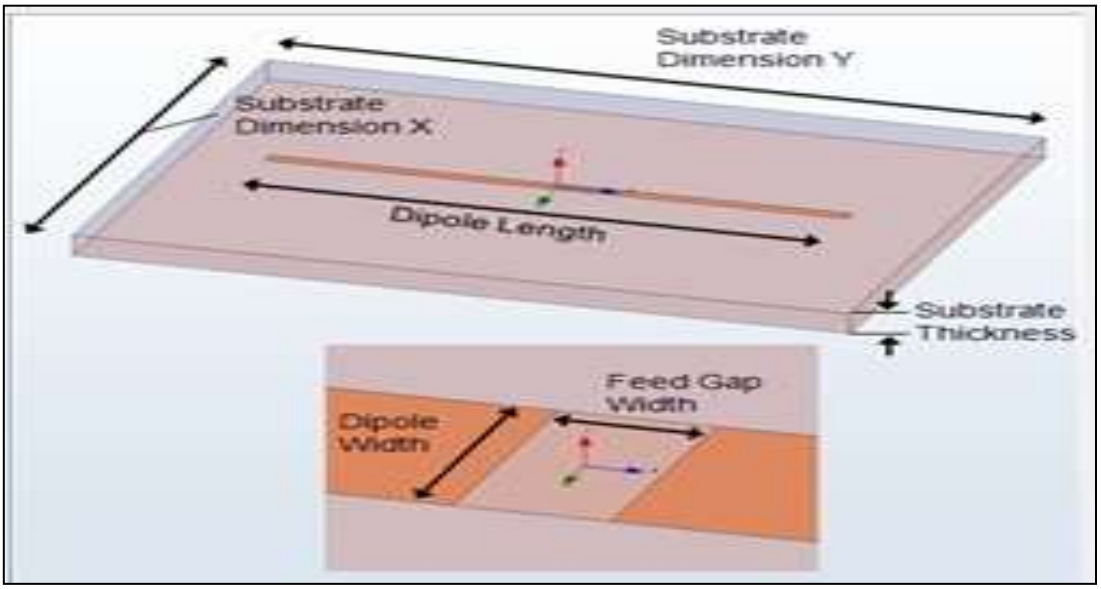

Figure (3.2): The planar dipole antenna.

Dimension of an antenna changes according to the resonant frequency, as a resonant frequency 0.9GHz and 1.8GHz has been chosen. The parameters used in the final model are shown in Table (3.3), and Table (3.4).

Table (3.3): Design parameters of the planar dipole antenna operating in 0.9GHz.

Parameter	Value	Unit
Resonant frequency(f)	0.9	GHz
Length of dipole	141.17	mm
Width of dipole	3.53	mm
Port Impedance(Z_0)	50	Ω
Feed Gap Length (G)	3.53	mm
Substrate thickness	62	mil
Substrate Dimension Along x	211.8	mm
Substrate Dimension Along y	282.3	mm

Table (3.4): Design parameters of the planar dipole antenna operating in 1.8 GHz.

Parameter	Value	Unit
Resonant frequency(f)	1.8	GHz
Length of dipole	68.18	mm
Width of dipole	1.7	mm
Port Impedance(Z_0)	50	Ω
Feed Gap Length (G)	1.7	mm
Substrate thickness	62	mil
Substrate Dimension Along x	102.3	mm
Substrate Dimension Along y	136.4	mm

3.2 Simulation Technique

A half wavelength dipole antenna (wire antenna) and planar dipole antenna operating at 0.9 GHz and 1.8 GHz are designed and simulated by using HFSS. Ansoft HFSS was used for the simulation and calculations of the dipole antennas. Tables (3.1), (3.2), (3.3), and (3.4) show the different input antenna dimensions and other parameters, whereas Figure (3.3) shows the view of designed half-wave dipole antenna and planar dipole antenna that operated at 0.9 GHz in HFSS simulator. In addition, figure (3.4) shows the view of designed half-wave dipole antenna and planar dipole antenna that operate at 1.8 GHz in HFSS simulator.

The designed antenna is characterized by measuring return loss, VSWR, radiation pattern, directivity, and gain. Moreover, figures (3.5) to (3.20) show the different output parameters after simulating in HFSS.

3.3 Results and Discussion

The half dipole antenna (wire antenna) and planar dipole antenna are simulated in high frequency structure simulator (HFSS). The simulation model is given in Figures (3.3-3.4). As shown in the Figure (3.3 a) and Figure (3.4 a), the proposed antenna consists of a two-cylinder radiator with a rectangular lumped port excitation between each arm of dipole to provide an RF excitation to antenna element. The structure is

then covered by a vacuum box to allow radiation of fields, radiating boundary condition will be applied to outer surface to act as infinite free space. Further, the faces of the vacuum box are individually selected for assigning the radiation boundary. After the simulation, the measured and simulated characteristics of the antenna are shown. From the far field report, the 3D polar plot is drawn. The numerical and experimental results regarding the radiation characteristics are presented and discussed.

Figures (3.5-3.6) show comparison of return loss curves for half dipole antenna (wire antenna) and planar dipole antenna at 900MHz and 1800MHz. From this analysis, the researcher noticed the operating frequency and return loss values for planar dipole antenna at 900MHz as shown in Fig. (3.5 b). Both parameters are lower than that for half dipole antenna at 900MHz as shown by Fig. (3.5 a). Fig. (3.6 a) illustrates that operating frequency and return loss values for planar dipole antenna are lower than that for half dipole antenna at 1800MHz.

The measured Voltage Standing Wave Ratio (VSWR) of the simulated antenna is given in Figures (3.7-3.8). Figures (3.9-3.12) show the comparison of smith chart for input impedance and polar plot for input impedance for the proposed antennas.

Figures (3.13-3.14) show the comparative analysis of rETotal in 3D for proposed antennas and the maximum values of rETotal are 9961.83mV, 10117mV, 1003.2mV, and 10065mV for half dipole antenna (wire antenna) and planar dipole antenna at 900MHz and 1800MHz respectively.

In figures (3.15-3.16), the 3D simulation of the radiation pattern of the antenna is noted. The researcher noticed that the dipoles have a radiation pattern, shaped like a toroids (doughnut) symmetrical about the axis of the dipole. The pattern shows that the antennas have omni-directional pattern. Red colored side shows highest gain part of a radiation pattern. In 3D pattern, both positive and negative are shown in same axis. Yellow colored side describes average gain pattern of dipole antenna, and blue colored shows the lowest gain part of a radiation pattern.

Figures (3.17-3.18) show the comparitive analysis of directivity in 3D for proposed antennas, and the maximum values of directivity are 2.3496dB, 2.3381dB, 2.3787dB, and 2.2937dB for half dipole antenna (wire antenna) and planar dipole antenna at 900MHz and 1800MHz respectively. Also, figures (3.19-3.20) show Radiation

pattern for half dipole antenna (wire antenna) and planar dipole antenna at 900MHz and 1800MHz.

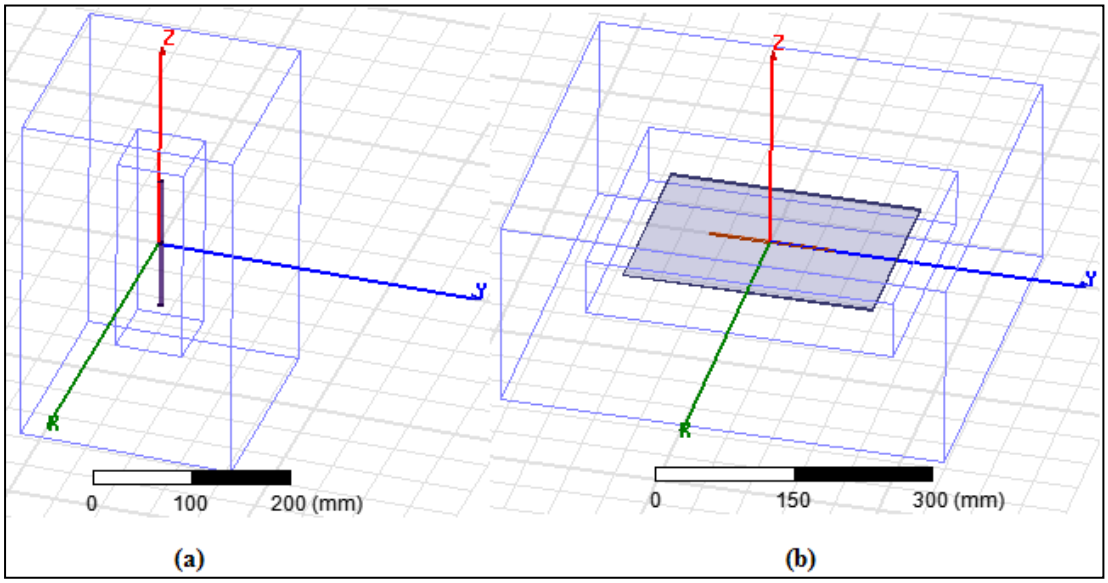

Figure (3.3): Designed antenna at 900 MHz for: (a) the half wave dipole antenna (wire antenna), (b) the planar dipole antenna.

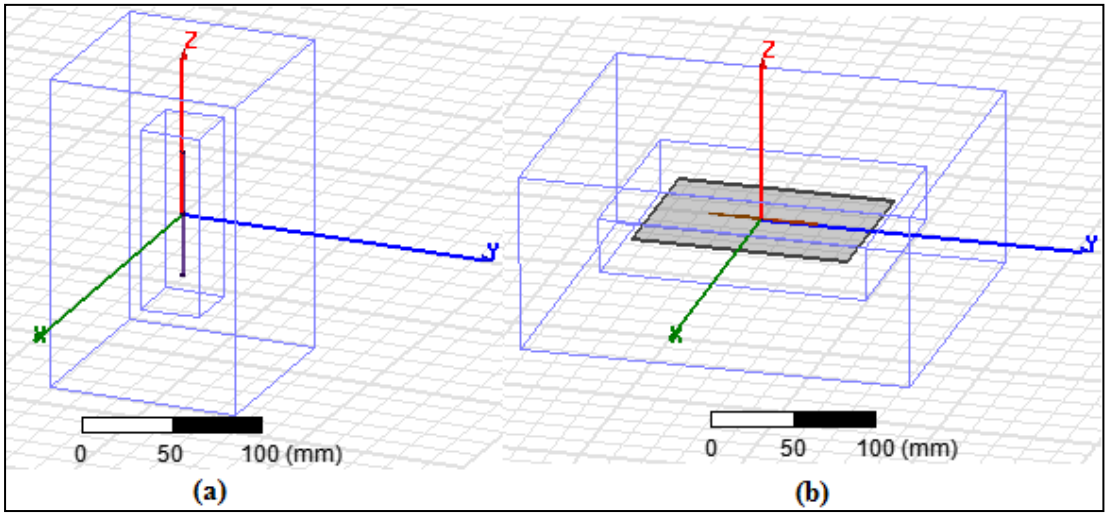

Figure (3.4): Designed antenna at 1800 MHz for: (a) the half wave dipole antenna (wire antenna), (b) the planar dipole antenna.

The plot of return loss for the above antenna is shown below:

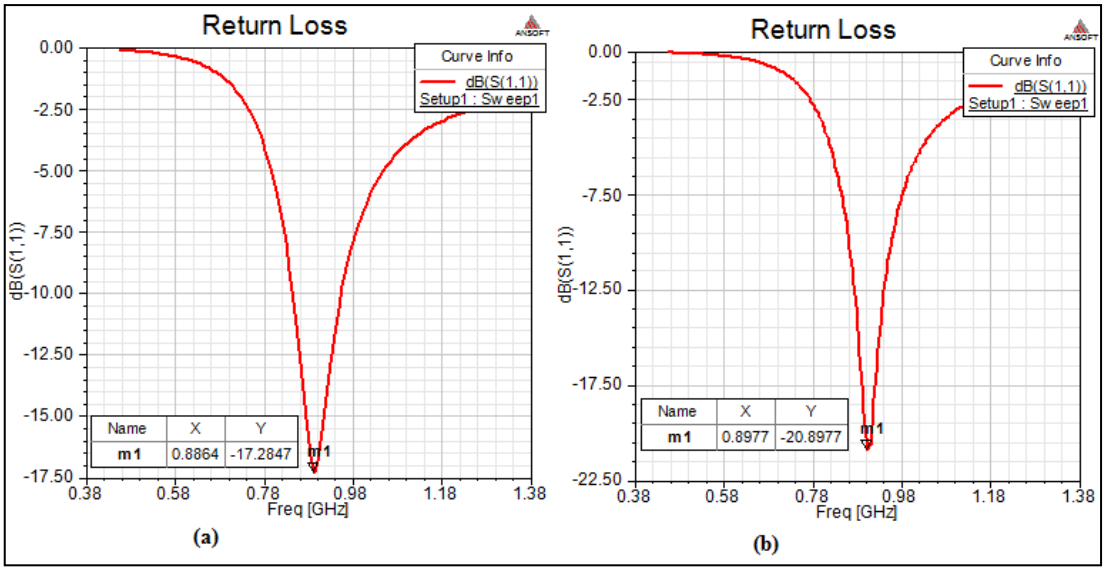

Figure (3.5): Relate Return Loss S_{11}[dB] for frequency at 900 MHz for: (a) the half wave dipole antenna (wire antenna), Return Loss: -17.28dB at 0.88 GHz Frequency, (b) the planar dipole antenna, Return Loss: -20.89dB at 0.89 GHz Frequency.

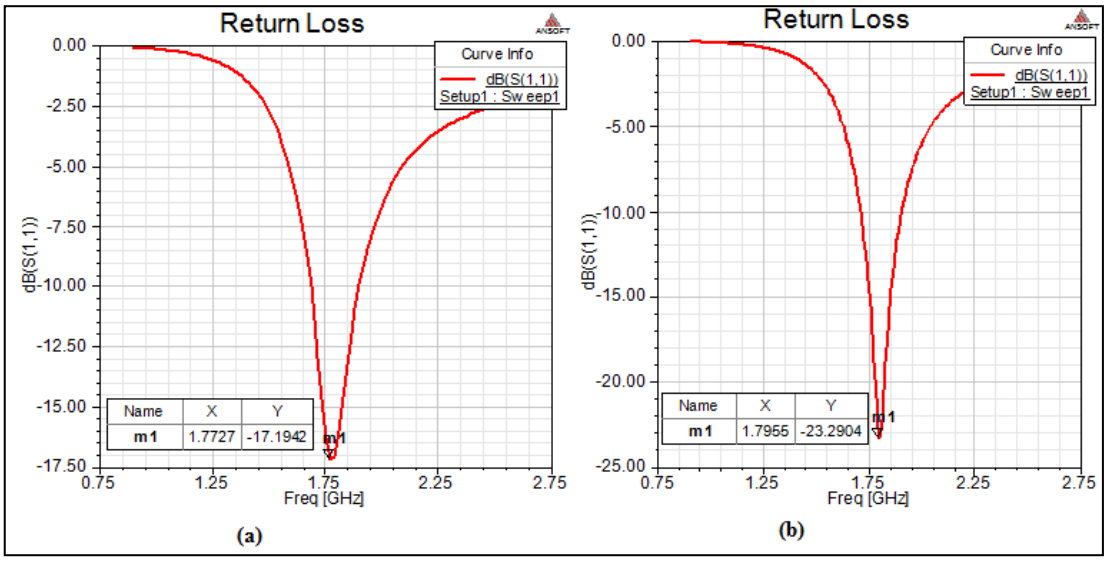

Figure (3.6): Relate Return Loss S_{11}[dB] for frequency at 1800 MHz for: (a) the half wave dipole antenna (wire antenna), Return Loss: -17.19dB at 1.77 GHz Frequency, (b) the planar dipole antenna, Return Loss: -23.29dB at 1.79 GHz Frequency.

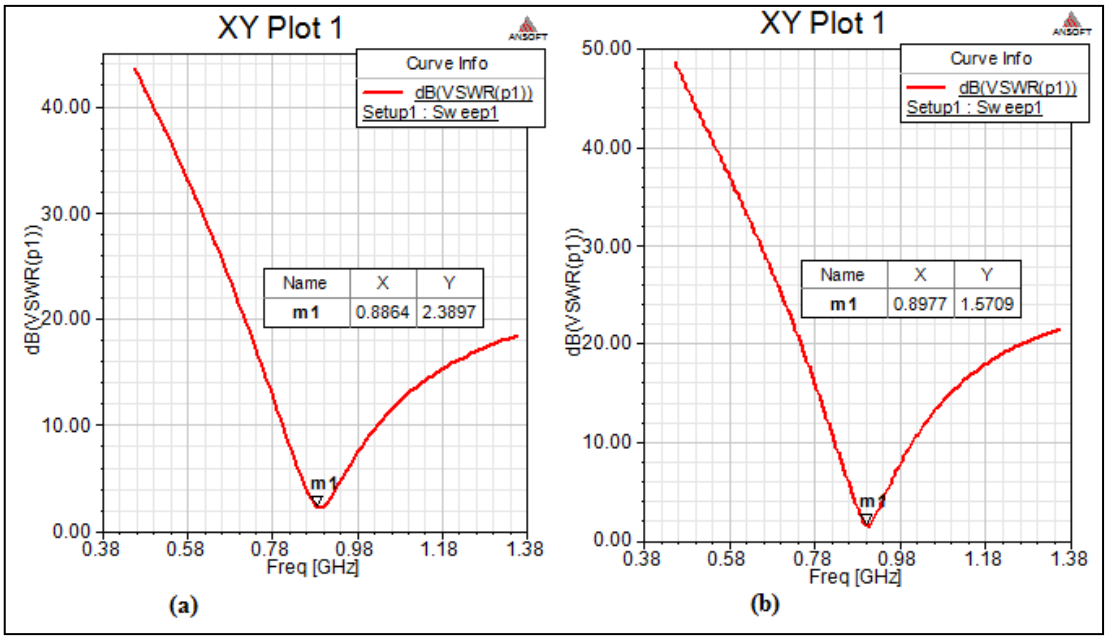

Figure (3.7): VSWP (Voltage Standing Wave Ratio) for frequency at 900 MHz for: (a) the half wave dipole antenna (wire antenna), VSWP: 2.38 at 0.88 GHz Frequency, (b) the planar dipole antenna, VSWP: 1.57 at 0.89 GHz Frequency.

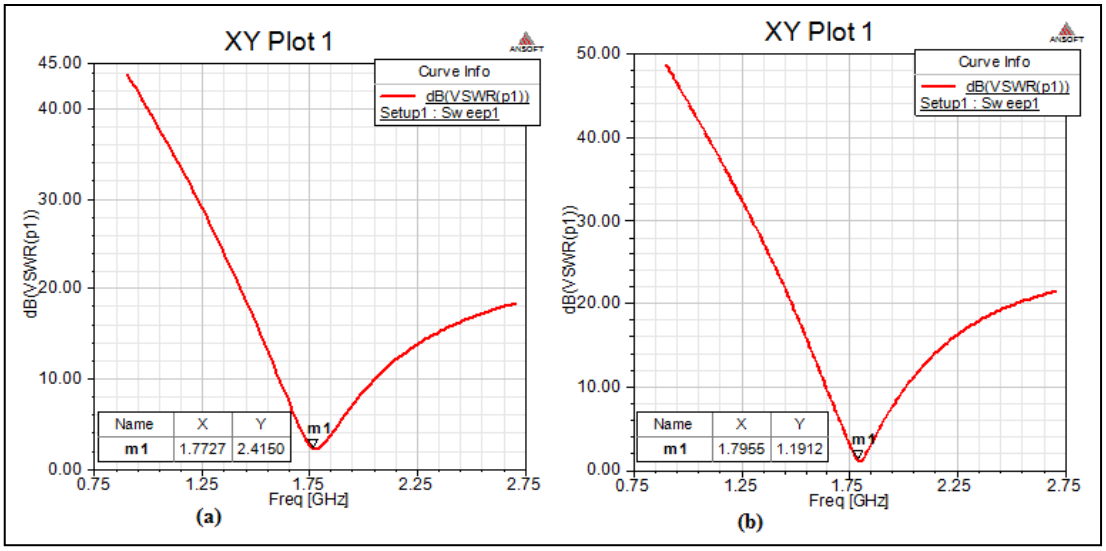

Figure (3.8): VSWP (Voltage Standing Wave Ratio) for frequency at 1800 MHz for: (a) the half wave dipole antenna (wire antenna), VSWP: 2.41 at 1.77 GHz Frequency, (b) the planar dipole antenna, VSWP: 1.19 at 1.79 GHz Frequency.

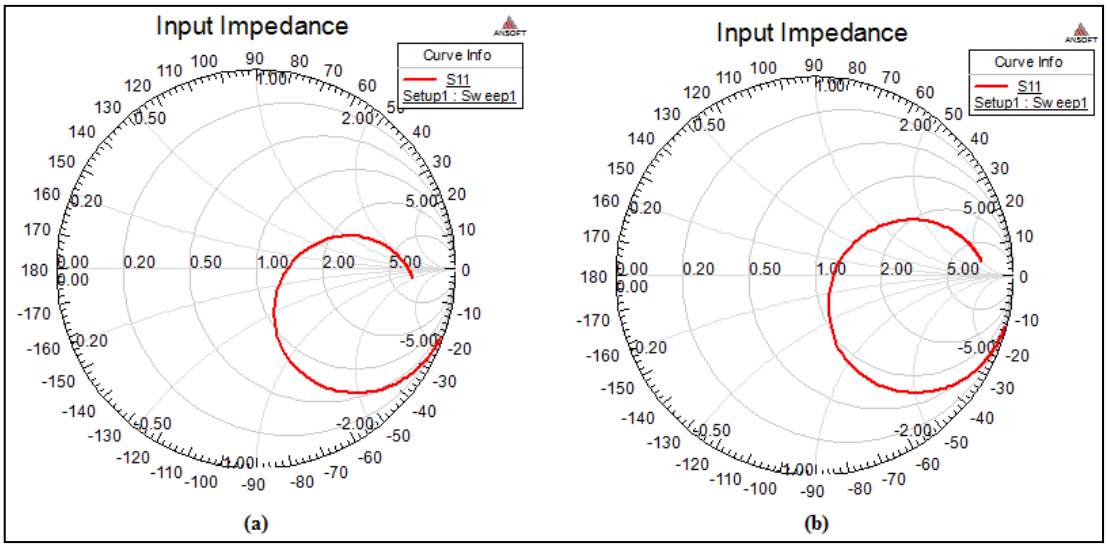

Figure (3.9): Smith chart for input impedance for frequency at 900 MHz for: (a) the half wave dipole antenna (wire antenna), (b) the planar dipole antenna.

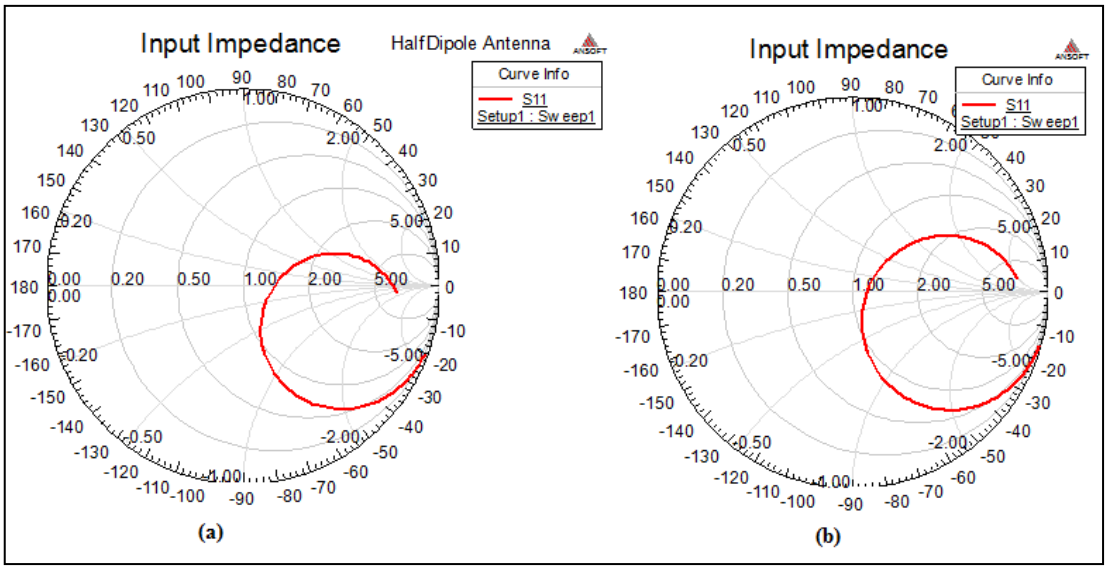

Figure (3.10): Smith chart for input impedance for frequency at 1800 MHz for: (a) the half wave dipole antenna (wire antenna), (b) the planar dipole antenna.

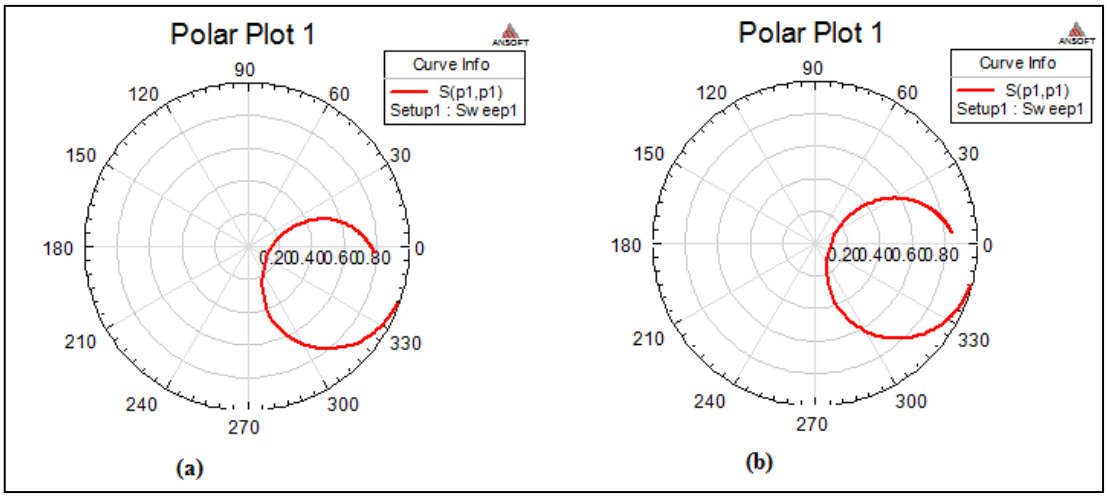

Figure (3.11): Polar Plot for input impedance for frequency at 900 MHz for: (a) the half wave dipole antenna (wire antenna), (b) the planar dipole antenna.

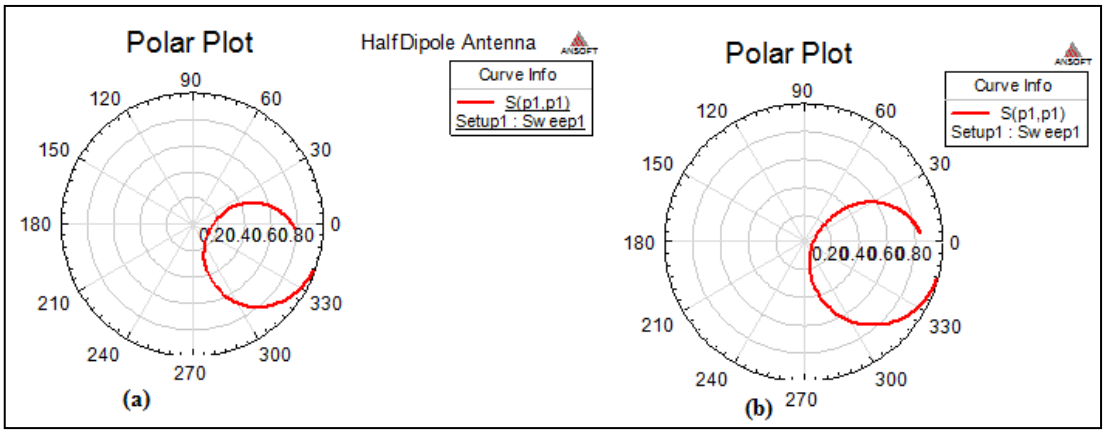

Figure (3.12): Polar Plot for input impedance for frequency at 1800 MHz for: (a) the half wave dipole antenna (wire antenna), (b) the planar dipole antenna.

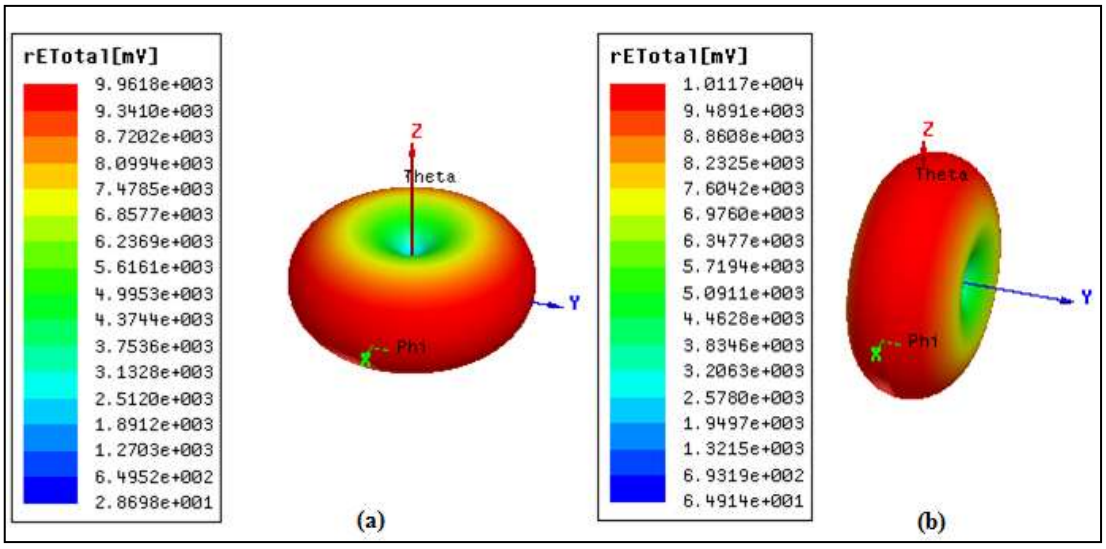

Figure (3.13): 3D Polar Plot for frequency at 900 MHz for: (a) the half wave dipole antenna (wire antenna), red area shows high rETotal and equals 9961.83mV, and blue area shows low rETotal and equals 28.6986 mV, (b) the planar dipole antenna, red area shows high rETotal and equal 10117mV, and blue area shows low rETotal and equals 64.91 mV.

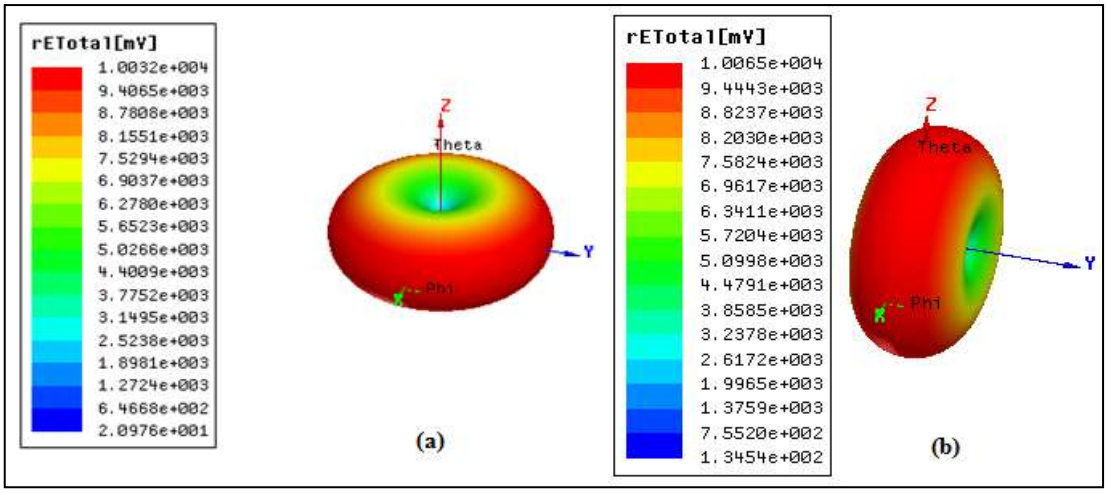

Figure (3.14): 3D Polar Plot for frequency at 1800 MHz for: (a) the half wave dipole antenna (wire antenna), red area shows high rETotal and equals 1003.2mV and blue area shows low rETotal and equals 20.976 mV, (b) the planar dipole antenna, red area shows high rETotal and equals 10065mV and blue area shows low rETotal and equals 134.54 mV.

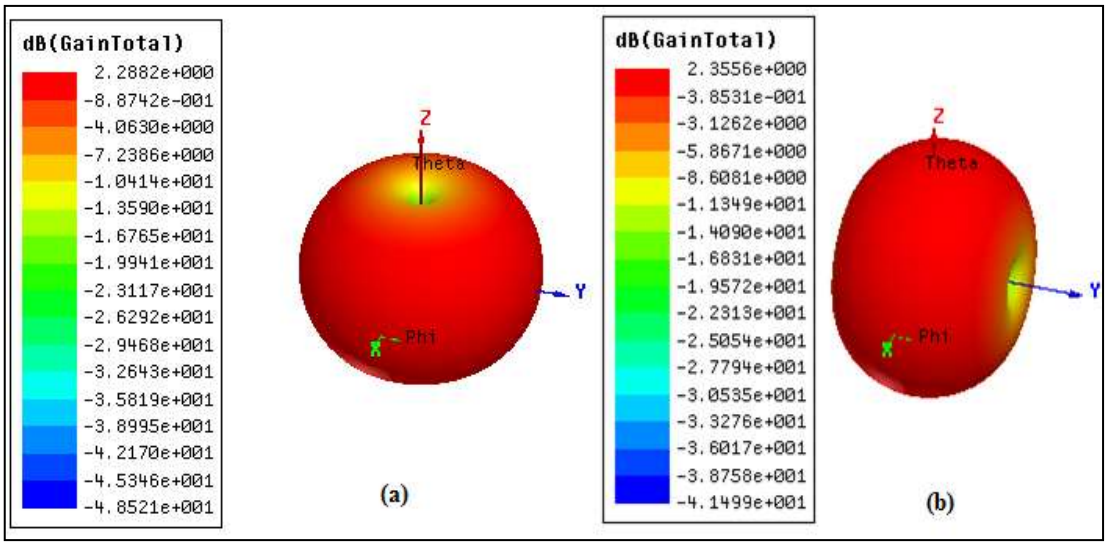

Figure (3.15): 3D Gain Plot for frequency at 900 MHz for: (a) the half wave dipole antenna (wire antenna), red area shows high gain and equals 2.2882dB and blue area shows low gain and equals -48.521dB, (b) the planar dipole antenna, red area shows high gain and equals 2.3556dB and blue area shows low gain and equals -41.499dB.

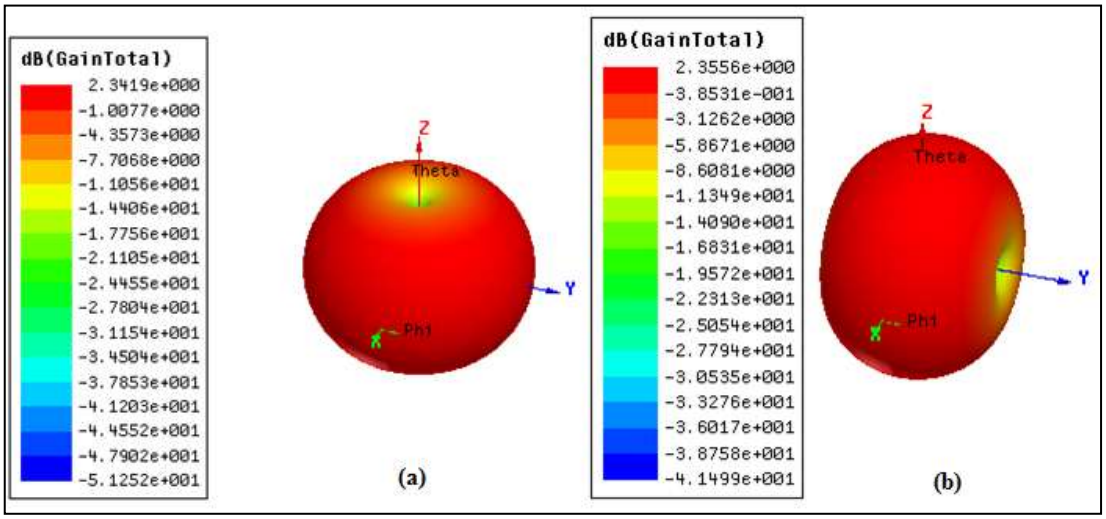

Figure (3.16): 3D Gain Plot for frequency at 1800 MHz for: (a) the half wave dipole antenna (wire antenna), red area shows high gain and equals 2.3419dB and blue area shows low gain and equals -51.252dB, (b) the planar dipole antenna, red area shows high gain and equals 2.3556dB and blue area shows low gain and equals -41.499dB.

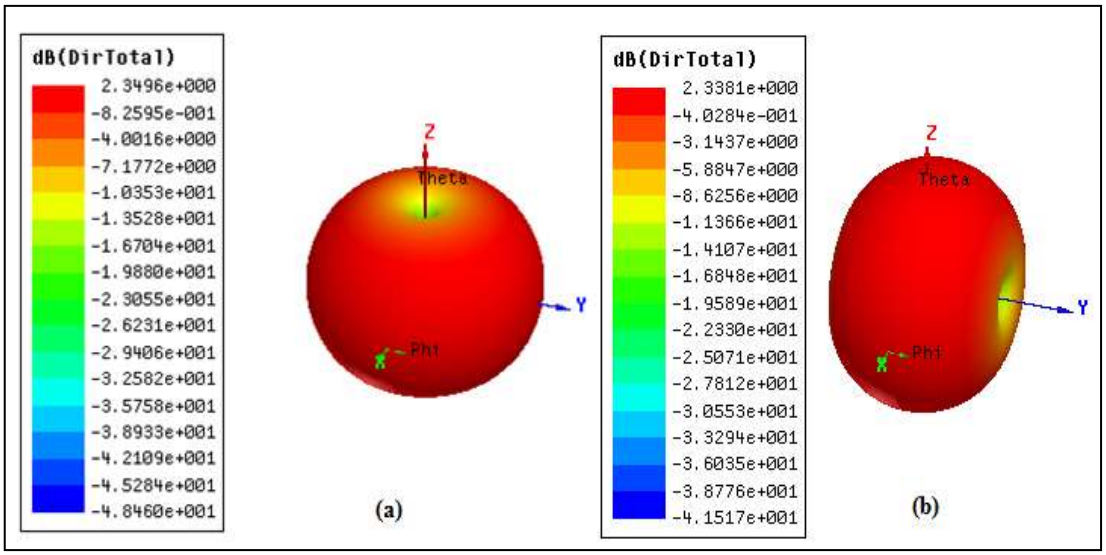

Figure (3.17): 3D Directivity Plot for frequency at 900 MHz for: (a) the half wave dipole antenna (wire antenna), red area shows high directivity and equals 2.3496dB and blue area shows low gain and equals -48.46dB, (b) the planar dipole antenna, red area shows high directivity and equals 2.3381dB and blue area shows low gain and equals -41.51dB.

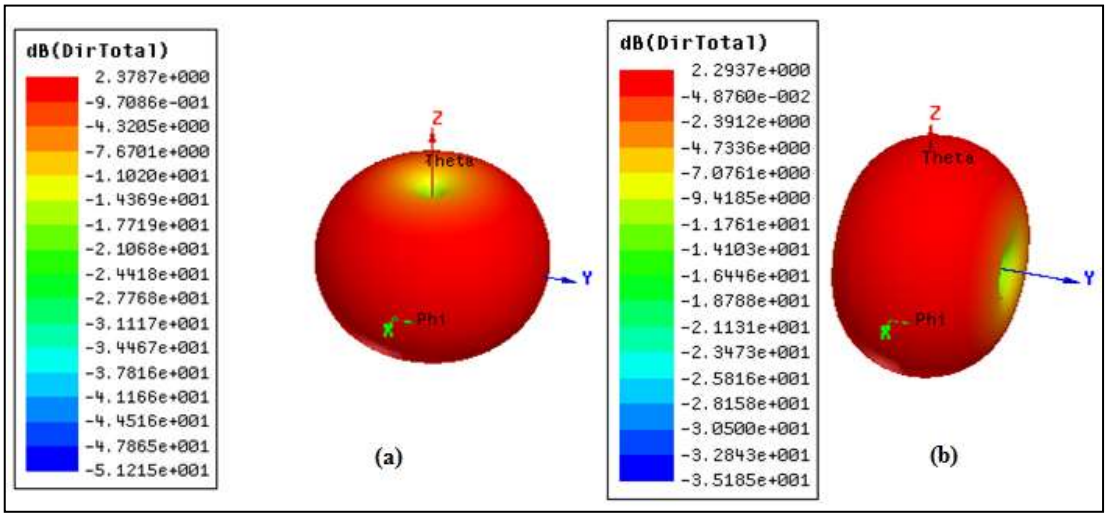

Figure (3.18): 3D Directivity Plot for frequency at 1800 MHz for: (a) the half wave dipole antenna (wire antenna), red area shows high directivity and equals 2.3787dB and blue area shows low gain and equals -51.215dB, (b) the planar dipole antenna, red area shows high directivity and equals 2.2937dB and blue area shows low gain and equals -35.185dB.

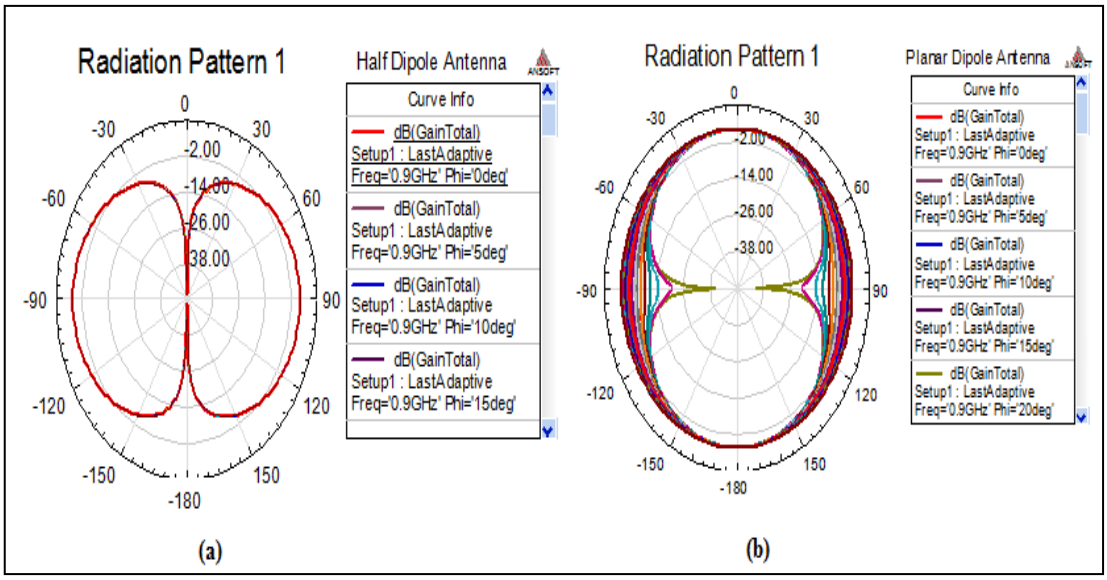

Figure (3.19): Radiation pattern for frequency at 900 MHz for: (a) the half wave dipole antenna (wire antenna), (b) the planar dipole antenna.

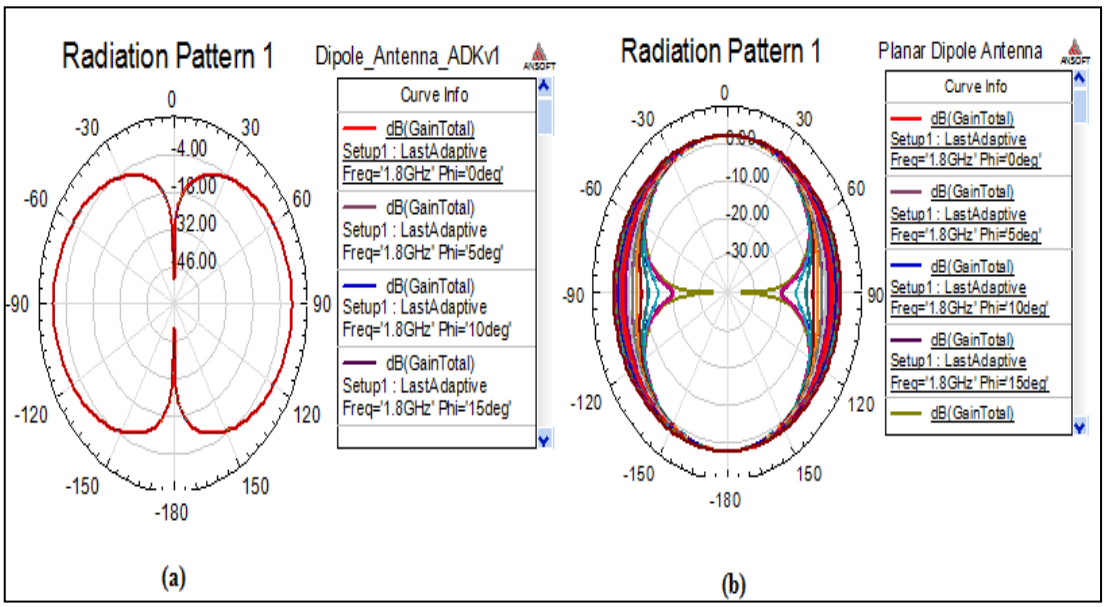

Figure (3.20): Radiation pattern for frequency at 1800 MHz for: (a) the half wave dipole antenna (wire antenna), (b) the planar dipole antenna.

Chapter Four

Simulation of Human Head Model Exposed to Mobile Phone Radiation Using FDTD

Chapter Four

Simulation of Human Head Model Exposed to Mobile Phone Radiation Using FDTD

Introduction

In order to overcome the limitations of classical methods, numerical methods were developed. Many numerical methods have been used to evaluate the power absorption into biological bodies. Other methods include the Method of Moments (MoM) (Harrington, 1993), the Finite Element Method (FEM) (Jianming, 2002), and the Finite Difference Time Domain (FDTD) method (Sullivan, 2000; Taflove, and Hagness, 2000; Kunz, and Luebbers, 1993; Elsherbeni, and Demir, 2009).

Numerical methods for the Maxwell equations are usually referred to as computational electromagnetic (CEM). The Maxwell equations can be solved in either the time domain or the frequency domain. Furthermore, the Numerical methods can be applied either on partial differential equation (PDE) formulation of the Maxwell equations or on a boundary integral formulation.

Time-domain methods can solve a problem for several frequencies in one single calculation, and they can follow the pulse evolution in time. The researcher concentrated the dissension on time domain methods (Auc Fai, 2006).

A numerical method that remedies the instabilities of the conventional FDTD is used to solve Maxwell's equations in a space-time dependent magneto-electric medium with direct application to the simulation of the recently proposed space-time cloak. The researcher utilized a dual grid FDTD method overlapped to the time domain to provide a stable approach for the simulation of magneto-electric medium with time and space varying permittivity, permeability and coupling coefficient. Hence, FDTD is essential in bio-electromagnetic and in the characterization of the interaction of EM fields with the tissues of the human body. This chapter presents the basic theory of the FDTD method and discusses the salient features of the Absorbing Boundary Conditions (ABCs).

From previous studies on the FDTD method to explore the effect of electromagnetic fields on layered biological tissues of the human body, Santosh S. Mhaske, Prof. G. A. Kulkarni, and Prof.Rahul L. Tayade suggested a planar multi-

layered model of the human head. This model consists of four planar layers of tissue human with different dielectric properties represented by (skin, fat, muscles, and kidney). The researchers investigated the effect of electromagnetic fields produced from dipole antenna on layered biological tissues with different dielectric properties, in the frequencies 900MHz. The interface distance between the air and the first life tissue is 5cm, 10cm, 15cm, 20cm, 25cm, and 30cm by FDTD method (Mhaske, Kulkarni, and Tayade, 2012).

Abu Ishaiba investigated the effect of electromagnetic fields produced from sector antenna on layered biological tissues. He calculated the electric field intensity, the magnetic field intensity, energy absorption (power density), and SAR distribution. The model consisted of three planar layers of tissues with different dielectric properties (skin, bone, and brain) in the frequencies 900MHz. The interface distance between the air and the first life tissue is 11cm, 13cm, and 15cm by FDTD method (Abu Ishaiba, 2012).

El Wasife studied the effect of electromagnetic fields produced from dipole antenna on layered biological tissues. A multi-layered head model was used to calculate the electric field intensity, the magnetic field intensity, energy absorption (power density), and SAR distribution. It consisted of four planar layers of tissues with different dielectric properties (skin, fat, muscles, and kidney) in the frequencies of 900MHz and 1800MHz. The interface distance between the air and the first life tissue is 30cm by FDTD method (El Wasife, 2011).

Elkhozondar, Shabat, El Wasife, and Osman investigated the effect of electromagnetic fields produced from mobile phone base station on layered biological tissues. A multi-layered was used to evaluate SAR and power density distribution. It consisted of four planar layers of tissues with different dielectric properties, skin, fat, muscles, and organs, in the frequencies 900MHz upon the interface between the air and the body tissue by FDTD method (EL-Khozodar, Shabat, EL-Wasife, and Osman, 2010).

In this chapter, the researcher used mat lab program which used finite-difference time-domain (FDTD) method to calculate the specific absorption rate (SAR) and the power density distribution inside a simple planar multi-layered human head model

exposed to electromagnetic field emitted from mobile phone operating in the 900MHz and 1800MHz.

4.1 Theory and Human Head Model

In this study, the human head is considered as a model of multilayered waveguide structure subjected to the radiation of dipole antenna of a mobile phone having dielectric properties for each layer which accords the frequency consideration. Dipole antenna is located at the left side of a human head with various gap distances. It is considered as near field radiation source for human head models. Figure (4.1) shows the three-dimensional realistic human head model with the dipole antenna used in this study at various gap distances between the antenna and the human head.

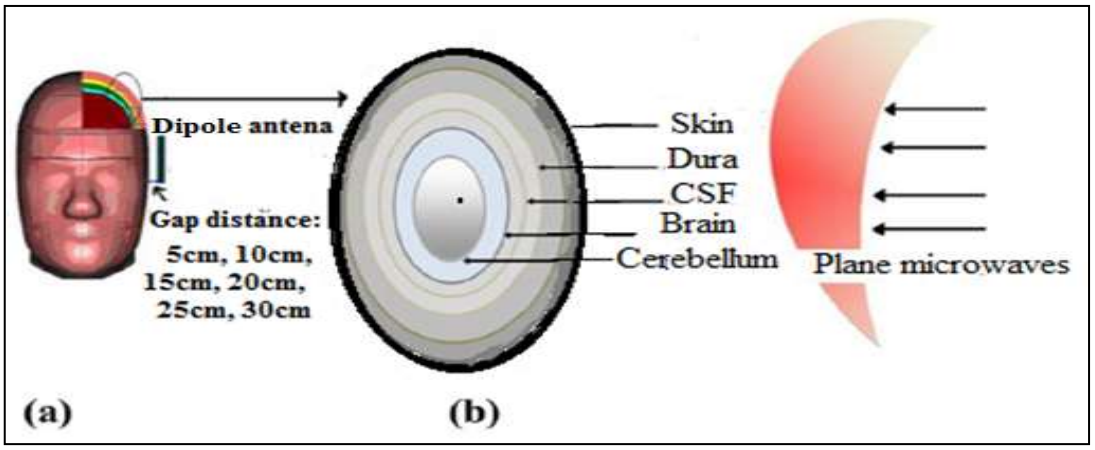

Figure (4.1): The Model of a human head. (a) Cross section human head model with mobile phone, (b) Plane microwaves irradiating a cranial model composed of five layers.

The proposed structure consists of five layers as biological body tissues. In this simulation, the core surrounded by five spherical shells represents the skin, dura, cerebrospinal fluid (CSF), brain, and cerebellum.

A schematic diagram of the multi-layer structure under consideration was shown in figure (4.2).

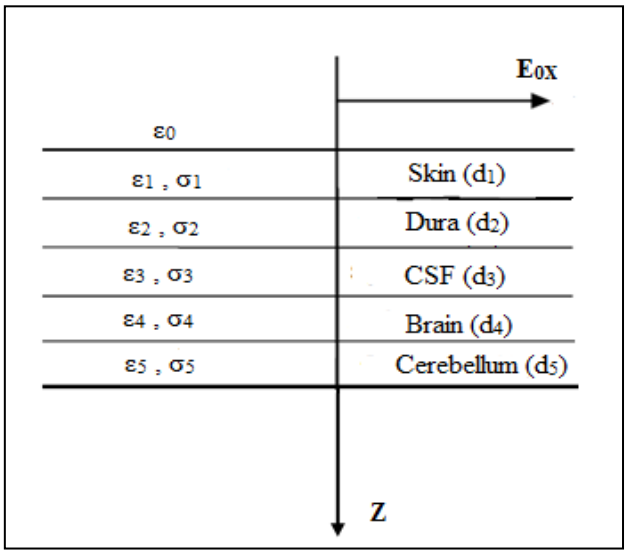

Figure (4.2): Planar multi-layered model of human head.

The layers are exposed vertically to electromagnetic waves with frequency equals 900MHz and 1800MHz upon the interface distance between the air and the first life tissue at 5cm, 10cm, 15cm, 20cm, 25cm, and 30 cm respectively. The electric field is assumed to propagate in the z direction with polarization at the x direction.

At 900MHz, the structure has layered media that consists of the skin of thickness of d_1 = 0.04023m, the dura of thickness d_2 = 0.037628m, the CSF of thickness d_3 = 0.019215m, the brain of thickness d_4 = 0.041536m, and the cerebellum layer of infinite thickness tissue.

At 1800MHz, the structure has layered media that consists of the skin of thickness d_1 = 0.028252 m, the dura of thickness d_2 = 0.026647m, the CSF of thickness d_3 = 0.015218m, the brain of thickness d_4 = 0.027256m, and the cerebellum layer of infinite thickness tissue.

4.2 Electric and Magnetic Field Interactions with Living Tissues

One of the most important aspects of bio-electromagnetics is the way electromagnetic fields interact with materials, for example, the mode the electric (E) and magnetic (H) fields affect human body. Because E and H were defined to account for forces among charges, the fundamental interaction of E and H with materials is that they exert forces on the charges in the materials.

Biological materials are lossy, and this loss changes the way the wave interacts with the material and its propagation behavior. A material is lossy if the conductivity σ is ≠0. Power will be dissipated in the lossy material as a wave passes through it, thus causing loss to the propagating wave. If power is dissipated in the material, the material will heat up, and this is what raises the concerns of RF waves' effect on human tissues (Furse, Christensen, and Durney, 2009).

In many electromagnetic field interactions, energy transfer is of prime consideration and concern. The electric field is transformed in the body into heat, which is the desired outcome of the therapy. For cell phones, the energy transfer must be under some predefined regulations. The E field can transfer energy to electric charges through the forces it exerts on them, but the H field does not transmit energy to charges. H effect is not prominent in EM biological interactions (Furse, Christensen, and Durney, 2009).

4.3 Electrical Properties of the Human Head

The electrical properties of human tissues (relative permittivity ε_r and conductivity σ) control the propagation, reflection, and attenuation of electromagnetic fields in the body. These properties strongly depend on the tissue type and the frequency of interest.

Body is a non-uniform space conductor where an electric current flows according to electric tissue conductivity. Body tissues have different resistances (impedances), and therefore different conductances.

- The highest resistance (Impedance) has the fat and bone tissues (R = 40-50 Ω/m).
- The lowest resistance (Impedance) has blood, liquor, and lymphatic fluid (R = 0.8 Ω/m).
- Resistance for dry skin is high (R=1000 Ω/m), and resistance for wet skin is low (R=50 Ω/m).

Table (4.1), and Table (4.2) show the electrical properties of the different tissues in the head model at 900 MHz, and 1800 MHz, which are the commonly used frequencies for cellular phones and wireless local area networks (Gabriel & Gabriel, 1996; "Dielectric Properties of the Body Tissues"). It is worth mentioning that the body is so weakly magnetic such that, generally, the relative permeability (μ_r) is assumed to be 1.

Table (4.1): Relative permittivity and conductivity of the layers of the human head model at frequency 900 MHz.

Tissue name	Conductivity (σ) [S/m]	Relative permittivity	Density(ρ) [Kg/m^3]	Penetration depth (d) [m]
Air	0	1	1.229	.05, .1, .15, .2, .25, and .3
Skin	0.86674	41.0405	1100	0.04023
Dura	0.96114	44.426	1050	0.037628
CSF	2.4126	68.638	1060	0.019215
Brain	0.94227	52.725	1030	0.041536
Cerebellum	1.2628	49.444	1030	0.030453

Table (4.2): Relative permittivity and conductivity of the layers of the human head model at frequency 1800 MHz.

Tissue name	Conductivity (σ) [S/m]	Relative permittivity	Density(ρ) [Kg/m^3]	Penetration depth (d) [m]
Air	0	1	1.229	.05, .1, .15, .2, .25, and .3
Skin	1.1847	38.872	1100	0.028252
Dura	1.3198	42.894	1050	0.026647
CSF	2.9236	67.2	1060	0.015218
Brain	1.3913	50.079	1030	0.027256
Cerebellum	1.7089	46.114	1030	0.021442

4.4 Finite-Difference Expressions for Maxwell's Equations in One Dimensions

In this model, it is assumed that only E_x and H_y components exist, so Eq. (2.14) becomes:

$$\frac{\partial \mathrm{E_x}}{\partial t} = \frac{1}{\varepsilon_\circ \varepsilon_\mathrm{r}}\left(\frac{\partial \mathrm{H_z}}{\partial y} - \frac{\partial \mathrm{H_y}}{\partial z} - \sigma \mathrm{E_x(t)}\right) \tag{4.1}$$

And Eq. (2.12) becomes:

$$\frac{\partial \mathrm{H_y}}{\partial \mathrm{t}} = -\frac{1}{\mu}\frac{\partial \mathrm{E_x}}{\partial \mathrm{z}} \tag{4.2}$$

These are the equations of a plane wave with the electric field oriented in the x-direction, the magnetic field oriented in the y-direction, both travel in the z-direction. Considering a typical substitution of central differences for the time and space derivatives in Eq. (4.1), we have initially:

$$\frac{\mathrm{E_x}^{n+1}(\mathrm{k}) - \mathrm{E_x}^{n}(k)}{\Delta t} = \frac{1}{\varepsilon_\circ \varepsilon_\mathrm{r}(\mathrm{k})}\left[-\frac{\mathrm{H_y}^{n+1/2}(k+1/2) - \mathrm{H_y}^{n+1/2}(k-1/2)}{\Delta z}\right] - \frac{\sigma(\mathrm{k})}{\varepsilon_\circ \varepsilon_\mathrm{r}(\mathrm{k})}\mathrm{E_x}^{n+1/2}(k) \tag{4.3}$$

Since E_x values at time-step n are not assumed stored in the computer's memory, we need some way to estimate such terms. A very good way is as follows, using what is called a semi-implicit approximation:

$$\mathrm{E_x}^{n+1/2}(k) = \frac{\mathrm{E_x}^{n+1}(k) + \mathrm{E_x}^{n}(k)}{2} \tag{4.4}$$

Here, E_x values at time-step n are assumed to be simply the arithmetic average of the stored values of E_x at the time-step n-1/2 and the yet-to-be computed new values of Ex at time-step n+1/2. Substituting Eq. (3.4) into Eq. (4.3), we obtain

$$\frac{E_x^{n+1}(k)-E_x^{n}(k)}{\Delta t} = \frac{1}{\varepsilon_\circ \varepsilon_r(k)}\left[-\frac{H_y^{n+1/2}(k+1/2)-H_y^{n+1/2}(k-1/2)}{\Delta z}\right] - \frac{\sigma(k)}{\varepsilon_\circ \varepsilon_r(k)}\left[\frac{E_x^{n+1}(k)+E_x^{n}(k)}{2}\right] \quad (4.5)$$

Rearrangement leads to

$$\frac{E_x^{n+1}(k)}{\Delta t}+\frac{\sigma(k)}{2\varepsilon_\circ \varepsilon_r(k)}E_x^{n+1}(k) = \frac{1}{\varepsilon_\circ \varepsilon_r(k)}\left[-\frac{H_y^{n+1/2}(k+1/2)-H_y^{n+1/2}(k-1/2)}{\Delta z}\right]+\frac{E_x^{n}(k)}{\Delta t} - \frac{\sigma(k)}{2\varepsilon_\circ \varepsilon_r(k)}E_x^{n}(k) \quad (4.6)$$

$$\frac{2\varepsilon_\circ \varepsilon_r(k)+\sigma(k)\Delta t}{2\varepsilon_\circ \varepsilon_r(k)\Delta t}E_x^{n+1}(k) = \frac{1}{\varepsilon_\circ \varepsilon_r(k)}\left[-\frac{H_y^{n+1/2}(k+1/2)-H_y^{n+1/2}(k-1/2)}{\Delta z}\right] + \frac{2\varepsilon_\circ \varepsilon_r(k)-\sigma(k)\Delta t}{2\varepsilon_\circ \varepsilon_r(k)\Delta t}E_x^{n}(k) \quad (4.7)$$

Dividing both sides by $\frac{2\varepsilon_\circ \varepsilon_r(k)+\sigma(k)\Delta t}{2\varepsilon_\circ \varepsilon_r(k)\Delta t}$ yields the desired explicit time step relation for $E_x^{n+1/2}(k)$:

$$E_x^{n+1}(k) = \frac{\frac{2\varepsilon_\circ\varepsilon_r(k)-\sigma(k)\Delta t}{2\varepsilon_\circ\varepsilon_r(k)\Delta t}}{\frac{2\varepsilon_\circ\varepsilon_r(k)+\sigma(k)\Delta t}{2\varepsilon_\circ\varepsilon_r(k)\Delta t}} E_x^{n}(k) +$$

$$\frac{2\Delta t}{2\varepsilon_\circ\varepsilon_r(k)+\sigma(k)\Delta t}\left[-\frac{H_y^{n+1/2}(k+1/2)-H_y^{n+1/2}(k-1/2)}{\Delta z}\right] \quad (4.8)$$

$$E_x^{n+1}(k) = \frac{1-\frac{\sigma(k)\Delta t}{2\varepsilon_\circ\varepsilon_r(k)}}{1+\frac{\sigma(k)\Delta t}{2\varepsilon_\circ\varepsilon_r(k)}} E_x^{n}(k) +$$

$$\frac{2\Delta t}{2\varepsilon_\circ\varepsilon_r(k)+\sigma(k)\Delta t}\left[-\frac{H_y^{n+1/2}(k+1/2)-H_y^{n+1/2}(k-1/2)}{\Delta z}\right] \quad (4.9)$$

Next, we discretize equation (4.2) and get:

$$\frac{H_y^{n+1/2}(k+1/2)-H_y^{n-1/2}(k+1/2)}{\Delta t} = \frac{1}{\mu(k+1/2)}\left[-\frac{E_x^{n+1/2}(k+1/2)-E_x^{n+1/2}(k+1/2)}{\Delta z}\right] \quad (4.10)$$

Rearrangement leads to

$$H_y^{n+1/2}(k+1/2) = H_y^{n-1/2}(k+1/2) + \frac{\Delta t}{\mu(k+1/2)}\left[-\frac{E_x^{n}(k+1)-E_x^{n}(k)}{\Delta z}\right] \quad (4.11)$$

To avoid computational problems due to the very different amplitudes of **E** and **H**, Taflove introduced a normalization of the **E** field (Sullivan, 2000; EL-Khozodar, Shabat, EL-Wasife, & Osman, 2010):

$$\check{\mathbf{E}} = \sqrt{\frac{\varepsilon_\circ}{\mu_\circ}}\,\mathbf{E} \tag{4.12}$$

Substituting this into equations of Eq. (4.9) and equations of Eq. (4.11) gives:

$$\widetilde{E}_x{}^{n+1}(k) = \frac{1 - \frac{\sigma(k)\Delta t}{2\varepsilon_\circ \varepsilon_r(k)}}{1 + \frac{\sigma(k)\Delta t}{2\varepsilon_\circ \varepsilon_r(k)}}\,\widetilde{E}_x{}^{n}(k) +$$

$$\sqrt{\frac{\varepsilon_\circ}{\mu_\circ}} \times \frac{2\Delta t}{2\varepsilon_\circ \varepsilon_r(k) + \sigma(k)\Delta t}\left[-\frac{H_y{}^{n+1/2}(k+1/2) - H_y{}^{n+1/2}(k-1/2)}{\Delta z}\right] \tag{4.13}$$

$$H_y{}^{n+1/2}(k+1/2) = H_y{}^{n-1/2}(k+1/2) + \sqrt{\frac{\varepsilon_\circ}{\mu_\circ}} \times \frac{\Delta t}{\mu(k+1/2)}\left[-\frac{E_x{}^{n}(k+1) - E_x{}^{n}(k)}{\Delta z}\right] \tag{4.14}$$

These equations can be directly implemented in a computer code, noting that the "1/2" in Eq. (4.13) and Eq. (4.14) do not need to be implemented in the computer code. The half a cell and half a time step are necessary in equations Eq. (4.13) and Eq. (4.14) just to remind us of the physical definitions of **E** and **H**, and to remind us that **E** and **H** are actually offset by half a cell and half a time step. This information, anyway, will never appear in our coding.

4.4.1 Stability Condition

The numerical algorithm is second order accurate in both space and time and is an explicit method; it requires an upper bound on the time step Δt for stability. The time increment Δt in FDTD is limited by the stability requirement known as the Courant-Friedrichs-Lewy (CFL) condition (Sullivan, 2000).

$$\Delta t \le \Delta t_{max} = \frac{\Delta z}{c_\circ \sqrt{n}} \tag{4.15}$$

where $c_\circ$ is the propagation speed of electromagnetic wave in free space, and n is the number of dimensions considered in the problem.

For 3D FDTD in a uniform grid, the stability requirement is:

$$\Delta t \leq \Delta t_{max} = \frac{1}{c_\circ \sqrt{\frac{1}{\Delta x^2} + \frac{1}{\Delta y^2} + \frac{1}{\Delta z^2}}} \tag{4.16}$$

In a cubic grid (where $\Delta z = \Delta x = \Delta y = \Delta$), (4.16) can be expressed as

$$\Delta t \leq \Delta t_{max} = \frac{\Delta}{c_\circ \sqrt{3}} \qquad (\Delta z = \Delta x = \Delta y = \Delta) \tag{4.17}$$

When getting two-dimensional simulation, $\Delta t = \Delta z/(c_\circ \sqrt{2}\ )$. We define the CFL number as,

$$\mathrm{CFL} = c_\circ \Delta t \sqrt{\frac{1}{(\Delta x)^2} + \frac{1}{(\Delta y)^2} + \frac{1}{(\Delta z)^2}} \tag{4.18}$$

For a linear, isotropic, non-dispersive, and homogeneous dielectric media with permittivity ε and permeability μ (the dielectric can have some losses in the form of non-zero conductivity σ), the time increment has to obey the stability condition as:

$$\mathrm{CFL} \leq 1 \leq \frac{1}{c_\circ \sqrt{\frac{1}{\Delta x^2} + \frac{1}{\Delta y^2} + \frac{1}{\Delta z^2}}} \tag{4.19}$$

A convenient time-step that satisfies the stability requirement for 1D, 2D and 3D is:

$$\Delta t = \frac{\Delta}{2c_\circ} = \frac{0.5\Delta}{c_\circ} \tag{4.20}$$

The equal sign"=" but not "≤" is used here, and $0.5 < 0.577 < 0.71 < 1$, Δt can be smaller, but cannot be bigger. Throughout this thesis, Δt will be determined by equation (4.20), which achieves the Courant stability condition. Therefore,

$$c_\circ \frac{\Delta t}{\Delta} = \frac{1}{\sqrt{\varepsilon_\circ \mu_\circ}} \frac{\Delta t}{\Delta} = \frac{1}{2} \tag{4.21}$$

Substituting equation (4.21) into Eq. (4.13) and Eq. (4.14), we get:

$$\widetilde{E}_x^{\,n+1}(k) = \frac{1-\frac{\sigma(k)\Delta t}{2\varepsilon_\circ\varepsilon_r(k)}}{1+\frac{\sigma(k)\Delta t}{2\varepsilon_\circ\varepsilon_r(k)}}\widetilde{E}_x^{\,n}(k) + \frac{1/2}{\varepsilon_r\left(1+\frac{\sigma(k)\Delta t}{2\varepsilon_\circ\varepsilon_r(k)}\right)}\times$$

$$\left[-H_y^{\,n+1/2}(k+1/2) \quad + H_y^{\,n+1/2}(k-1/2)\right] \tag{4.22}$$

$$H_y^{\,n+1/2}(k+1/2) = H_y^{\,n-1/2}(k+1/2) + \frac{1}{2}\left[-\widetilde{E}_x^{\,n}(k+1) + \widetilde{E}_x^{\,n}(k)\right] \tag{4.23}$$

We use the computer equations and simulate a sinusoidal wave hitting a human body tissue that has a dielectric constant and conductivity according the frequency.

4.4.2 Cell Size Determination

The researcher chose the cell size in a FDTD formulation that is similar to any approximation procedure. To obtain higher accuracy in solution, the grid size has to be smaller. Hence, the time step will be smaller. The spatial sampling rate is required to be between 10 samples per wavelength to 20 samples per wavelength (Kunz, Luebbers, 1993; Sullivan, 2000).

Naturally, the worst-case scenario must be assumed, and this will involve looking at the highest frequencies that will be simulated and determining the corresponding wavelength. For instance, suppose we run simulations at 900 GHz and 1800 GHz; in free space, EM energy will propagate at the wavelength of (Sullivan, 2000):

$$\lambda = \frac{c_\circ}{f} \tag{4.24}$$

where $c_\circ$ is the propagation speed of electromagnetic wave in free space, and f is frequency of electromagnetic wave. For a system excited by a sinusoidal source of 900 GHz, the wavelength is 0.333 meter. If the sampling rate is 20, the spatial step for one dimension (cell size) can be chosen to be:

$$\Delta \leq \frac{\lambda}{20} = \frac{0.333}{20} = 0.01\text{m} \tag{4.25}$$

where ($\Delta z = \Delta x = \Delta y = \Delta$). Then, time-step for one dimension will be:

$$\Delta t = \frac{\Delta z}{2c_\circ} = \frac{0.333/20}{2 \times 3 \times 10^8} = 1.6 \times 10^{-11}\ \text{s} \ \cong\ .016 \times 10^{-9}\ \text{ns} \qquad (4.26)$$

Similarly, the wavelength for a sinusoidal source of 1800 GHz is 0.166 meter. If the sampling rate is 20, the spatial step for one dimension (cell size) can be chosen to be:

$$\Delta \leq \frac{\lambda}{20} = \frac{0.166}{20} = 0.008 \qquad (4.27)$$

Then, time-step for one dimension will be:

$$\Delta t = \frac{\Delta}{2c_\circ} = \frac{0.166/20}{2 \times 3 \times 10^8} = 1.3 \times 10^{-11}\ \text{s} \ \cong\ .013 \times 10^{-9}\ \text{ns} \qquad (4.28)$$

However, if we simulate EM propagation in biological tissues, we must look at the wavelengths in the tissue with the highest dielectric constant, because this will have the corresponding shortest wavelength. Because the tissues in the head have thin thicknesses, steps must be small enough to represent all tissues with a very small average (Rhattoy, Lahmer, and Zatni, 2010).

4.4.3 Absorbing Boundary Conditions (ABC's)

We cannot simulate the propagation of the signal indefinitely, and we need to terminate the simulation in the FDTD grid. It is necessary to terminate the computational domain to conform to the available computational resources. Most electromagnetic problems entail a structure whose behavior is studied in an unbounded domain. Since it is impossible to simulate infinite physical domains, the computational space is terminated by absorbing boundary conditions that effectively simulate an unbounded region by preventing reflections from the edges (Mur, 1981; Sullivan, 2000).

Most of the Absorbing Boundary Conditions (ABCs) can be grouped into two categories. One category is ABCs derived from differential equations (analytical ABCs). The other category is ABCs using material absorbers (material ABCs). Analytical ABCs are simulated by approximating the wave equation at the boundary

while the material ABCs incorporate a lossy medium to physically absorb the incident wave. Mur's first-order and second-order absorbing boundary conditions are examples of ABCs derived from differential equations (Taflove, 1995; Rao, 2004). Suppose we look for a boundary condition at the beginning of the head, then

$$\text{distance} = c_\circ \Delta t = c_\circ \frac{\Delta z}{2c_\circ} = \frac{\Delta z}{2} \tag{4.29}$$

Model, where $k = 1$. In fact, that if we use Δt given by Eq. (4.20) ($\Delta t = \Delta z/2c_\circ$). For a wave that goes toward a boundary in free space, it travels at a speed $c_\circ$, the speed of light. So, it travels in one time step of the FDTD algorithm. This equation explains that it takes two time steps for a wave front to cross one cell. Therefore, a common sense approach is E_x at next time step = E_x at present time step, written in symbols, it is:

(E_x at time step n, at spatial step 1) = (E_x at time step $n-1$, at spatial step 2).

Note that the wave travels from spatial step 2 to spatial step 1, along the negative x direction. The absorbing boundary condition for the 1D case can be therefore expressed by:

$$E_x^{\,n}(1) = E_x^{\,n-1}(2) \tag{4.30}$$

It is relatively easy to implement this condition. Simply, the value of E_x (2) is stored for two time steps, delay may happen due to the interlaced computation of the electric and magnetic field, and then it is used in E_x (1). Boundary conditions, which have been implemented at the left end forE_x, while for the right end, the dielectric properties of the last layer (cerebellum) in consideration have to be taken into account:

$$\text{distance} = v\Delta t = \frac{c_\circ}{\sqrt{\varepsilon_r}} \frac{\Delta z}{2c_\circ} = \frac{\Delta z}{2\sqrt{\varepsilon_r}} \cong \frac{\Delta z}{s} \tag{4.31}$$

Where v is the speed of the wave inside the tissue, and s is equal to or higher than two. Distance that the wave travels depends on the dielectric properties of the medium.

So, the number of time steps, needed for the wave to travel one cell, will vary according to the frequency of interest. This equation explains that it takes s time

steps for a wave front to cross one cell. The absorbing boundary condition for the 1D case can be therefore expressed by:

$$E_x^{\,n}(KE) = E_x^{\,n-s}(KE-1) \tag{4.32}$$

Where KE is the cell at the end of the model. The value of E_x (KE-1) has to be stored for s time steps, and then used in the calculation of E_x (KE).

4.4.4 Source Signals

The selection of source signal is also important since it represents the antenna used in mobile phone. Commonly used source signals are the sinusoidal signal or the Gaussian pulse; it is preferred to use a modulated signal in order to avoid high frequency at the beginning of the simulation. Other choices, in order to reduce the error, include using the so-called "soft" source, where the source signal of interest is added in the source point to the previous value of the field. In other words, for example, if the following is a "hard" source (Sullivan, 2000).

$$E_x(kE) = \sin\left(2 \times \pi \times f \times \Delta t\right) \tag{4.33}$$

Where f frequency of electromagnetic wave. The following is instead a "soft" source

$$E_x(kE) = E_x(kE) + \sin\left(2 \times \pi \times f \times \Delta t\right) \tag{4.34}$$

4.4.5 Calculation of Specific Absorption Rate (SAR)

We calculate SAR distribution cell inside the head from the converged solutions of FDTD expressions by deriving it from Maxwell's equations. **E** and **H** are first determined analytically or numerically from Maxwell's equations. The SAR (W/kg) is then calculated by the following equation (Ali, and Ray, 2014)

$$SAR_i = \frac{\sigma_i |E_i|^2}{2\rho_I} \tag{4.35}$$

Where, E is the root means square (r.m.s) value of the electric field in V/m, σ is the conductivity of the head in S/m and ρ_i is the i^{th} tissue density of the head in Kg/m³.

Since the electric fields are now available, the dissipated power density in each layer can also be calculated using the following equation:

$$P_i = \frac{\sigma_i |E_i|^2}{2} = \rho_I \, SAR_I \qquad (4.36)$$

Eq. (4.35) is a point relation, so it is often called the local SAR. The space-average SAR for a body or a part of the body is obtained by calculating the local SAR at each point in the body and averaging over the part of the body being considered.

4.5 Calculation Techniques

To implement the code for the calculation of the fields, SAR and power density obeying equations Eq. (4.22), Eq. (4.23), Eq. (4.35), and Eq. (4.36) were used to:

a. Define the size KE of the arrays **E**, **H,** SAR, and P that, once we chose the spatial, it would correspond to the absolute size of the computational domain. We can write this in matlab code as such follows:

```
ex = zeros(1,KE);
hy = zeros(1,KE);
cb = zeros(1,KE);
p = zeros(1,KE);
sar = zeros(1,KE);
```

where

```
KE = 45.
```

b. Determine the necessary time step according to our resolution and excitation signal, noting that the cell size dx and the time step dt are specified explicitly. We did this because we need dt in calculation of source from Eq. (4.33).The cell size dx is only specified from Eq. (4.25), and Eq. (4.27), because it is needed to calculate dt from Eq. (4.26), and Eq. (4.28). Re writing Eq. (4.33) in matlab code gives the following:

```
source = sin (2* pi * frequency * dt (1,1) * n);
ex (1,2) = source.
```

This source is used in matlab code at 900 MHz, and 1800 MHz.

c. Implement a cycle to compute the fields for a certain number of time steps. Within this cycle, we need to include a cycle to calculate the various EX (K)

according to equation (4.22) for all the cells of the domain KE, and the excitation signal at the source point KS, also, a cycle to calculate the various HY (K) according to equation (4.23) for all the cells of the domain KE. From Eq. (4.22), Eq. (4.23), Eq. (4.35) and Eq. (4.36), we can get the computer equation as such follows:

```
ex (1,k) = ca * ex (1,k) + cb * (hy (1,k-1) – hy (1,k));
hy (1,k) = hy (1,k) + 0.5 * (ex(1,k) – ex (1,k+1));
p (1,k ) = (s (1,k) * (abs (ex (1,k)))^2) / 2;
sar (1,k) = p (1,k) / r (1,k);
```

where:

```
eaf = dt (1,k) * s(1,k) / (2 * permittivity (1,k) * 8.85e-12);
ca = (1-eaf) / (1+eaf);
cb = 0.5 / (permittivity (1,k) * (1+eaf)).
```

These are the Ex, Hy, P, and SAR that we want to evaluate when the distance between the cell phone and the human head model changes at frequency 900 MHz, and 1800 MHz. Figures (4.3) to (4.26) show the different output of the distribution of electromagnetic fields, second, power density, SAR by a planar multi-layered model to human head; its (Skin, Dura, Cerebrospinal Fluid, Brain, and Cerebellum) after simulating in matlab.

4.6 Results and Discussions

Human head is considered as a model of multilayered waveguide structure in this study. The model is subjected to the radiation of dipole antenna of a mobile phone having dielectric properties for each layer differ according the frequency. Dipole antenna located at the left side of a human head with various gap distances is considered as near field radiation source for human head models. The results are illustrated in many Figures. Figures (4.3 -4.6 a) show many intervals that are, the range from 0 to 5 that represents a free space, the interval from five to nine that represents skin, the interval from nine to twelve we supposed a Dura tissue. Furthermore, the range from twelve to fourteen represents CSF, in addition, the interval from fourteen to eighteen occupies the brain, and from eighteen to twenty-one occupies cerebellum.

Figure (4.3 a) shows that an electromagnetic pulse is radiated from a source located in free space, but when the pulse strikes the human body interface the wave propagates more slowly and the pulse length is shorter, skin amplitude decreases to 0.154 V/m, dura amplitude is 0.086 V/m, CSF amplitude is 0.025 V/m, and pulse amplitude will decrease more to zero in cerebellum through brain. Obviously, figure (4.4 a) shows the relation between Magnetic field in y-dimension and time step where signal amplitude decreases when it hits the human body and goes through the skin at 0.790A/m, dura at 0.397A/m, even reached zero at cerebellum over CSF, and brain. Also, figure (4.5 a) illustrates that power density is zero in free space and increases to maximum at skin equal to 0.032 W and less in dura to 0.010 W, and finally reaches zero in cerebellum via CSF, and brain. The relation between SAR versus time step is explained in Figure (4.6 a), that it increases from zero at free space to 2.91×10^{-5} W/Kg at skin and decreases again to 9.38×10^{-6} W/Kg at dura, CSF to 3.44×10^{-6} W/Kg, back to zero again in cerebellum amidst brain.

All different intervals are shown in figures (4.3-4.4 b). They show that ranges (0-6), (6-9), (9-13), (13-15), (15-18), and (18-21) represent free space, skin, dura, CSF, brain, and cerebellum respectively. Figure (4.3 b) shows that a signal amplitude begins in free space and decreases to 0.094 V/m in skin. In addition, the maximum beak equals 0.005 V/m in dura, to zero in cerebellum through CSF, and brain. Figure (4.4 b) explains connection between Magnetic field in y-dimension and time step where signal amplitude decreases when it hits the human body and goes through the skin at 0.186 A/m, dura at 0.167 A/m, and reaches zero at cerebellum over CSF, and brain. Moreover, figure (4.5 b) illustrates that the power density is zero in free space and increases to maximum in skin to 0.0053 W, and it decreases to reach zero in cerebellum, dura, CSF, and brain. In figure (4.6 b), the specific absorption rate (SAR) increases from zero at free space to 4.87×10^{-6} W/Kg at skin, and it decreases again back to zero in cerebellum amidst dura, CSF, and brain.

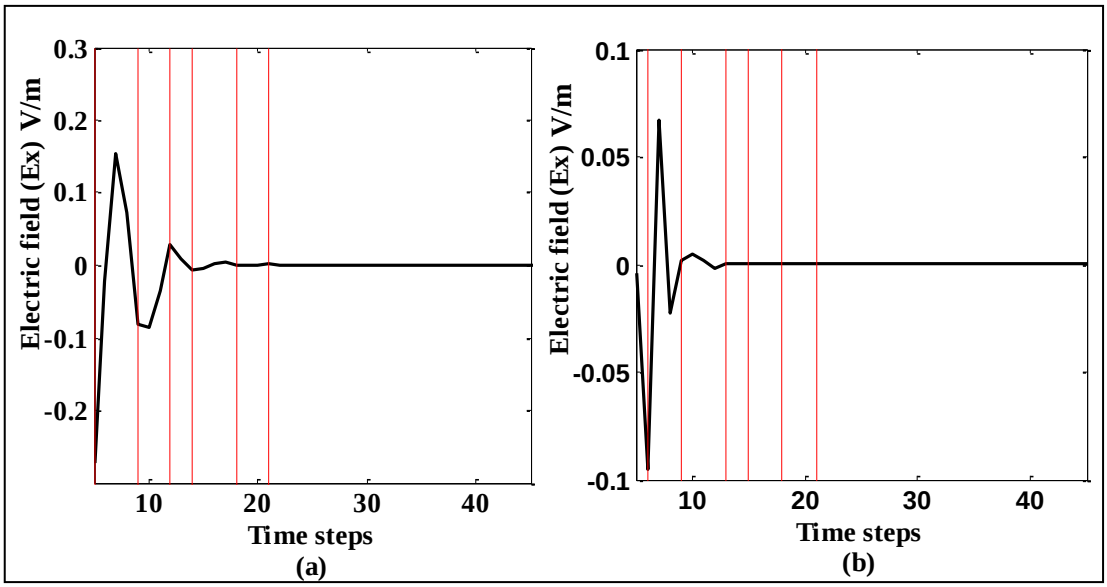

Figure (4.3): Simulation of the propagation of electric field at 3000 iteration in five layers of human tissue for distance of 5cm at: (a) f= 900MHz, λ=.33m, Δz= λ/20=.01m, Δt=.6ns and (b) f= 1800MHz, λ=.16m, Δz= λ/20=.008m, Δt=27.7ns.

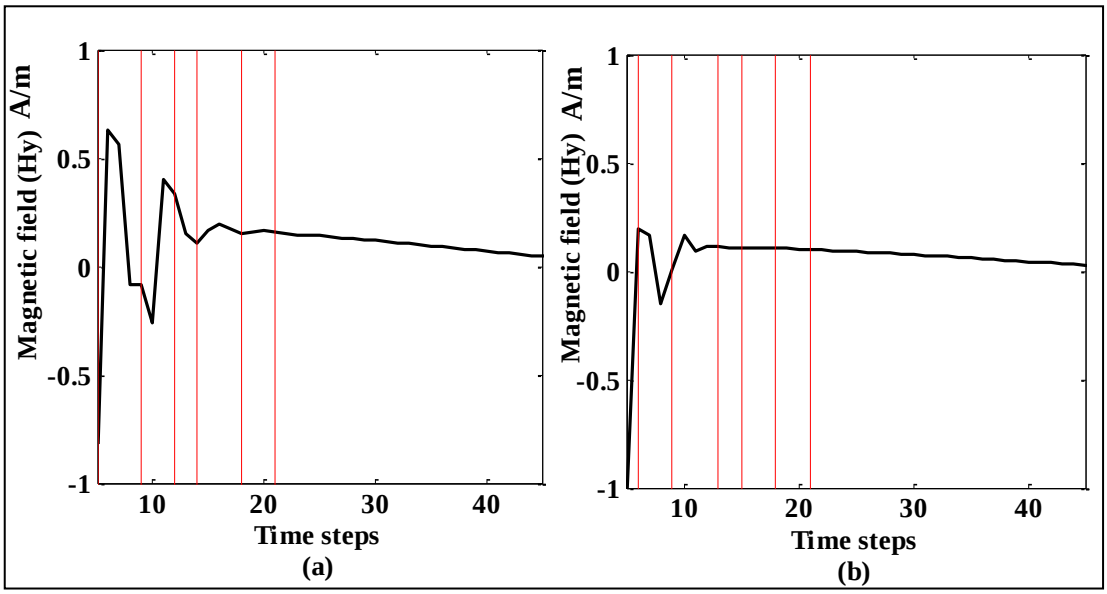

Figure (4.4): Simulation of the propagation of magnetic field at 3000 iteration in five layers of human tissue for distance of 5cm at: (a) f= 900MHz, λ=.33m, Δz= λ/20=.01m, Δt=.6ns and (b) f= 1800MHz, λ=.16m, Δz= λ/20=.008m, Δt=27.7ns.

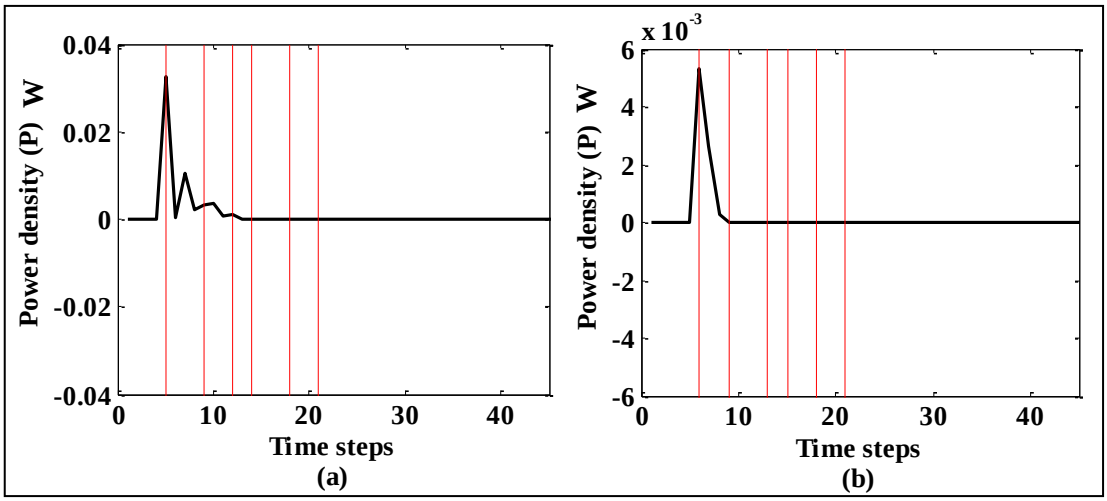

Figure (4.5): Power density at 3000 iteration in five layers of human tissue for distance of 5cm at: (a) f= 900MHz, λ=.33m, Δz= λ/20=.01m, Δt=.6ns and (b) f= 1800MHz, λ=.16m, Δz= λ/20=.008m, Δt=27.7ns.

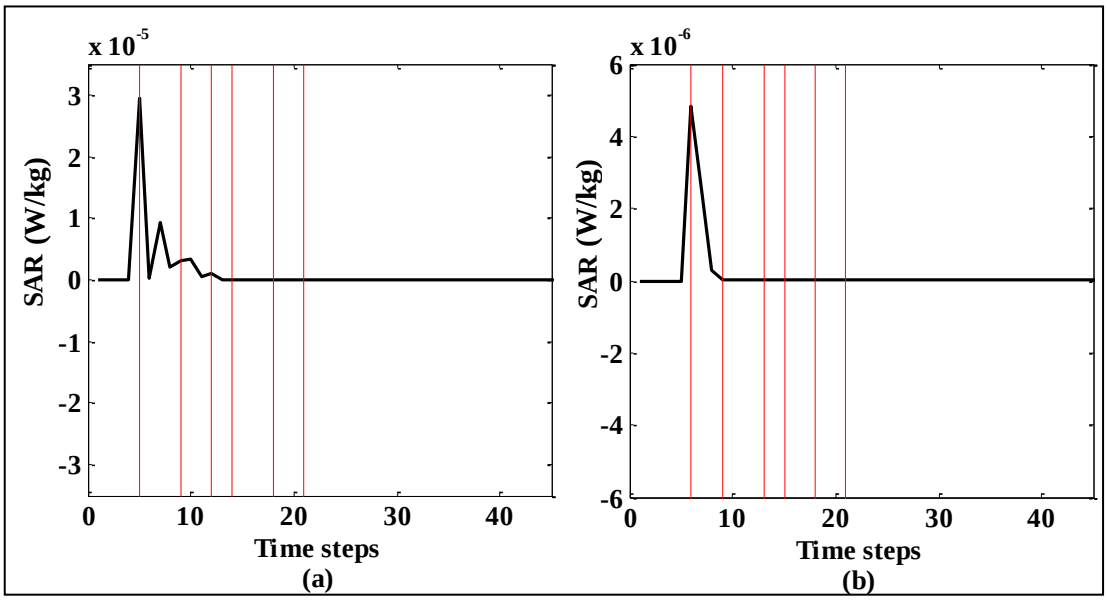

Figure (4.6): SAR at 3000 iteration in five layers of human tissue for distance of 5cm at: (a) f= 900MHz, λ=.33m, Δz= λ/20=.01m, Δt=.6ns and (b) f= 1800MHz, λ=.16m, Δz= λ/20=.008m, Δt=27.7ns.

According to figures (4.7-4.10 a), the ranges (0-10), (10-14), (14-17), (17-19), (19-23), and (23-26) represent free space, skin, dura, CSF, brain, and cerebellum respectively. Electromagnetic pulse in figure (4.7 a) grows at distance 10 cm, when it is measured, it achieves line of sight where signal amplitude starts in free space when it pummels the human body, 0.41 V/m at skin, dura amplitude is 0.184 V/m, CSF amplitude is 0.087 V/m, and pulse amplitude will decrease more to zero in cerebellum via brain. Figure (4.8 a) shows that Magnetic field in y-dimension signal amplitude increases at distance 10 cm, and when measured while it pounds the human body and goes over the skin at 0.913 A/m, it reaches zero at cerebellum through dura, CSF, and brain. Power density in figure (4.9 a) increases more than when measured at 5 cm and becomes 0.418 W in skin, dura in 0.072 W, CSF in 0.016 W, to zero in cerebellum during brain. Figure (4.10 a) shows that SAR increases more than when measured at 5 cm where it becomes 3.5×10^{-4} W/Kg in skin, 6.62×10^{-5} W/Kg in dura, to zero in cerebellum through CSF, and brain.

Furthermore, figures (4.7), (4.8), (4.9), and (4.10 b) show many intervals again, that the ranges (0-12, 12-16, 16-19, 19-21, 21-24, and 24-27 represent free space, skin, dura, CSF, brain, and cerebellum respectively. Figure (4.7) shows that a signal amplitude increases more than when measured at distance 5 cm; it begins in free space when pummels the human body at 0.182 V/m at skin, Dura amplitude is 0.012 V/m, to zero in cerebellum via CSF, and brain. Figure (4.8 b) shows that the Magnetic field in y-dimension signal amplitude increases at distance 10 cm, and when measured while it pounds the human body and goes over the skin at 0.657A/m, till it reaches zero at cerebellum vai dura, CSF, and brain. Power density in figure (4.9 b) increases more than when measured at 5 cm where it becomes 0.032W in skin, to zero in cerebellum via dura, CSF, and brain. Figure (4.10 b) shows that SAR increases more than when measured at 5 cm where it becomes 2.604×10^{-5} W/Kg in skin, to zero in cerebellum vai dura, CSF, and brain.

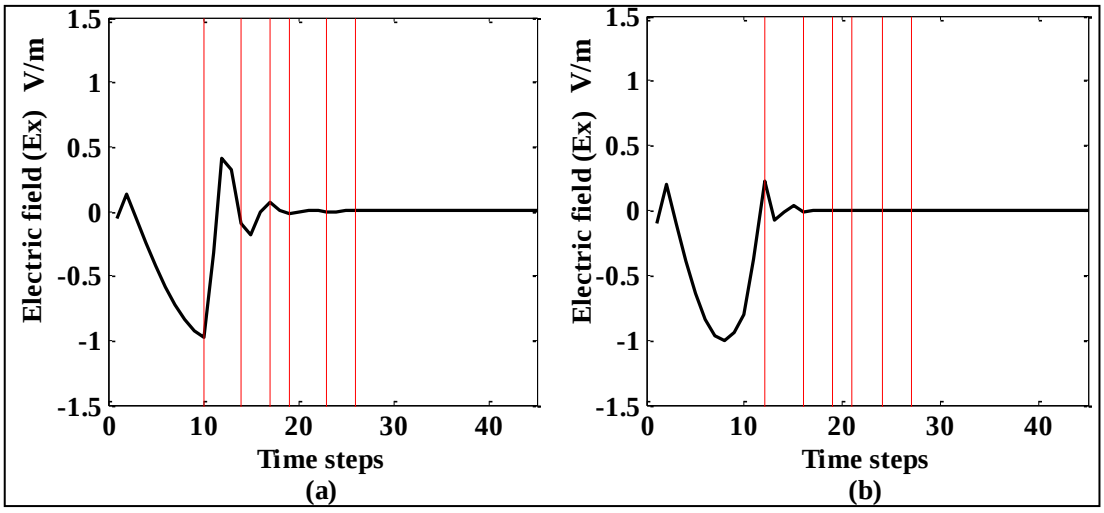

Figure (4.7): Simulation of the propagation of electric field at 3000 iteration in five layers of human tissue for distance of 10cm at: (a) f= 900MHz, λ=.33m, Δz=λ/20=.01m, Δt=.6ns and (b) f= 1800MHz, λ=.16m, Δz= λ/20=.008m, Δt=27.7ns.

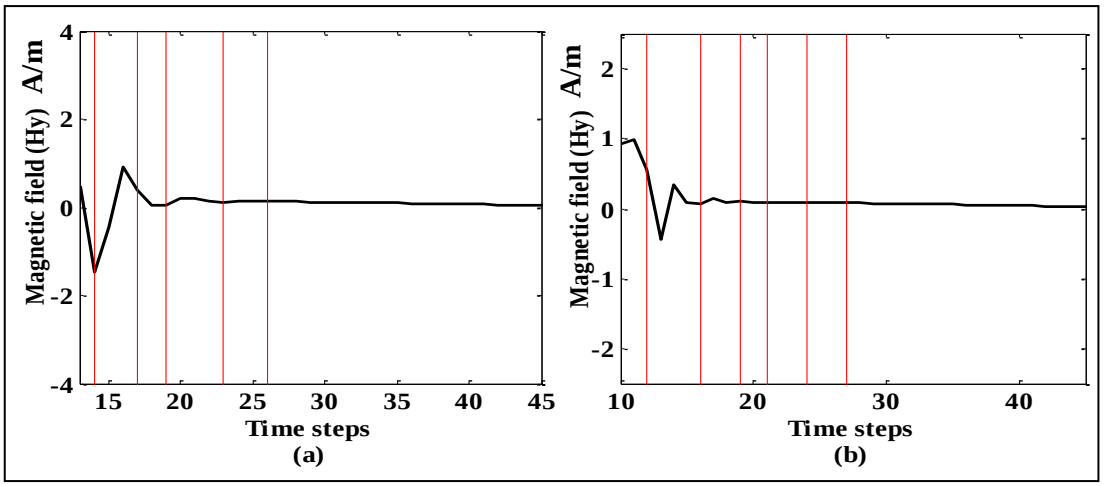

Figure (4.8): Simulation of the propagation of magnetic field at 3000 iteration in five layers of human tissue for distance of 10cm at: (a) f= 900MHz, λ=.33m, Δz=λ/20 =.01m, Δt=.6ns and (b) f= 1800MHz, λ=.16m, Δz= λ/20=.008m, Δt=27.7ns.

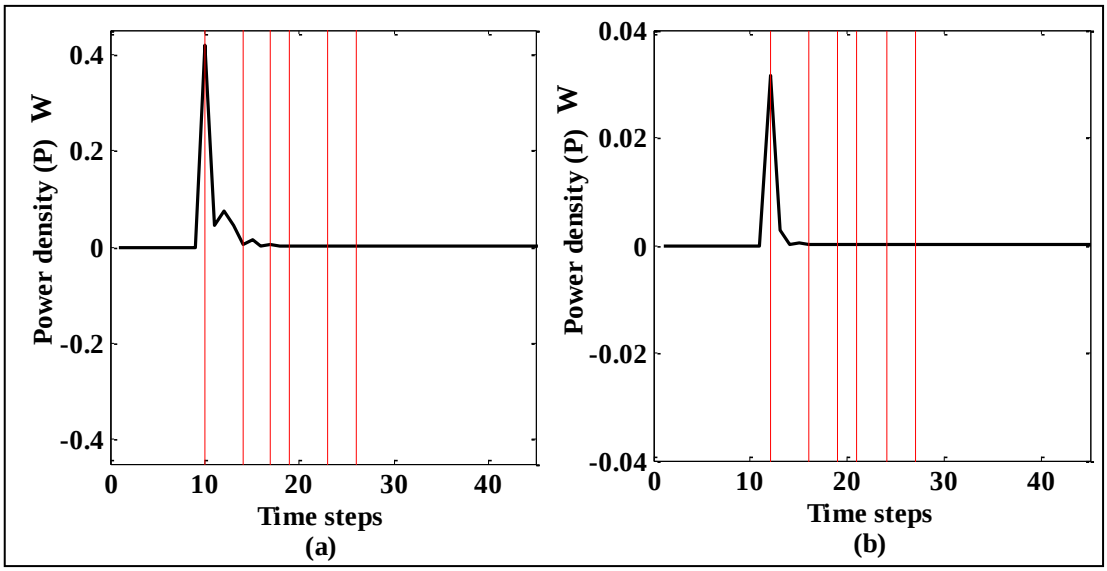

Figure (4.9): Power density at 3000 iteration in five layers of human tissue for distance of 10cm at: (a) f= 900MHz, λ=.33m, Δz=λ/20 =.01m, Δt=.6ns and (b) f= 1800MHz, λ=.16m, Δz= λ/20=.008m, Δt=27.7ns.

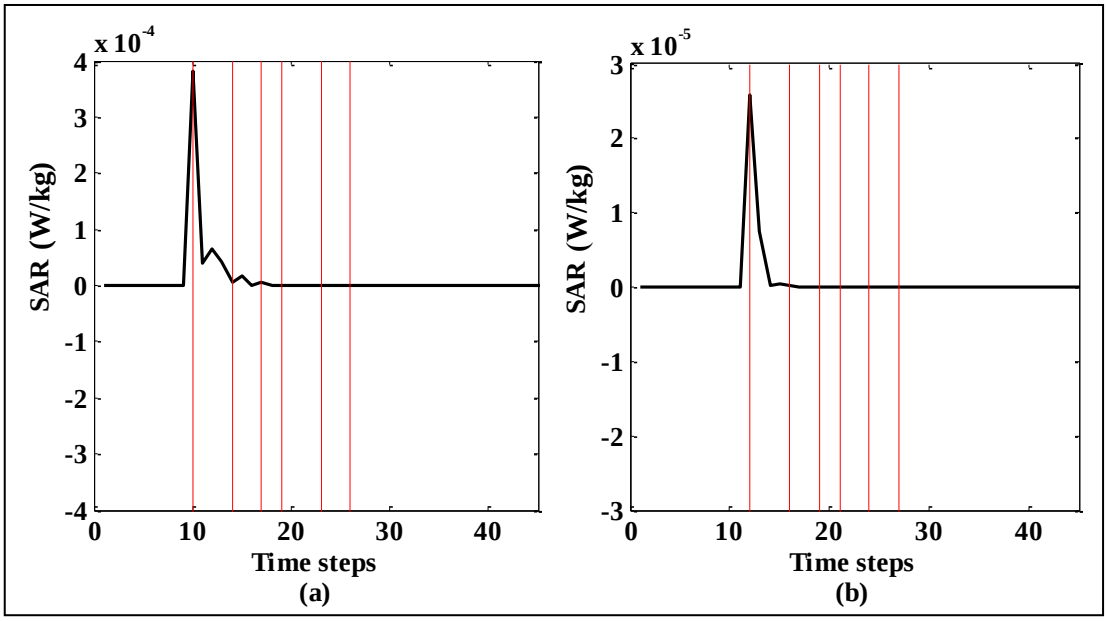

Figure (4.10): SAR at 3000 iteration in five layers of human tissue for distance of 10cm at: (a) f= 900MHz, λ=.33m, Δz=λ/20=.01m, Δt=.6ns and (b) f= 1800MHz, λ=.16m, Δz= λ/20=.008m, Δt=27.7ns.

According to figures (4.11), (4.12), (4.13) and (4.14 a), the position of five human tissues is set at value (0 to 15) which represents free space, the interval of (15-19) occupies skin tissue, and the range (19-22) is in Dura, and the value (22-24) represents CSF, the brain is in domain of (24-28), and value of (28-31) is cerebellum. Figure (4.11 a) shows that the electromagnetic pulse is measured when it achieves line of sight where signal amplitude begins in free space while it strikes the human body, skin amplitude is 0.119 V/m, dura amplitude is 0.025 V/m, and pulse amplitude will decrease more to zero in cerebellum via CSF, and brain. Fig. (4.12 a) shows the connection between Magnetic field in y-dimension and time step where signal amplitude is less when it strikes the human body and goes through the skin at 0,927 A/m, dura at 0.326 A/m, till it reaches zero at cerebellum vai CSF and brain. In figure (4.13 a), Power density reaches 0.0062 W in skin and decreases to 0.0003 W in dura, and finally becomes zero at cerebellum vai CSF and brain. Figure (4.14 a) shows that SAR reaches the extreme in skin at 5.64×10^{-6} W/Kg and decreases to 2.92×10^{-7} W/Kg in dura and finally becomes zero at cerebellum via CSF and brain.

Figures (4.11-4.14 b) shows the ranges of (0-18, 18-22, 22-25, 25-27, 27-30, and 30-33) that represent free space, skin, dura, CSF, brain, and cerebellum respectively. Figure (4.11 b) shows that signal amplitude at skin is 0.157 V/m in skin and zero in cerebellum via dura, CSF, and brain. Figure (4.12 b) shows the connection between Magnetic field in y-dimension and time step where signal amplitude is less when it strikes the human body and goes through the skin at 0.274, dura at 0.113 A/m, till it reaches zero at cerebellum via CSF and brain. In figure (4.13 b), Power density reaches 0.014 W in skin, and decreases to zero in cerebellum via dura, CSF and brain. In figure (4.14 b), SAR reaches its maximum in skin at 1.31×10^{-5} W/Kg and decreases to zero in cerebellum via dura, CSF and brain.

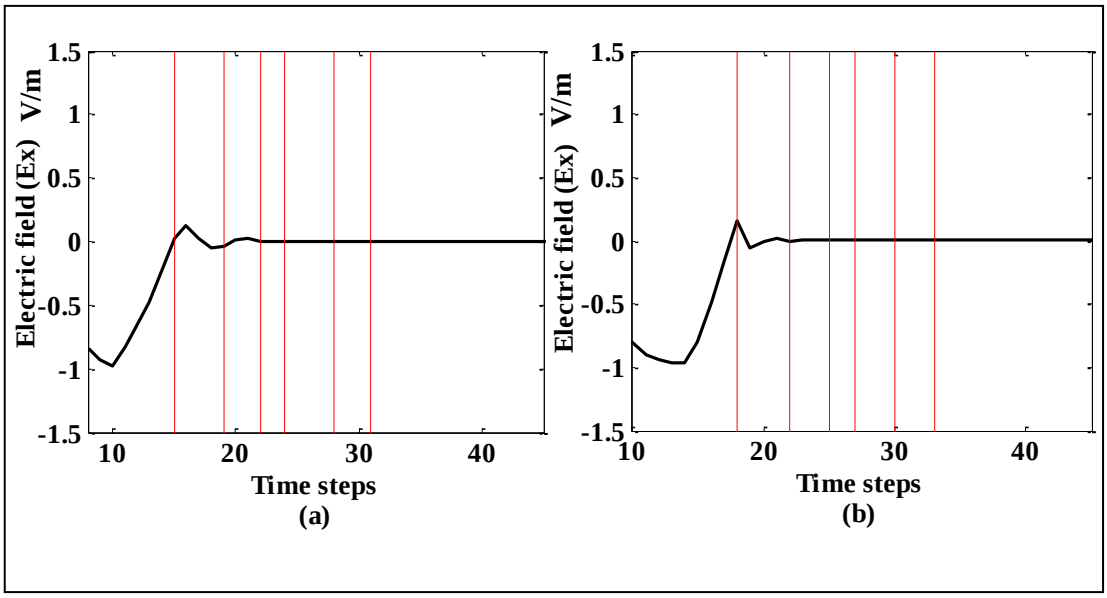

Figure (4.11): Simulation of the propagation of electric field at 3000 iteration in five layers of human tissue for distance of 15cm at: (a) f= 900MHz, λ=.33m, Δz=λ/20=.01m, Δt=.6ns and (b) f= 1800MHz, λ=.16m, Δz= λ/20=.008m, Δt=27.7ns.

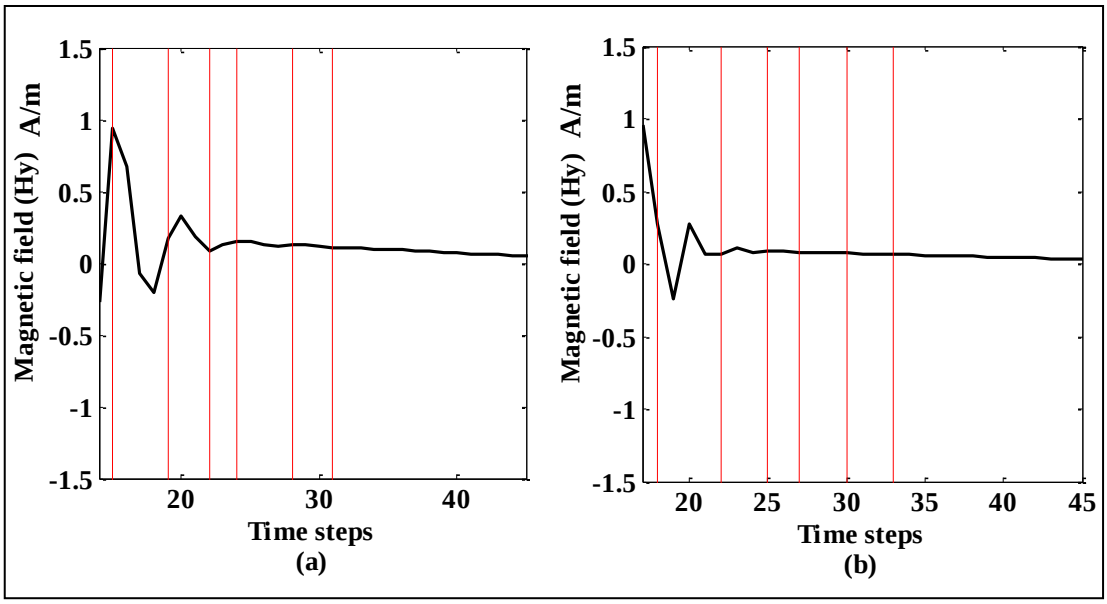

Figure (4.12): Simulation of the propagation of magnetic field at 3000 iteration in five layers of human tissue for distance of 15cm at: (a) f= 900MHz, λ=.33m, Δz=λ/20 =.01m, Δt=.6ns and (b) f= 1800MHz, λ=.16m, Δz= λ/20=.008m, Δt=27.7ns.

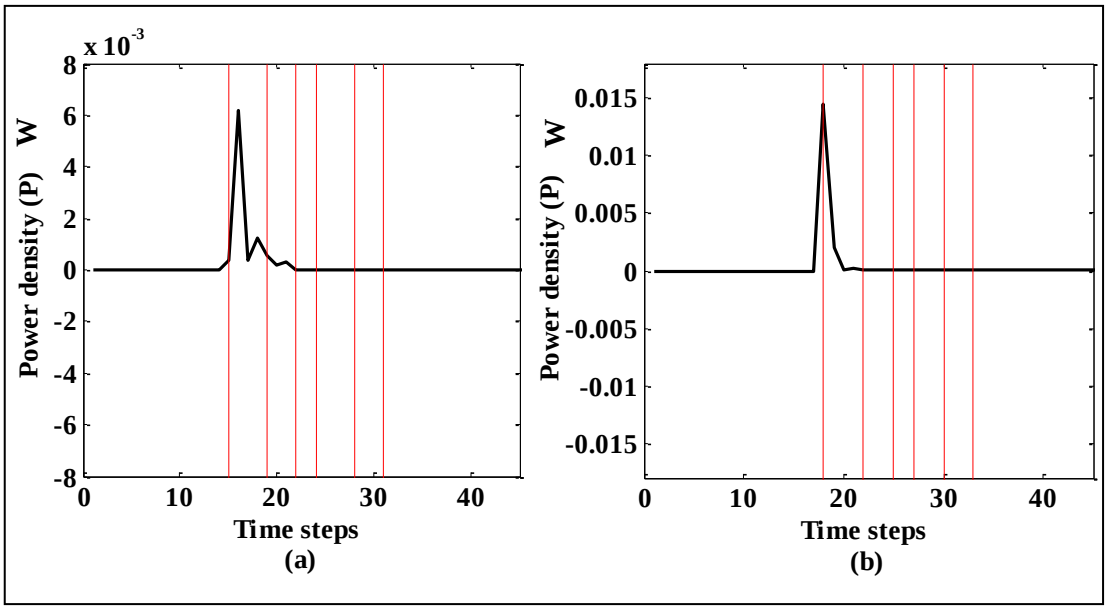

Figure (4.13): Power density at 3000 iteration in five layers of human tissue for distance of 15cm at: (a) f= 900MHz, λ=.33m, Δz=λ/20 =.01m, Δt=.6ns and (b) f= 1800MHz, λ=.16m, Δz= λ/20=.008m, Δt=27.7ns.

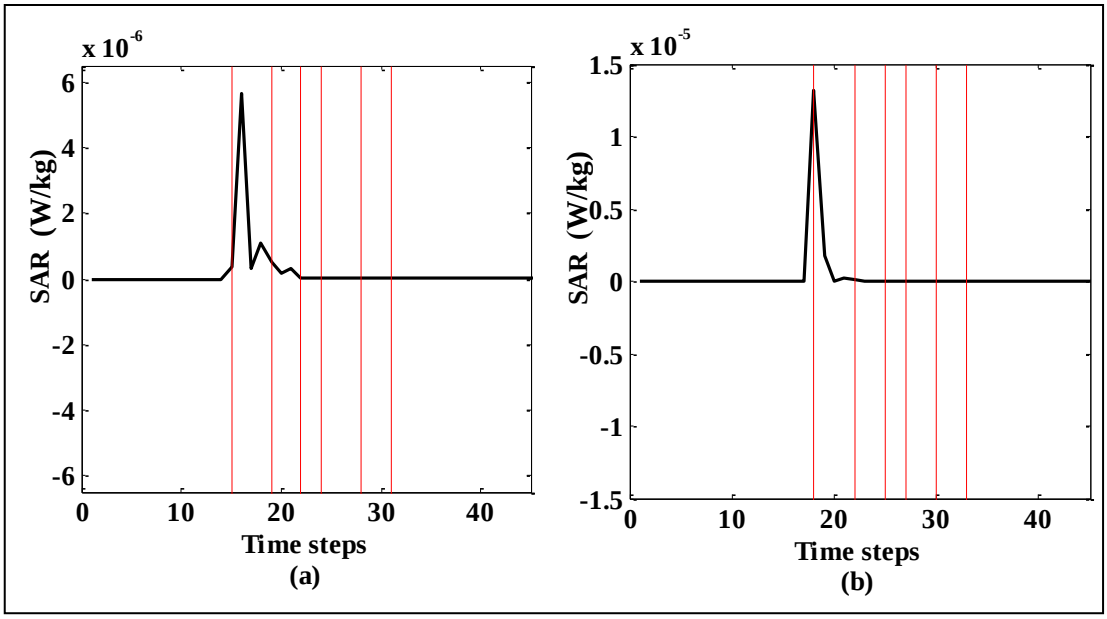

Figure (4.14): SAR at 3000 iteration in five layers of human tissue for distance of 15cm at: (a) f= 900MHz, λ=.33m, Δz=λ/20=.01m, Δt=.6ns and (b) f= 1800MHz, λ=.16m, Δz= λ/20=.008m, Δt=27.7ns.

Figures (4.15-4.18 a) show that the intervals from (0-20), (20-24), (24-27), (27-29), (29-33), and (33-36) represent free space, skin, dura, CSF, brain, and cerebellum respectively. In figure (4.15 a), electric field pulse increases more than when measured at distance 15 cm and equals 0.097 V/m in skin, 0.017 V/m in dura, and pulse amplitude decreases to zero in cerebellum. Figure (4.16 a) shows the relation between Magnetic field in y-dimension and time step where signal amplitude decreases when it strikes the human body and goes through the skin at 0.843 A/m, dura at 0.278 A/m, and zero at cerebellum over CSF and brain. Figure (4.17 a) shows that Power density becomes .004 W in skin and zero in cerebellum via dura, CSF and brain. In figure (4.18 a), SAR reaches 3.721×10^{-6} W/Kg in skin and zero in cerebellum.

Figures (4.15-4.18 b) confirm that the ranges (0-25), (25-28), (28-31), (31-33), (33-37), and (37-39) represent free space, skin, dura, CSF, brain, and cerebellum respectively. Also, figure (4.15 b) shows that a signal amplitude begins in free space and decreases to 0.081 V/m in skin and zero in cerebellum via dura, CSF, and brain. Figure (4.16 b) shows the relation between Magnetic field in y-dimension and time step where signal amplitude decreases when it strikes the human body and goes through the skin at 0.355 A/m, and zero at cerebellum via dura, CSF, and brain. Figure (4.17 b) shows that Power becomes .0087 W in skin to zero in cerebellum via dura, CSF and brain. In figure (4.18 b) shows that SAR amounts to 7.21×10^{6} W/Kg in skin and decreases to zero in cerebellum.

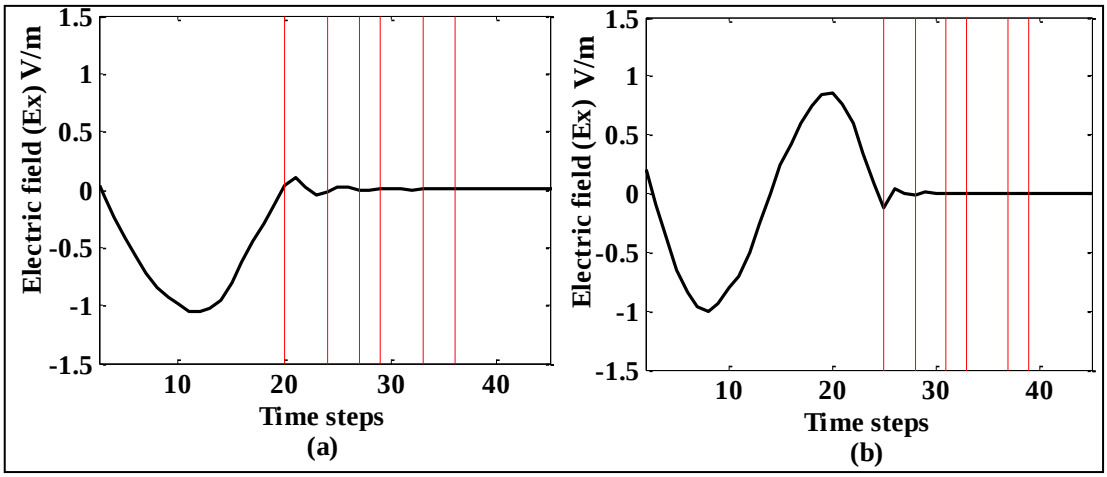

Figure (4.15): Simulation of the propagation of electric field at 3000 iteration in five layers of human tissue for distance of 20cm at: (a) f= 900MHz, λ=.33m, Δz=λ/20=.01m, Δt=.6ns and (b) f= 1800MHz, λ=.16m, Δz= λ/20=.008m, Δt=27.7ns.

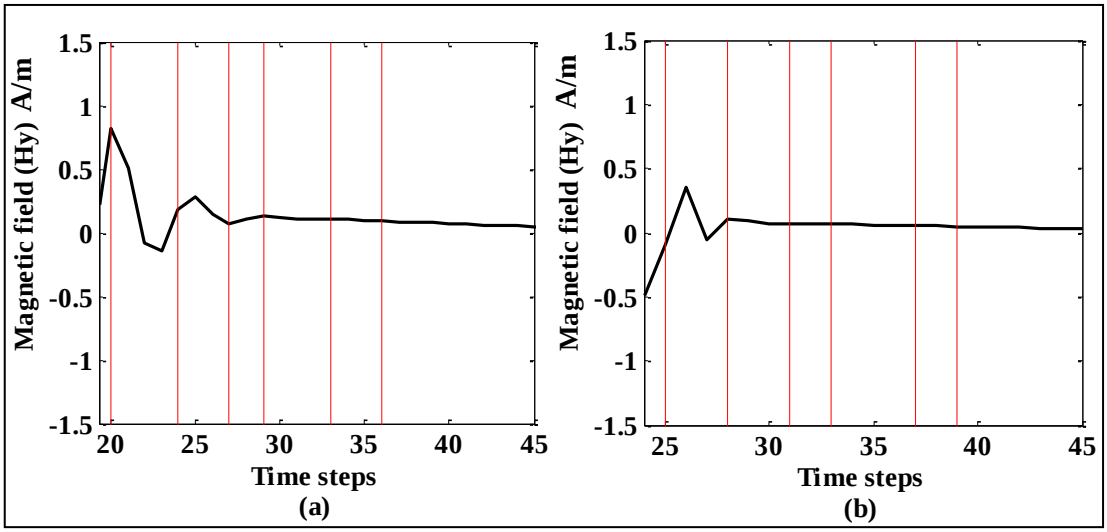

Figure (4.16): Simulation of the propagation of magnetic field at 3000 iteration in five layers of human tissue for distance of 20cm at: (a) f= 900MHz, λ=.33m, Δz=λ/20 =.01m, Δt=.6ns and (b) f= 1800MHz, λ=.16m, Δz= λ/20=.008m, Δt=27.7ns.

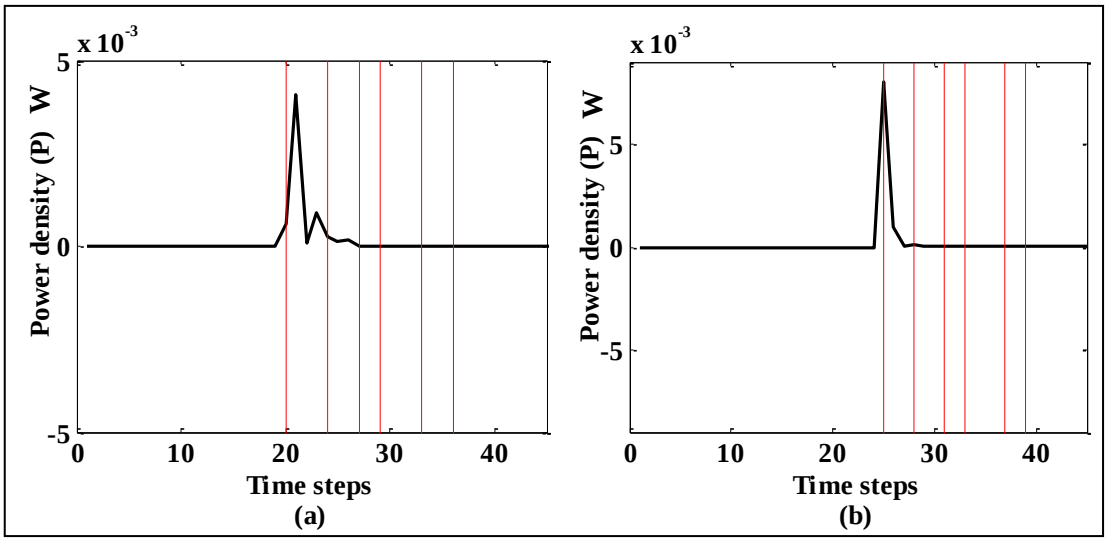

Figure (4.17): Power density and time steps at 3000 iteration in five layers of human tissue for distance of 20cm at: (a) f= 900MHz, λ=.33m, Δz=λ/20 =.01m, Δt=.6ns and (b) f= 1800MHz, λ=.16m, Δz= λ/20=.008m, Δt=27.7ns.

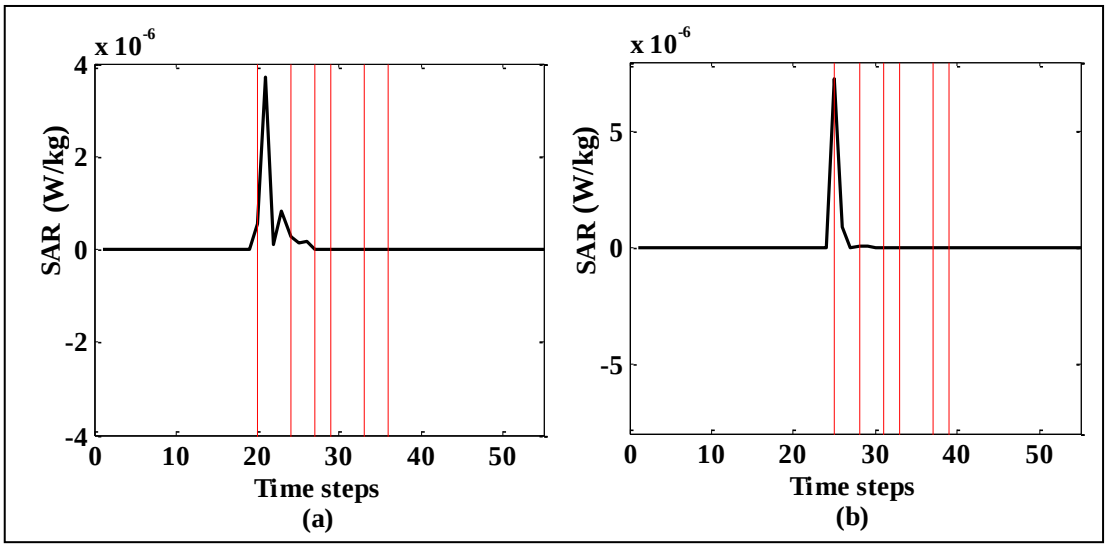

Figure (4.18): SAR at 3000 iteration in five layers of human tissue for distance of 20 cm at: (a) f= 900MHz, λ=.33m, Δz=λ/20=.01m, Δt=.6ns and (b) f= 1800MHz, λ=.16m, Δz= λ/20=.008m, Δt=27.7ns.

Figures (4.19-4.22 a) show the ranges (0-25), (25-29), (29-32), (32-34), (34-38), and (38-41) which represent free space, skin, dura, CSF, brain, and cerebellum respectively. Figure (4.19 a) shows that electromagnetic amplitude increases more than when measured at distance 20 cm. Here, a signal amplitude in skin equals 0.239 V/m, dura amplitude is 0.055 V/m, and pulse amplitude decreased to zero in cerebellum amidst dura, CSF, and brain. Figure (4.20 a) shows that in Magnetic field in y-dimension, signal amplitude decreases when it strikes human body and goes through the skin at 2.002 A/m, dura at 0.488, until it reaches zero at cerebellum. Also, figure (4.21 a) shows that Power density is zero in free space and increases to maximum at skin and equals 0.024 and decreases in dura to 0.001 W, and finally it reaches zero in cerebellum. In figure (4.22 a), the rapport between SAR versus time step increases from zero at free space to 2.256×10^{-5} W/Kg at skin and decreases again to 1.411×10^{-6} W/Kg at dura, until it backs to zero again in cerebellum.

As shown in figures (4.19-4.22 b), the ranges from (0-31, 31-34, 34-38, 38-40, 40-43, and 43-46) represent free space, skin, dura, CSF, brain, and cerebellum respectively. Figure (4.19 b) shows that signal amplitude in skin is 0.818 V/m and 0.086 V/m in dura, and zero in cerebellum amidst CSF, and brain. Figure (4.20 b) shows that in Magnetic field in y-dimension, signal amplitude decreases when it strikes human body and goes through skin at 1.02 A/m, until it reaches zero at cerebellum. Meanwhile, figure (4.21 b) shows that power density is zero in free space and increases to maximum at skin and equals 0.397 W, to zero in cerebellum through dura, CSF, and brain. Figure (4.22 b) shows that SAR increases more than when measured at 20 cm where it becomes .00361 W/Kg in skin and zero again in cerebellum.

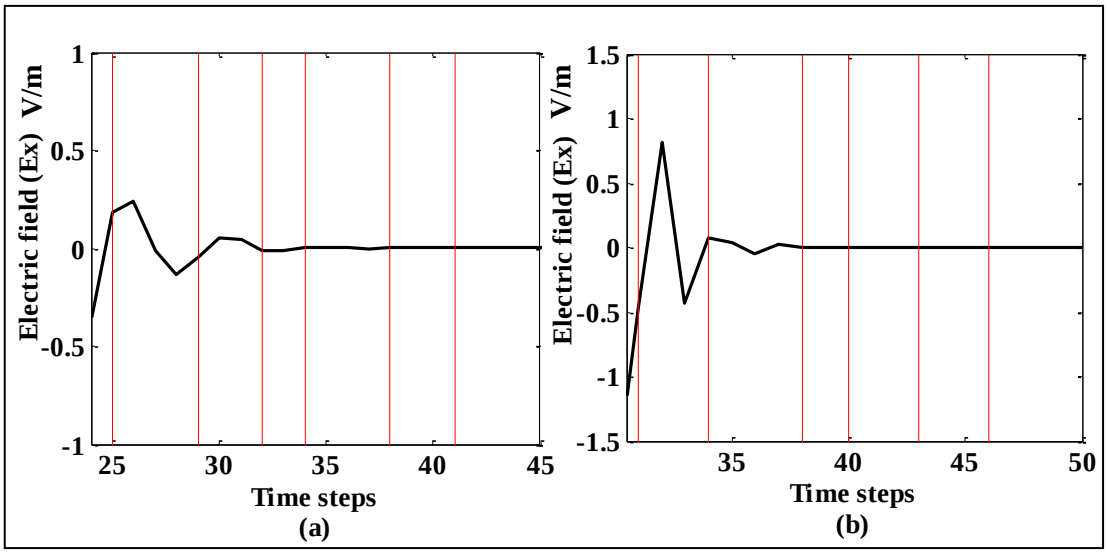

Figure (4.19): Simulation of the propagation of electric field at 3000 iteration in five layers of human tissue for distance of 25cm at: (a) f= 900MHz, λ=.33m, Δz=λ/20=.01m, Δt=.6ns and (b) f= 1800MHz, λ=.16m, Δz= λ/20=.008m, Δt=27.7ns.

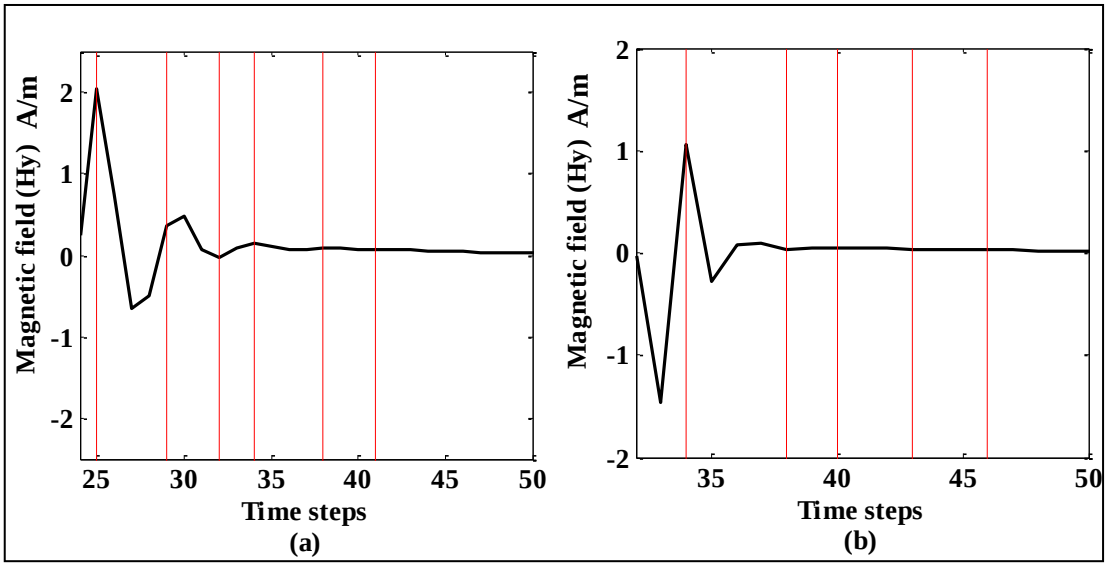

Figure (4.20): Simulation of the propagation of magnetic field at 3000 iteration in five layers of human tissue for distance of 25cm at: (a) f= 900 MHz, λ=.33m, Δz=λ/20 =.01m, Δt=.6ns and (b) f= 1800MHz, λ=.16m, Δz= λ/20=.008m, Δt=27.7ns.

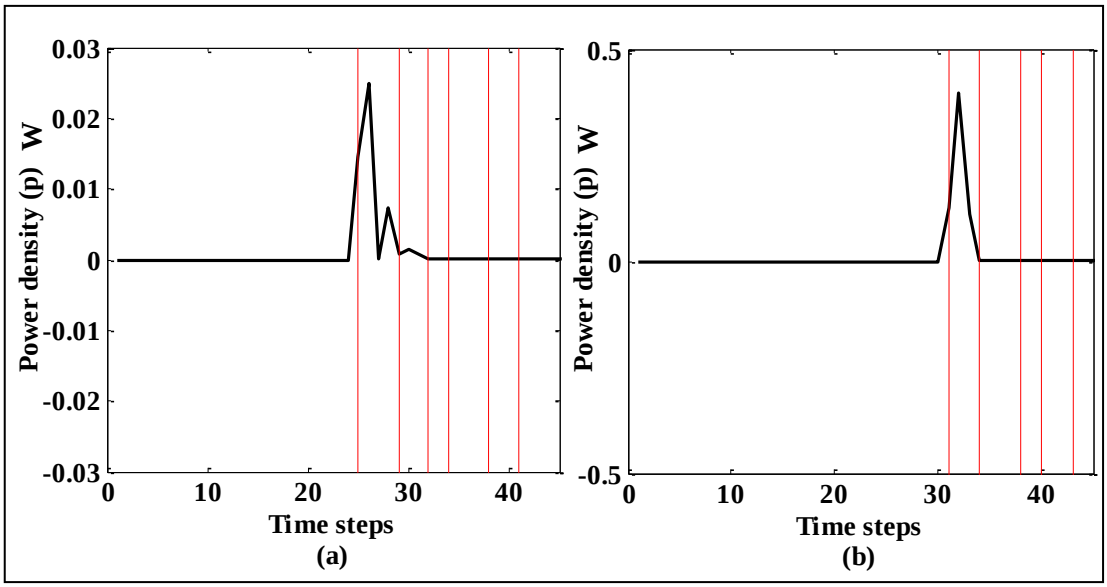

Figure (4.21): Power density at 3000 iteration in five layers of human tissue for distance of 25cm at: (a) f= 900MHz, λ=.33m, Δz=λ/20 =.01m, Δt=.6ns and (b) f= 1800MHz, λ=.16m, Δz= λ/20=.008m, Δt=27.7ns.

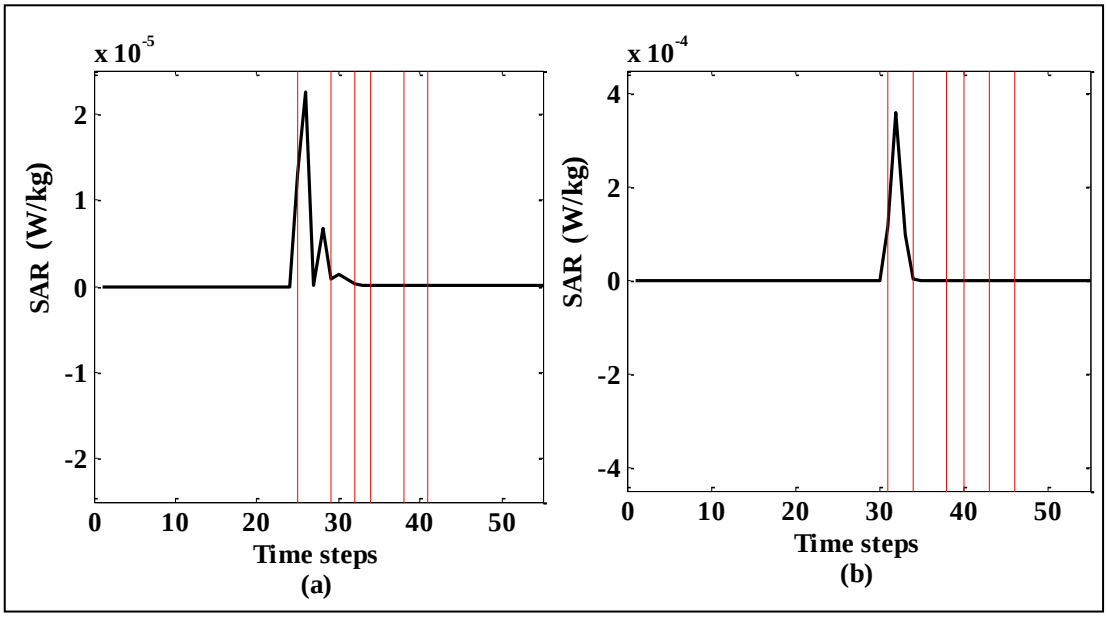

Figure (4.22): SAR at 3000 iteration in five layers of human tissue for distance of 25cm at: (a) f= 900MHz, λ=.33m, Δz=λ/20=.01m, Δt=.6ns and (b) f= 1800MHz, λ=.16m, Δz= λ/20=.008m, Δt=27.7ns.

Moreover, figures (4.23-4.26 a) show that the ranges of (0-30), (30-34), (34-37), (37-39), (39-43), and (43-46) represent free space, skin, dura, CSF, brain, and cerebellum respectively. Figure (4.23 a) shows that a signal amplitude equals 0.07 V/m in skin, and pulse amplitude decreases to zero in cerebellum. Figure (4.24 a) indicates that in Magnetic field in y-dimension, a signal amplitude decreases when it whips the human body and goes over the skin at 0.616 A/m, dura at 0.201 A/m, until it reaches zero at cerebellum. Figure (4.25 a) shows that power density reaches .011 W in skin and decreases more to zero in cerebellum. SAR is measured at distance 30 cm. Figure (4.26 a) shows that SAR reaches 1.08×10^{-5} W/Kg in skin and decreases to 5.47×10^{-7} W/Kg in dura, and finally it becomes zero in cerebellum.

Figures (4.23-4.26 b) show that the ranges of (0-37), (37-41), (41-44), (44-46),(46-49), and (49-52) represent free space, skin, dura, CSF, brain, and cerebellum respectively. Figure (4.23 b) shows that signal amplitude is 0.114 V/m in skin and reaches zero in cerebellum in dura, CSF, and brain. Figure (4.24 b) shows that in Magnetic field in y-dimension, signal amplitude decreases when it whips human body and goes in the skin at 0.188A/m, and it reaches zero in the cerebellum. Figure (4.25 b) shows that power density reaches .0078 W in skin and decreases to zero in cerebellum. In figure (4.26 b), SAR is measured at 30 cm and equals 7.047×10^{-6} W/Kg.

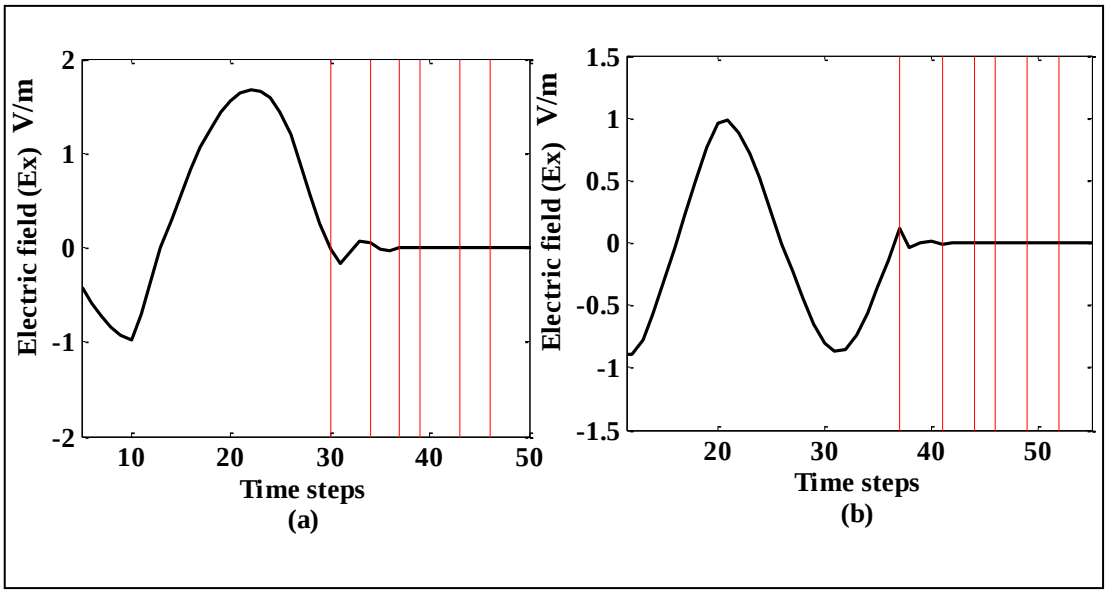

Figure (4.23): Simulation of the propagation of electric field at 3000 iteration in five layers of human tissue for distance of 30cm at: (a) f= 900MHz, λ=.33m, Δz=λ/20=.01m, Δt=.6ns and (b) f= 1800MHz, λ=.16m, Δz= λ/20=.008m, Δt=27.7ns.

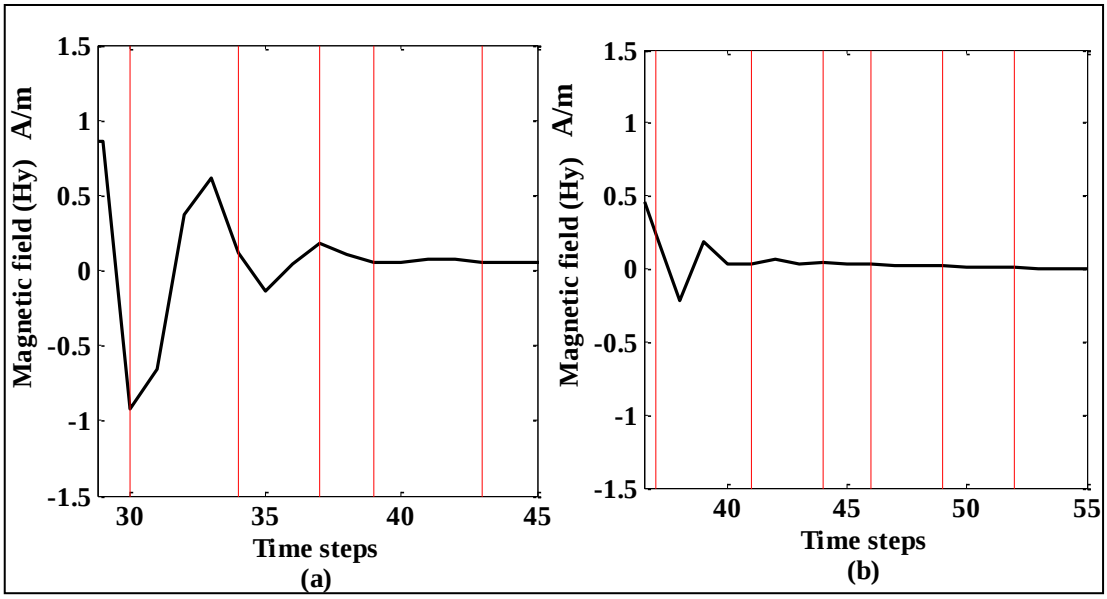

Figure (4.24): Simulation of the propagation of magnetic field at 3000 iteration in five layers of human tissue for distance of 30cm at: (a) f= 900MHz, λ=.33m, Δz=λ/20 =.01m, Δt=.6ns and (b) f= 1800MHz, λ=.16m, Δz= λ/20=.008m, Δt=27.7ns.

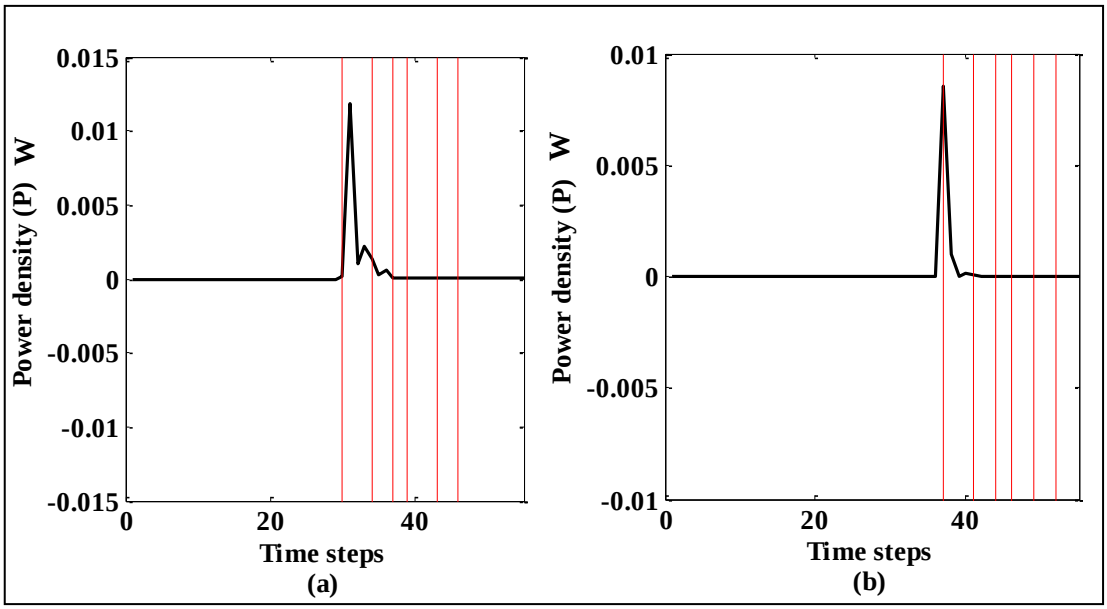

Figure (4.25): Power density at 3000 iteration in five layers of human tissue for distance of 30cm at: (a) f= 900MHz, λ=.33m, Δz=λ/20 =.01m, Δt=.6ns and (b) f= 1800MHz, λ=.16m, Δz= λ/20=.008m, Δt=27.7ns.

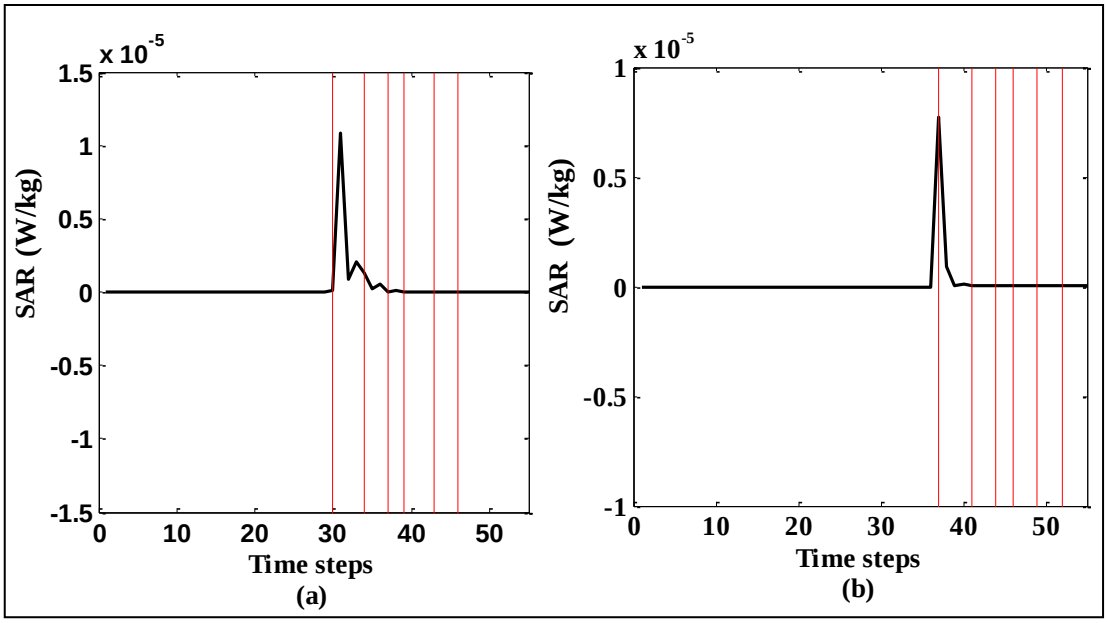

Figure (4.26): SAR at 3000 iteration in five layers of human tissue for distance of 30cm at: (a) f= 900MHz, λ=.33m, Δz=λ/20=.01m, Δt=.6ns and (b) f= 1800MHz, λ=.16m, Δz= λ/20=.008m, Δt=27.7ns.

Conclusions

Conclusions

In this thesis, the researcher proposed to study the effect of RF wave radiated from dipole antenna in cellular phones operating in GSM (900 MHz and 1800 MHz) on human head by using Matlab software. It also investigated the signal properties in free space and the change of the signal after hitting human head and going through head layers (skin, Dura, Cerebro-Spinal Fluid (CSF), brain, and Cerebellum).

Through simulating electromagnetic waves emitted from dipole antenna about (5cm, 10cm, 15cm, 20cm, 25cm, and 30cm) away from human's head; the behavior of the wave from the moment of emission to the moment of infiltrating the scalp and the cerebellum is examined. A multi-layered head model was used; the five layers represent skin, dura, CSF, brain, cerebellum respectively. FDTD method is used to study the distribution of the electromagnetic fields in body tissues, the absorbent power, and SAR distribution.

It is found that the electromagnetic of GSM signal in free space and after striking the human head interface propagates more slowly, and the amplitude decreases through skin, Dura, Cerebro Spinal Fluid (CSF), brain until it reaches zero in Cerebellum.

Specific Absorption Rate (SAR) and power density distribution at human head layers have higher values in outer section of head consisting of skin and dura that is because they come closer to the antenna source.

As the distance of mobile phone, radiations from the tissue layer decrease, the EM wave radiations penetrate deeper up to the cerebellum layer. In addition, Figures show that the effect of frequency 900 MHz by mobile phone, global system mobile (GSM) is more than the frequency 1800 MHz on human head.

Moreover, at distance 5 cm, the electric field value is 0.154 V/m in skin, 0.086 V/m in dura, but the electric field value at distance 30 cm is 0.07 V/m in skin at 900 MHz. Further, the electric field value is 0.094 V/m in skin and 0.005V/m in dura at distance 5 cm, yet, the electric field value at distance 30 cm is 0.114 V/m at 1800MHz.

Also, at distance 5 cm, the power density value equals 0.032 W in skin and 0.010 W in dura. Meanwhile, the SAR value is equal to 2.91×10^{-5} W/Kg in skin and 9.38×10^{-6}

W/Kg in dura at 900 MHz, but power density value is equal to 0.0053 W in skin, and the SAR value is equal to 4.87×10^{-6} W/Kg at 1800 MHz.

In addition, at distance 30 cm, the power density value is equal to 0.011 W in skin, and the SAR value is equal to 1.08×10^{-5} W/Kg in skin and 5.47×10^{-7} W/Kg in dura at 900 MHz. However, power density value is equal to 0.0078 W in skin, and the SAR value is equal to 7.047×10^{-6}W/Kg at 1800 MHz.

References

References

Abu Ishaiba, S. A. (2012). "*The Effect of sector Antennas on Human Head Model in Term of Electromagnetic Radiation and SAR Distribution."* (Master Thesis). The Islamic University of Gaza.

Ackson, J., & David, J. (1999). *Classical Electromagnetic*. (3rd ed.). New York: John Wiley and Sons.

Adey, W. R. (1997). *Bioeffects of Communication Fields*. New York: Chapman and Hall.

Ali, M. F., & Ray, S. (2014, June 4). "*FDTD*- based SAR analysis in human head using irregular volume averaging techniques of different resolutions at GSM 900 band." *Indian Journal of Radio & Space Physics*, 43, 235-242.

Andersson, *U. (2001). Finite-Domain Method*s *for Maxwell Equations. (n.d.).* Stockholm*:* Kungl Tekniska Tekniska.

Andrews, L. (2009). *Encyclopedia of Applied Spectroscopy*. Weinheim: WILEY-VCH.

Assefa, N., & Tsige, Y. (2003). *Human Anatomy and Physiology*. the Ethiopia: USAID.

Attwood, S. S. (1995). *Radio Wave Propagation Experiments*. Columbia University Press 3, 25-30.

Auc Fai, C. (2006). *The Finite Difference Time Domain Method for Computational Electromagnetics*. Research Project towards the degree of Bachelor of Engineering, University of Southern Queensland, Faculty of Engineering and Surveying.

Balanis, A. (2005). *Antenna theory analysis and design*. (3rd ed.). Canada: John Wiley & Sons, INC, Hoboken, New Jersey.

Balanis, A. (2011). *Introduction to the Finite-Difference Time-Domain (FDTD) Method for Electromagnetics.* Arizona State University*:* the Morgan & Claypool Publishers series.

Bath, A., Thakur, A., Sharma, J., Prasad, B. (2014). "Analyzing the Different Parameters of Dipole Antenna." *International Journal of Electrical & Electronics Engineering (IJEEE), 1*(1), 1694- 2426.

Bender, L., Harding, D., Jackson, T., Kennedy, D., Lee, G., & Stokes, J. (2005). *Brain and Nervous System.* USA: Facts on File, INC.

Bhargavi, K., KE, B., & Nageswar, P. (2013, April). "Mobile Phone Radiation Effects on Human Health." *International Journal of Computational Engineering Research, 3* (4).

Butcher , G. (n.d). *Tour of the Electromagnetic Spectrum*. New York: InDyne and V! Studios, INC.

Carr, J. (2001). *Practical Antenna Handbook.* (4th ed.). New York: McGraw-Hill.

Chatterjee, R. A. (2001). *Antenna Theory and Practice*. New Delhi: New Age International.

Chatterjee, R., & Neelakanta, P. S. (2003). *Antennas for Information Super Skyways: An Exposition on Outdoor and Indoor Wireless Antennas*. England: Institute of Physics.

Chen, J. (2010). *A Hybrid Spectral-Element / Finite-Element Time-Domain Method for Multiscale Electromagnetic Simulations.* (Doctoral Dissertation), Duke University, North Carolina.

Cheng, K. D. (1998). *Field and Wave Electromagnetic*. (2nd ed.). New York: Addison-Wesley Publishing Company, INC.

Christ, A., Samaras,T., Klingen, A., & Kuster, N. (2006). Characterization of the electromagnetic near-field absorption in layered biological tissue in the frequency range from 30 MHz to 6000 MHz. *institute of physics publishing*, 51 (2006), 4951–4965. doi:10.1088/0031-9155/51/19/014.

Chu, S. T., and Chaudhuri, S. K. (1995). Finite-Difference Time-Domain Method for optical wave guide analysis, *progress In Electromagnetic Research(PIER)*, 11, 255–300.

Connor, F. R. (1989). Introductory Topics in Electronics and Telecommunication Antennas. *Edward Arnold . 1*(4), 2-4.

Derrickson, H. & Gerard, T. O. (2005). *Principles of Anatomy and Physiology*. (12th ed.). New York: Wiley.

Dielectric Properties of the Body Tissues. Retrieved July 30, 2016, from: http://niremf.ifac.cnr.it/tissprop/htmlclie/htmlclie.htm.

EL-Khozodar, H., Shabat, M., EL-Wasife, K., & Osman, A. (2010). Modeling the Effect of Electromagnetic Waves produced by Mobile Phone base station on Human body Tissue. *Journal Natural sciences*, 12, 81-87.

Elsherbeni, A., & Demir V. (2009). *The Finite-Difference Time-Domain Method forElectromagnetics with MATLAB Simulations*. Scitech Inc., Raleigh, NC.

EL-Wasife, K. (2011). Power Density and SAR in Multi-Layered Life Tissue at Global System Mobile (GSM) Frequencies. *Journal of Electromagnetic Analysis and Applications*, 3, 328-332. doi:10.4236/jemaa.2011.38052.

Encyclopædia Britannica. (2016). *Cerebrospinal fluid (CSF).* Retrieved March 22, 2016, from: https://www.britannica.com/science/cerebrospinal-fluid.

Fujimoto, k .y. (1999). *Mobile Antenna Systems*. British Library: hand book Artech House , INC.

Fung, C. (2011). *Basic Antenna Theory and Application.* Project for Degree Bachelor of Science, the Worcester polytechnic institute.

Furse, C., Christensen D. A., & Durney, C. H. (2009). *Basic Introduction to BioElectromagnetics*. (2nd ed). CRC Press.

Furse, C., Christensen, D. A., & Durney, C. H. (2009). *Basic Introduction to BioElectromagnetics* (2nd ed.). CRC Press.

Gabriel, C., & Gabriel, S. (1996) .Compilation of the Dielectric Properties of Body Tissues at RF and Microwave Frequencies. *Internet Document*. Retrieved November 30, 2015, from: http://niremf.ifac.cnr.it/docs/DIELECTRIC/Report.html.

Gandhi, O. P., & Lazzi, G. (1996). Electromagnetic Absorption in The Human Headand Neck for Mobile Telephones at 835MHz and 1900 MHz. *IEEE Trans on Microwave Theory and Techniques MTT, 1*(44), 1886-1897.

Grove, G.(n.d.). *All about Antennas*. Monitoring Times.

Hallas, J. R. (n.d.). *Basic Antennas understanding practical Antennas and Desigin.* the USA: The national association for Amateur Radio (ARR L).

Hao, Y., Mittra, R. (2009). FDTD Modeling of Metamaterials Theory and Applications. USA: Artech House, inc.

Harrington, R. F. (1993). *Field Computation by Moment Methods*. Piscataway: Wiley- IEEE Press.

Hawkins, J.N.A.(1936). *Radio Antennas Handbook.* (2 th ed.). the USA: Radio, Ltd.

Hoehn, K. A. & Nicpon, E. L. (2007). *Human Anatomy & Physiology*. (7th ed.).San-Francisco: Benjamin Cummings.

Huang , Y., & Boyle , *K*. (2008). *Antennas from theory to practice*. (1st ed.). the USA: A John Wiley and Sons, Ltd.

Hyland, G. (2000). The physiological and environmental effects of non-ionizing electromagnetic radiation. *In Working document for the STOA Panel*. pp 297-574. European Parliament, Directorate General for Research, Directorate A, The STOA Programme.

Igarashi, K., Nishino, K. O., & Nayar, S. K. (2005). *The Appearance of Human Skin.* USA: the National Science Foundation.

James, W. (1991). *Antenna Here is a Dipole.* In ("Rus") Healy. NJ2L.

Jensen, R. (2000). *Remote sensing of the environment*. (2nd ed.). the USA: Prentice Hall.

Jianming, J. (2002). *The Finite Element Method in Electromagnetics*. (2nd ed.). Wiley-IEEE Press.

Jurgens, T. G., Taftove, A., Umashanker, K., & Moore, T.G. (1992). Finite-Difference Time-Domain Modeling of Curved Surfaces, *IEEE Transactions on antennas and propagation, 40*(4), 357–366.

Kawano, K., Kitoh, T. (2001). *Introduction to Optical Waveguide Analysis: Solving Maxwell's Equation*. John Wiley and Sons, INC.

Kenneth, R., & Repacholi, H. (2004). Biological Effects of Radiofrequency Fields: Does Modulation Matter? . *Radiation Research, 1*(162), 164-168.

Know Your Brain. (2012, October 20). *National Institute of Neurological Disorders and Stroke*. Bethesda: National Institutes of Health (NIH).

Kraus, D. (1997). *Antennas* (2nd ed.). New York: Tata McGraw-Hill.

Kunz, K. S., & Luebbers, R. J. (1993). *The Finite-Difference Time-Domain Method for Electromagnetics*. CRC, Boca Raton, FL.

Kunz, K. S., Luebbers, R. J. (1993). Time *Domain Method for Electromagnetics*. New York*: CRC Press.*

Lucas, J. (2015). *What Is Electromagnetic Radiation?*. Retrieved March 22, 2015, from: http://www.livescience.com/38169-electromagnetism.html.

Mhaske, S., Kulkarni, G. A., & Tayade, R. L. (2012). SAR in Life Tissue at GSM Frequencies. *International Journal of Advanced Research in Computer Science and Software Engineering, 2*(4).

Millgan, *T. A. (2011). Modern antenna design.* (2nd ed.). New Jersey*:* A John Wiley & Sons, INC.

Mohsenin, N. (1984). *Electromagnetic Radiation Properties of Foods and Agricultural Products*. New York: CRC Press.

Morris, R., & Fillenz, M. (2003). *Neuroscience: the Science of the Brain*. UK: The British Neuroscience Association.

Mousa, A. (2011, February 20). "Electromagnetic Radiation Measurements and Safety Issues of some Cellular Base Stations in Nablus." *Journal of Engineering Science and Technology Review, 4*(1), 35-42.

Mur, G. (1981). "Absorbing boundary conditions for the finite-difference approximation of the time-domain electromagnetic-field equations." *IEEE Transactions on Electromagnetic Compatibility, 23*(4), 377–382.

Nicolas, E., & Lautru, D. (2001). Specific Absorption Rat Assessment Based on A selective Isotropic Measuring System for Electromagnetic Field. *IEEE Trans Electromagnet, 1*(50), 397-40.

Orfanidis, S. J. (1999). *Electromagnetic Waves and Antennas*. New York: Rutgers University P.

Orugu, R. R., Srinivas, K., Raju, V. R., Krishna, Ch. R., Babu, D.N. (2013). "Analyzing Planar Dipole Antenna with Different Arm Widths Operating at 1 GHz." *International Journal of Engineering and Innovative Technology (IJEIT), 3*(2), 2277- 3754.

Paker, S., & Sevgi, L. (1998). "FDTD Evaluation of the SAR Distribution in a Human Head Near a Mobile Cellular Phone." *ITU Electronics and Communication Engineering Department, and Marmara Research Center, Information Technologies Research Institute, 6*(3).

Parameswari, S., Kumar, N. (2015). Tri-Band Half wave Dipole antenna for Wireless Communication Application. *International Journal of Emerging Technology in Computer Science & Electronics (IJETCSE), 12*(4), 0976- 1353.

Patel, N., Vo, K., & Hernandez, M. (2015). *Electromagnetic Radiation*. Retrieved on September 25, 2015, from: http://chem.libretexts.org/Core/Physical_and_Theoretical_Chemistry/Spectroscopy/Fundamentals/Electromagnetic_Radiation.

Rahman, M. M. (2013). "Mobile Phone - A Technical Evaluation On Electromagnetic Exposure And Specific Absorption Rate (SAR) For Human Safety." *International journal of technology enhancements and emerging engineering research, 1* (4), 2347-4289.

Rao, B. V. (2004). *Parallel FDTD Maxwell Solver* (Research Project towards the degree of Bachelor of Electronics & Telecommunication Engineering), Pune University, Alandi (D).

Retriev, W. (2011). "Electromagnetic Fields and Public Health Base Stations and Wireless Technologies." *Health Topics A to Z*, 1-7.

Rettner, R. (2016). *The Human Body: Anatomy, Facts & Functions*. Retrieved March 22, 2016, from: http://www.livescience.com/37009-human-body.html.

Rhattoy, A., Lahmer, M., & Zatni, A. (2010, December). *FDTD* based SAR analysis in human head using irregular volume averaging techniques of different resolutions at GSM 900 band. *ICGST-DSP Journal*, *10*(1), 9-18.

Sabbah, A. I. (2010). *Evaluation of SAR and temperature elevation in a multI-layered human head model exposed to RF radition (*Unpublished Master Thesis), Jordan University of Science and Technology, Jordan.

Schelkunoff, S. A., & Friis, H. T. (1952). *Applied mathematics series*. New York: Bell Telephone Laboratories, INC.

Schneider, J. B. (2016). *Understanding the Finite-Difference Time-Domain Method*. (n.p.).

Sharma, R. S. (n.d.). Effect of Electro-Magnetic Field (EMF) on Human Health. *In Indian Council of Medical Research.* New Delhi –110 029.

Skolnik, M. I. (1962). *Introduction to Radar System*. the USA: McGraw-Hill.

Skolnik, M. I. (1990). *Radar Handbook.* (2nd ed.). the USA: McGraw-Hill.

Smartphone cellular mobile phone antenna design. (2015). *antenna-theory.* Retrieved on November 15, 2015, from: http://www.antenna-theory.com/design/cellantenna.php.

Smitha, C. K., & Narayanan, N. K. (2016). Increase in Specific Asorption Rate (SAR) of Mobile Phone – A Threat to Human. *International Research Journal of Electronics and computer Engineering*, *2*(2), 1-5.

Stallings, W. (2005). *Wireless communications and Network.* (2nd ed.). Pearson Education, INC.

Stewart, W. (2007). *Mobile Phones and Health:* A report from the Independent Expert Group on Mobile Phones (Rep. NO. 2000). London: HESE.

Student bmj. (2011). December). The meninges and common pathology. (n.p.), 19.

Sullivan, D. (2000). *Electromagnetic Simulation Using the FDTD Method*. (2nd ed.). New York*:* the Institute of Electrical and Electronics (IEEE Press), INC.

Taflove, A. (1980). Application of the finite-difference time-domain method to sinusoidal steady state electromagnetic penetration problems. *IEEE Transactions on Electromagnetic Compatibility, 22(3), 191–202.*

Taflove, A. (1995). *Computational Electromagnetic*s*: the* finite-Difference time-domain method*.* London*:* Artech House, INC.

Taflove, A. (2016, June 7). *Allen Taflove*. Retrieved July 30, 2016, from: https://en.wikipedia.org/wiki/Allen_Taflove.

Taflove, A., & Hagness, S. (2000). *Computational Electrodynamics: the Finite-Difference Time-Domain Method*. (2nd ed.). Boston: Artech House.

Taflove,A., Brodwin, M. E. (1975). Numerical solution of steady-state electromagnetic scattering problems using the time-dependent Maxwell's equations. *IEEE Transactions on Microwave Theory and Techniques, 23(8), 623–630*.

Tan, D. (2012). Modeling the Specific Absorption Rate Distribution of a Smartphone. *ANSYS, INC.*

Tawde, P. (2015). Half wave dipole antenna for satellite communication applcation. *International Journal of Advance Research in Science and Engineering, 4*(4), 2319- 8354.

Tempfli, K., kerle, N., Huurneman, C., & Janssen, L. F. (2009). *Principles of Remote Sensing*. (4th ed.). The Nether land: The International Institute for Geo-Information Science and Earth observation (ITC).

The human brain. (2016). *Information, awareness & policy.* England: Health and care information you can trust.

Umashankar, K. R., Taflove, A. (1982). A novel method to analyze electromagnetic scattering of complex objects. *IEEE Transactions on Electromagnetic Compatibility*, 397–405.

Umran, S. I., Robert A. M. (2011). *Numerical Electromagnetic The FDTD Method. the United States of America: Cambridge University Press.*

Vulama, D. (2009, May). Underestimation of EMF/NIR Exposure for Children for Mobile Telephones and for Electronic, *Article Surveillance (EAS) Systems,* Retrieved November 30, 2015, from: http://www.nesucanada.com/.

Wikipedia, (n.d.). *Cellular network*. Retrieved March 22, 2016, from: https://en.wikipedia.org/wiki/Cellular_network.

Wikipedia. (2014, April). *Electromagnetic radiation*. Retrieved April 29, 2015 from: https://en.wikipedia.org/wiki/Electromagnetic_radiation.

Wikipedia. (2015, October 2, a). *Mobile phone radiation and health*. In. Retrieved November 30, 2015, from: https://en.wikipedia.org/wiki/Mobile_phone_radiation_and_health.

Wikipedia (2016, October 22, b). *Antenna (radio).* Retrieved October 30, 2016, from: https://en.wikipedia.org/wiki/Antenna_(radio).

Wikipedia, (2016, July 25, c). *Finite-difference time-domain method.* Retrieved July 30, 2016, from: https://en.wikipedia.org/wiki/Finite-difference_time-domain_method.

Wikipedia, (2016, June 23, d). *Computational electromagnetics.* Retrieved on July 30, 2016, from: https://en.wikipedia.org/wiki/Computational_electromagnetics.

Yee, K. (1966). "Numerical solution of initial boundary value problems involving Maxwell's equations in isotropic media." *IEEE Transactions on Antennas and Propagation, 14(3), 302–307.*

Z.El Dein, A., Amr, A. E. (2010, June 30 - July 2). *Specific Absorption Rate (SAR) Induced in Human Heads of Various Sizes When Using a Mobile Phone*. Paper presented at Proceedings of the World Congress on Engineering, London, U.K.

Zhang, Z. (2011). *Antenna desgin for modle devices*. (1st ed.). China: John Wiley & Sons (Asia) Pte Ltd.

Appendix

Appendix 1:

Ansoft HFSS Simulator used to design half wave length dipole antenna and planar dipole antenna

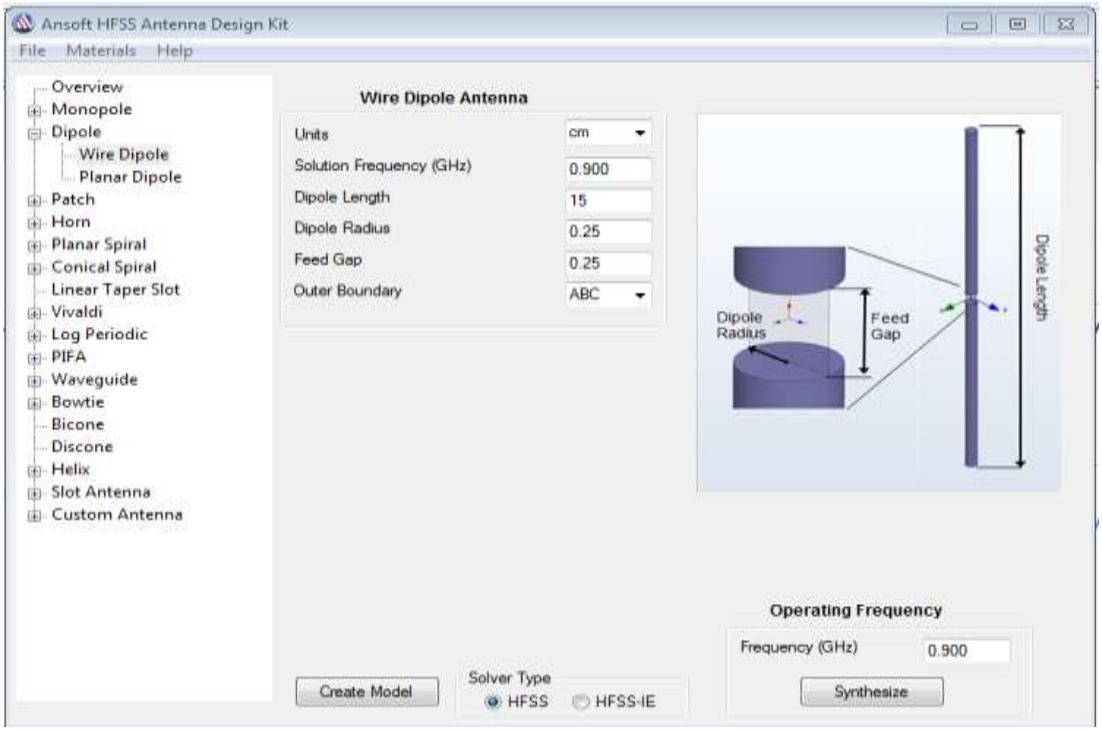

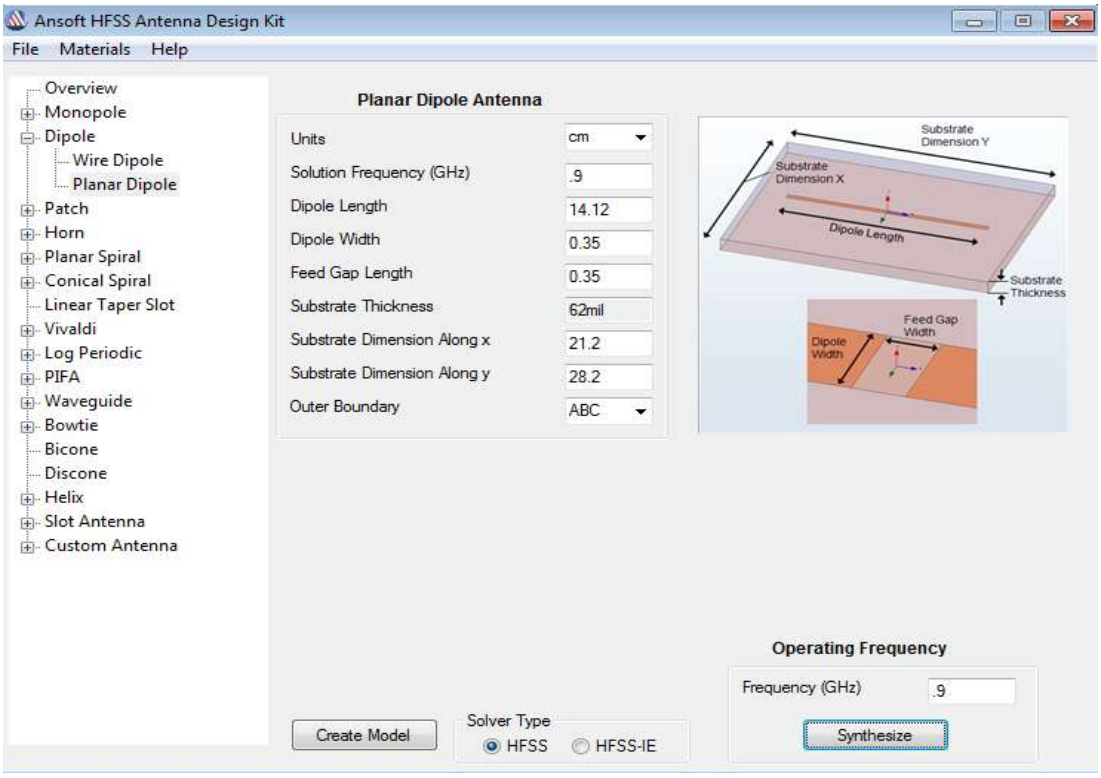

Appendix 2:

Simulation of EM wave hitting human head model by matlab program

```
clear all
clc
permeability = 4*pi*1e-7;  %Free Space
permittivity = 8.85e-12;    %Free Space
c = 1/sqrt(permeability*permitivity);
m=45;
ex = zeros(1,m);
hy = zeros(1,m);
dt = zeros(1,m);
p = zeros(1,m);
sar = zeros(1,m);
dx = .008;
iteration = 3000;
for n = 1:iteration
   for k = 2:45
      eaf = dt(1,k) * s(1,k) / (2*permitivity(1,k)*8.85e-12);
      ca = (1-eaf) / (1+eaf);
      cb = 0.5 / (permitivity(1,k) * (1+eaf));
      ex (1,k) = ca * ex(1,k) + cb * (hy(1,k-1) - hy(1,k));
   end
   source = sin(2*pi*1800*10^(6)*dt(1,1)*n);
    ex(1,2) = source;
   % Boundaries
   if n>2
      KE = 45;
      Kc = 10;
      % dielectric edge
      ex(1,kc) = ex_left_b1_m2;
      ex_left_b1_m2 = ex_left_b1_m1;
      ex_left_b1_m1 = ex(1,kc-1);
```

```
    end
    for k = 1:44
        hy(1,k) = hy(1,k) + 0.5 * (ex(1,k) - ex(1,k+1));
    end
    for k = 1:45
       p (1,k) = (s(1,k) * (abs(ex(1,k)))^2) / 2;
    end
    for k = 1:45
       sar(1,k) = p(1,k) / r(1,k);
    end
    plot(ex);
    plot(hy);
    plot(p);
    plot(sar);
end
```